DISS. ETH No. 24425

Use of fibronectin binding peptides to measure mechanical strain of fibronectin fibers in tissue

A thesis submitted to attain the degree of

Doctor of Sciences (Dr. sc. ETH Zürich)

presented by

SIMON ARNOLDINI

MSc ETH in Material Science, ETH Zürich

born on 08.08.1988

citizen of Austria

accepted on the recommendation of

Prof. Dr. Dr. h.c. Viola Vogel, examiner

Dr. Martin Behe, co-examiner

Prof. Dr. Oliver Distler, co-examiner

2017

Summary

The extracellular matrix (ECM) plays an important role in tissue homeostasis and as mechanical anchorage for cells. Especially the ECM protein fibronectin (Fn) represents a crucial factor in early development of organisms, in wound healing, but also in several pathologies, such as cancer or fibrotic disorders. These pathologies have frequently been reported to go along with an increase in tissue stiffness, mediated in part by an enhanced expression of collagen-I, an enhanced enzymatic crosslinking of ECM residues, as well as an increased number of highly contractile, activated fibroblasts, so called myofibroblasts. However, despite growing knowledge on alterations in tissue mechanics in cancer, it remains unclear whether and how changed tissue stiffness can impact the strain state of protein fibrils and thus the display and accessibility of potential binding sites on these fibers. Given the knowledge of mechanically induced opening up of cryptic motifs and destruction of binding epitopes on Fn and the sheer abundance of binding sites for a variety of growth factors, cytokines, integrins and other matrix proteins, the question arises, to what extent and which of these binding sites are affected by a changed mechanical strain state of fibronectin protein fibers in tissues. However, to address this important question in a satisfactory way, methods and probes for the measurement of Fn fiber strain in tissues are missing, as previously proposed methods are either only applicable *in vitro*, or have unknown binding mechanism and affinities.

Therefore, the aim here is to introduce and establish the Fn binding peptide FnBPA5, originating from bacterium S. *aureus*, as a novel strain probe to specifically bind to relaxed Fn fibers in tissue and *in vivo* to ultimately find correlations with functional aspects triggering Fn relaxation in different systems. Utilization of this novel strain probe enables a first of its kind assessment and comparison of the mechanical strain of Fn fibers in different tissue. First, the strain sensitive binding of FnBPA5 peptide is assessed via binding capability to relaxed or stretched manually pulled Fn fibers and comparison of FnBPA5 binding with Fn-FRET ratio in fibroblast cell culture matrices. In a second step FnBPA5 is then utilized as a strain probe to visualize Fn fiber strain in tissue sections and *in vivo,* to investigate the physiological strain state in organs, and assess alterations of this parameter in pathologic situations.

The herein presented data reveal, that FnBPA5 shows preferential binding to relaxed Fn fibers in an *in vitro* assay of manually pulled Fn fibers, as well as in comparison with the Fn-FRET probe in human dermal fibroblast cell culture experiments. FnBPA5 is found to exhibit high affinity binding to both plasma Fn and relaxed Fn fibers with a dissociation constant in the nanomolar range, similar to currently used antibodies against fibronectin, and has an adequate plasma stability for *in vivo* applications. *Ex vivo* tissue staining of tumor tissue with FnBPA5 shows that areas of relaxed Fn fibers, exhibiting high FnBPA5 binding to Fn, coincide with presence of mature collagen fibers and alpha-smooth muscle actin (α-SMA) expressing cells. *In vivo* experiments using ^{111}In-radiolabeled FnBPA5 derivative reveals specific uptake in tumors and other organs with enhanced retention in tumors compared to other organs in a mouse prostate cancer (PC-3) xenograft tumor model.

Tissue stainings of PC-3 tumor tissue sections and sections from healthy organs reveal no binding to tissue sections from healthy organs, with binding of FnBPA5 only observable in tumor tissue sections, suggesting a highly stretched state of Fn fibers in healthy organs and relaxation of Fn fibers only occuring in tumor tissue. Co-staining of FnBPA5 with cell contractility marker α-SMA reveals higher FnBPA5 binding to Fn in areas adjacent to α-SMA expressing cells, suggesting a relaxation of Fn in these areas, triggered by yet unknown mechanisms. A model of lymph node swelling using lymph nodes from mice injected with lymphocytic choriomeningitis virus (LCMV) or CpG oligodeoxynucleotide adjuvant compared to untreated lymph nodes only shows binding of FnBPA5 to lymph node tissue sections from LCMV infected mice, compared to the other two experimental groups leading to the notion that infection and partial destruction of lymph node fibroblasts as previously reported for LCMV is responsible for Fn relaxation, with physiological lymph node swelling, as observed for CpG, leaving Fn fiber strain unchanged.

It was further investigated whether different glycosaminoglycans (GAGs), such as heparin, clinically used low molecular weight heparin derivatives, as well as hyaluronic acid and synthetically sulfated hyaluronic acid, bind to and are capable of changing Fn conformation. Additionally, given the fact that one major binding site for GAGs on Fn is overlapping with the bacterial binding site also used by FnBPA5, competitive binding studies with different GAGs and FnBPA5 were carried out revealing only little potential of these GAGs to efficiently block FnBPA5 binding to manually pulled Fn fibers.

In summary, this thesis introduces a novel class of peptide probes, showcased here using the S. *aureus* Fn binding peptide FnBPA5, being capable of visualizing relaxed Fn fibers in tissue sections and *in vivo*. The usage of such probes could lead to a better understanding of the dynamic interplay of matrix composition, cellular forces and mechanical strain of Fn fibers and how this is altered in pathologies, such as cancer or fibrotic disorders. The herein presented characterization of an *in vivo* tumor model and *ex vivo* tissue stainings from cancer and lymph node model gives first evidence that the FnBPA5 peptide can serve as an important novel tool to characterize alterations in Fn fiber strain upon pathological changes in tissues. Ultimately, it can be envisioned that bacterial peptide probes, after careful trial experiments can be clinically exploited for diagnosis of pathologic tissue changes affecting Fn strain state, or even for targeting such changes *in vivo*.

Zusammenfassung

Die extrazelluläre Matrix (EZM) spielt eine wichtige Rolle in der Gewebshomeostase und als mechanisches Stabilisationsnetzwerk der Zellen. Das extrazelluläre Protein Fibronektin (Fn) spielt eine Schlüsselrolle in der Frühentwicklung von Organismen und in der Wundheilung, aber auch in verschiedenen Krankheiten, beispielsweise in Krebs oder krankhaften fibrotischen Veränderungen. Ein Charakteristikum dieser Krankheiten ist eine erhöhte mechanische Steifigkeit des Gewebes, welche aus Veränderungen verschiedener Faktoren resultiert. Erhöhte Expression von Kollagen-I, erhöhte enzymatische Vernetzung von Proteinfasern in der EZM, sowie einen erhöhten Anteil an kontraktilen, aktivierten Fibroblasten, sogenannten Myofibroblasten. Obwohl die Veränderungen der Gewebssteifigkeit in diesen Krankheiten bekannt sind, bleibt es weiterhin unklar, wie dieses veränderte mechanische Umfeld den Verstreckungsgrad von Proteinfasern und damit die Präsentation von potentiellen Bindungsstellen auf diesen Fasern verändert oder beeinträchtigt. Aufgrund der grossen Anzahl von Bindungsstellen für Wachstumsfaktoren, Cytokine, Integrine und andere Matrixproteine innerhalb des Proteins Fibronektin und dem Vorhandensein verschiedener mechanisch aktivierbarer Bindungsstellen stellt sich die Frage, ob und inwiefern einige dieser Bindungsstellen von einem veränderten Verstreckungsgrad von Fn-Fasern im Gewebekontext verändert werden können. Für eine befriedigende Beantwortung dieser Frage fehlen jedoch wirksame Methoden und Mittel um den Verstreckungsgrad von Fn Fasern in Geweben zu bestimmen. Bisher vorgeschlagene Ansätze sind entweder nur für *in vitro* Experimente geeignet, oder der genaue Mechanismus beziehungsweise die Bindungsaffinitäten sind nicht bekannt.

Das Ziel der vorliegenden Arbeit ist es, die bakterielle Peptidsequenz FnBPA5 des Bakteriums S. *aureus,* als neues Mittel zur Messung des Verstreckungsgrades und zur spezifischen Bindung an relaxiertes Fibronektin in Gewebe und *in vivo* einzuführen und zu etablieren. Weiters werden Zusammenhänge mit funktionellen Aspekten die für diese Fn-Relaxation verantwortlich sind untersucht.

Die hier präsentierten Resultate zeigen eine präferentielle Bindung von FnBPA5 an relaxierte manuell gezogenen Fn Fasern *in vitro*, sowie eine verstärkte Peptidbindung zu relaxierten Fn-Fasern in humaner Fibroblasten Zellkultur, die mit Fn-FRET visualisiert wurden. Affinitätsmessungen zu Plasma Fibronektin und zu relaxierten Fibronektin Fasern zeigen eine hohe Affinität von FnBPA5 mit Werten der Dissoziationskonstanten im nanomolaren Bereich, vergleichbar mit der Affinität von Antikörpern. Weiters wird gezeigt, dass die Stabilität von FnBPA5 in Blutplasma adäquat für die *in vivo* Nutzung des Peptids ist. Färbungen von Tumor Gewebsschnitten zeigen, dass Bereiche von relaxiertem Fibronektin, mit starker Peptidbindung zu Fibronektin, mit der erhöhten Präsenz von Kollagen und alpha smooth muscle actin (α-SMA) exprimierenden Zellen koinzidieren. *In vivo* Experimente mit Hilfe von ^{111}In radiomarkiertem FnBPA5 in Mäusen mit Prostatakrebs (PC-3) Xenografts durchgeführt, zeigen die spezifische Aufnahme des Peptids in Tumoren und anderen Organen mit verlängerter Verweildauer in Tumoren verglichen mit anderen Organen.

Färbung von Gewebsschnitten von PC-3 Tumoren und gesunden Organen mit FnBPA5 zeigten ausschliesslich für Tumorschnitte eine spezifische Bindung von FnBPA5 mit praktisch keiner Bindung zu Gewebsschnitten der gesunden Organe. Dies legt nahe, dass Fibronektin Fasern in gesundem Gewebe stark gestreckt sind und eine Faser Relaxierung nur in Tumoren beobachtbar ist. Eine Ko-Färbung von FnBPA5 mit dem Zellkontraktilitätsmarker α-SMA zeigt weiters, dass die Bindung von FnBPA5 an Fn Fasern in Bereichen mit α-SMA exprimierenden Zellen stark erhöht ist, was auf eine Relaxierung der Fn Fasern in diesen Bereichen basierend auf einem noch unklaren Mechanismus hinweist. Weiters wurde ein Modell der Lymphknoten-Schwellung untersucht und Bindung von FnBPA5 zeigt sich nur in Lymphknoten von Mäusen, welche mit dem Lymphozytischen Choriomeningitis Virus (LCMV) infiziert wurden, nicht jedoch für Lymphknoten von Kontrollmäusen und Mäusen welche mit CpG Oligodeoxynucleotid Adjuvanten behandelt wurden. Dieses Resultat suggeriert, dass die Infektion mit LCMV und die damit einhergehende partielle Zerstörung des Fibroblasten Netzwerks im Lymphknoten, welche für diese Infektion berichtet wurde, für die Relaxierung der Fibronektin Fasern verantwortlich zeichnet. Physiologisches Anschwellen der Lymphknoten, wie es mit dem CpG Adjuvanten getestet wurde zeigt hingegen keine signifikante Relaxierung der Fibronektin Fasern innerhalb des Lymphknotens.

In einer weiteren Reihe von Experimenten wurde getestet, ob verschiedenen Glycosaminoglycane (GAGs), beispielsweise Heparin, sowie klinisch genutzte niedermolekulare Heparinderivate, als auch Hyaluronsäure und synthetisch sulfatierte Hyaluronsäure, an Fibronektin binden und ob sie dazu in der Lage sind die Fibronektin Konformation zu beeinflussen. Aufgrund der Überlappung der Bindungsstelle von Heparin und anderen GAGs an Fibronektin mit der Bindungsstelle von bakteriellen Peptiden wurde eine kompetitive Bindungsstudie mit verschiedenen GAGs und FnBPA5 durchgeführt. Diese Experimente zeigen jedoch nur geringes Potential dieser Glycosaminoglycane die Bindung von FnBPA5 an Fn Fasern zu blockieren.

Die vorliegende Arbeit führt hier, beispielhaft am Fn bindenden Peptid FnBPA5 von S. *aureus,* eine neuartige Klasse von Peptidsensoren zur Visualisierung von relaxierten Fibronektinfasern in Geweben und *in vivo* ein. Die Anwendung dieser neuen Methodik hat Potential zum besseren Verständnis der dynamischen Interaktion zwischen Matrixzusammensetzung, zellulären Kräften und mechanischem Verstreckungsgrad von Fn Fasern beizutragen. Dies ist von speziellem Interesse für Krebs oder fibrotischen Erkrankungen, in welchen das Gleichgewicht dieser Faktoren gestört ist. Die hier gezeigte Charakterisierung eines *in vivo* Tumormodells und *ex vivo* Gewebsschnitt Färbungen von Krebs- und Lymphknoten-Schwellungsmodellen weist klar darauf hin, dass das FnBPA5 Peptid als wichtiges Instrument zur Charakterisierung von pathologischen Veränderungen der EZM in Geweben dienen kann. Nach weiteren Charakterisierungsschritten kann die Entwicklung klinisch einsetzbarer bakterieller Peptide zur Diagnose von pathologischen Veränderungen von Geweben, beziehungsweise zum spezifischen Ansteuern von relaxiertem Fn *in vivo* als Vision für die Zukunft definiert werden.

Table of content

Chapter 1

Scope of the Thesis

Motivation and Significance

Malignant transformations often go along with a disorganization of the extracellular matrix (ECM) and a change in cellular contractility. Already in 1986 Dvorak and coworkers reported specific similarities between the tumor microenvironment and wounds, with striking resemblances of stromal tumor compartments to granulation tissue of wounded skin [1,2]. This analogy of tumors with non-healing wounds imply however, that specific mechanisms that govern the return to tissue homeostasis in a wound healing situation must be compromised in tumors. Continuous deposition of matrix molecules with an ultimate loss of organ function due to fibrotic lesions, is however not exclusively observed in cancer, but also in fibrotic diseases, such as idiopathic pulmonary fibrosis, or systemic sclerosis, with transforming growth factor beta being a key mediating factor, as described by Zeisberg and others [3,4]. What tumor stroma and fibrotic tissue have in common is the need for neo-vascularization, the presence of inflammatory cells, as well as an increased presence of the contractile myofibroblast phenotype, going along with aberrant deposition, as well as a changed composition and crosslinking of extracellular matrix residues [5-7]. Considering those drastic differences in tissue organization, the question arises how the changed matrix organization impacts strain state of individual protein fibers within it. This is of special importance facing the fact that one of the most abundantly present ECM protein, fibronectin (Fn) with known upregulation in both cancer and fibrosis [8,9], has several binding sites to important growth factors, namely binding sites for the latent TGF-β complex [10] and binding sites for VEGF [11], bone morphogenic protein 1 [12], as well as PDGF [13] and VEGF [14] with heparin acting as co-receptor strongly enhancing heparin interaction between growth factor and Fn. The latent TGF-β complex was reported to be activated from its inactive form via mechanical forces [15,16] and VEGF and PDGF have been found to exhibit a changed binding affinity to fibronectin depending on the presence of heparin [13,14]. Furthermore there is evidence, that the abundantly reported increase in collagen content and crosslinking [7], has a functional impact on how cells interact with fibronectin, respectively how cellular contractile forces are transmitted to Fn fibers [17,18].

The question thus arises how the overall increase in tissue rigidity in cancer and fibrotic tissues [19,20] correlates with changes in strain state of fibronectin fibers and whether this could change affinities of some of its binding ligands. As no measurement probe for fibronectin in tissue is available so far we establish in this work the use of novel peptide probes derived from bacterial fibronectin binding proteins [21,22] specifically binding to relaxed, but not to stretched Fn fibers. We demonstrate the functionality of the probe *in vitro* in a manually pulled Fn fiber assay and in cell culture in comparison to Fn-FRET, showing preferential binding to relaxed Fn fibers in both model systems. We further examined the *in vivo* biodistribution in a cancer mouse model and

could observe a specific uptake and prolonged retention of the peptide probe in tumors and ultimately utilized the FnBPA5 peptide to probe *ex vivo* tissue sections to assess differences in Fn strain between healthy and cancerous tissue. Correlative co-stainings with different markers reveal an increased binding to Fn in areas containing highly contractile, alpha smooth muscle actin expressing cells in tumor tissue, thus challenging the current dogma of a linear relationship between enhanced contractility and highly stretched matrix proteins, at least for fibronectin. Swelling of lymph nodes is presented here as a second model for fast tissue growth with known changes in tensional state of fibroblastic cells [23,24], with up to now unknown consequences for ECM fibers within, giving additional information and insight on possible fields of use for FnBPA5 as a new strain probe for Fn in different pathological tissue models.

In summary, the introduction of the FnBPA5 peptide probe has great potential to open up the doors for future research to improve diagnostics by helping to explore how alterations of tensional homeostasis affect the mechanical strain of Fn fibrils in health and disease. This could ultimately lead to a better understanding of the mechano-chemical signaling at the cell-ECM interface in different microenvironmental niches. The early detection of abnormalities in Fn strain state with the exact knowledge of its consequences on the molecular level may then ultimately lead to a more efficient targeting of respective diseases.

Specific Aims

This dissertation focuses on 3 specific aims. Firstly, the bacterial Fn binding peptide FnBPA5 is established and characterized as a novel tool to probe the tensional state of fibronectin fibers in tissue and *in vivo*. After conducting proof-of-principle experiments, this peptide probe is utilized in a second step to probe tissue samples to investigate changes in Fn fiber strain in different systems (tumor versus healthy tissue and swollen lymph nodes of virus infected or adjuvant treated mice versus naïve lymph nodes). The binding of different glycosaminoglycans (GAGs) to Fn, the consequent change of fibronectin's conformation assessed via Fn-FRET, and the investigation of a possible competition of GAGs with binding of FnBPA5 to manually pulled Fn fibers and cell culture matrices is furthermore elaborated in the third aim of this thesis.

Specific aim 1 (Chapter 3)

It remains unclear how well documented mechanical changes on the tissue level, observed in cancer and other pathological processes [7,23-25], influence the strain state of protein fibers within the ECM and thus potentially also the functional display of binding sites on these fibers. Therefore we strived to exploit here the strain sensitive binding properties of the S. *aureus* derived Fn binding peptide FnBPA5 [21,22] to establish a novel probe to measure changes in Fn fiber strain in tumor tissue and *in vivo*.

To address this unmet need, we used a combination of methods ranging from the manually pulled Fn fiber assay [26] to the use of a fluorescence resonance energy transfer (FRET) probe for Fn in cell culture [27,28] to assess and characterize the binding of fluorescently labeled FnBPA5 peptide. Tumor tissue sections from PC-3 tumor xenograft mice were then probed using fluorescently labeled FnBPA5, and radiolabeled ^{111}In-FnBPA5 was used for *in vivo* single photon emission computed tomography (SPECT) and biodistribution studies.

We confirmed previously predicted strain sensitive binding behavior of FnBPA5 to Fn from steered molecular dynamics computational simulations [29] and could show preferential binding of FnBPA5 to mechanically relaxed Fn fibers, if compared to stretched ones using a manually pulled Fn fiber assay [26]. Before testing this new probe *in vivo* we assessed mechanosensitive binding in cell culture in comparison to previously established Fn-FRET probe [27] and could show a correlation of higher FnBPA5 binding to relaxed Fn fibers, as visualized via Fn-FRET. Binding affinity to both plasma and fibrillar Fn was measured, with affinities in the nanomolar range, in line with previous affinity measurements of the same peptide to proteolytic Fn fragments in solution [30]. *Ex vivo* tissue stainings show specific heterogeneous binding pattern of FnBPA5 to Fn indicating that both stretched and highly relaxed strain states of Fn fibers coexist in tumor tissue. Increased presence of collagen and alpha-SMA expressing cells were observed to be supportive factors for Fn relaxation and thus FnBPA5 binding in tumor tissue sections. *In vivo* biodistribution of radiolabeled FnBPA5 derivative in a PC-3 tumor xenograft mouse model showed a specific accumulation in many organs, predominantly in liver, spleen and tumor. High kidney uptake was shown to be unspecific as scrambled negative control showed similar kidney uptake with no specific uptake

in any other organs. Most interestingly, the biodistribution reveals a higher retention time of FnBPA5 in tumors compared to other organs, indicating high affinity binding of FnBPA5 to tumor tissue *in vivo*.

Arnoldini, S., Moscaroli, A., Chabria, M., Hilbert, M., Hertig, S., Schibli, R., Behe, M., Vogel, V., "Novel peptide probes to assess the tensional state of fibronectin fibers in cancer", accepted, Nature Communications (2017)

Specific aim 2 (Chapter 4)

As nothing is known on the strain state of Fn fibers in tissue and organs, the second aim of this thesis is focused on the application of the newly established fibronectin strain probe, based on the peptide FnBPA5, for the characterization of Fn fiber strains in histological tissue sections. A further objective of this section is to establish first correlations between changed Fn fiber strain in different settings and factors such as increased number of highly contractile cells, reported to be important in cancer progression [7,31].

Tissue sections from adult mouse tissue from a prostate cancer (PC-3) tumor xenograft model, was used and differences between tumor tissue sections and tissue sections from healthy organs (kidney, liver, lung, heart) were assessed. As changes in Fn fiber strain are likely not restricted to cancer, but also occur in other pathological processes, we strived to establish a second model system to assess Fn fiber strain in tissue. The process of lymph node swelling upon immunological challenge is known for a long time in medicine, however only recently researchers presented mechanistic insight how lymph nodes can withstand the drastic net influx of cells upon lymph node swelling without rupturing, proposing an externally triggered downregulation of contractility of fibroblastic reticular cells (FRCs), the lymph node's fibroblasts [23,24,32]. Based on their findings we asked, using two different models of lymph node swelling, whether we could see an effect on Fn fiber strain compared to the untreated control. Popliteal lymph node tissue sections from naïve mice and from mice treated with Lymphocytic Choriomeningitis Virus (LCMV) and CpG adjuvant were therefore probed with FnBPA5 to determine potential changes in Fn fiber strain upon lymph node swelling between different treatments.

No significant binding of FnBPA5 to tissue sections from liver, kidney, heart, and lung could be observed, indicating a highly stretched state of Fn fibers in these healthy tissue sections, whereas relaxed Fn fibers showing high FnBPA5 binding could only be observed in tumor tissue. To further clarify the question whether binding of FnBPA5 is indeed triggered by strain-dependent changes within tumor tissue, we stained tissue for alpha smooth muscle actin, a marker for highly contractile myofibroblasts often observed in tumor stroma [33,34]. Strikingly, in tumor tissue sections, we could find a clear correlation of increased FnBPA5 binding to fibronectin in areas containing α-SMA expressing cells, whereas barely any FnBPA5 bound to Fn in areas lacking myofibroblasts. α-SMA expressing cells were also observed in lung, however no binding of FnBPA5 to lung tissue was observed. Interestingly, probing the lymph node swelling model upon treatment with Lymphocytic Choriomeningitis Virus (LCMV) [35] or CpG oligodeoxynucleotide adjuvant [36], revealed no change in Fn fiber strain for swollen lymph nodes from adjuvant treated mice, albeit lymph nodes were clearly enlarged in size and cellularity. Only for

lymph nodes derived from mice treated with lymphocytic choriomeningitis virus (LCMV) an increased binding of FnBPA5 and thus a relaxation of Fn fibers could be observed, with previously reported destruction of the lymph node fibroblast network upon LCMV virus infection [35] as potential underlying factor. Untreated control did not show any binding of FnBPA5 to Fn within lymph nodes. This indicates that LCMV, known to attack and compromise the reticular fibroblasts [35], thus interfering with the mechanical continuum of the lymph node, leads to a significant change in Fn fiber strain.

Arnoldini, S., Jaramillo, D., Moscaroli, A., Oxenius, A., Behe, M., Vogel, V., "Strain sensitive peptides for the characterization of fibronectin fiber strain in cancer and lymph node swelling", Manuscript in preparation, submission planned for late 2017

Specific aim 3 (Chapter 5)

While heparin is known to be able to change fibronectin conformation for quite some time [37,38], it remains open, to what extent other, more abundantly available heparan sulfates are capable to alter Fn in a similar way. Given the fact, that heparin and several bacterial Fn binding peptides bind to the same domains at the N-terminus of Fn, we further asked whether natural hyaluronic acid (HA), synthetically sulfated hyaluronic acid (sHA), heparin and clinically used low molecular weight heparin derivatives compete with FnBPA5 binding to Fn. This question is based on previous findings reporting blocking of S. *aureus* and S. *epidermidis* adhesion to Fn coated surfaces in the presence of heparin [39,40] and a more recent report of partial blocking of S. *dysgalactiae* Fn binding peptide B3C to manually pulled Fn fibers [41].

To elucidate this, different heparan sulfate proteoglycans were tested on human bone marrow stromal cell (hBMSC) fibronectin matrices and Fn conformation was assessed using Fn-FRET. Additionally, potential competitive binding between heparin, a synthetically sulfated hyaluronic acid and the peptide FnBPA5 to Fn was studied in manually pulled Fn fiber assays.

As synthetically sulfated hyaluronic acid (sHA) was, unlike its unsulfated natural derivative, reported in a previous study to change Fn conformation similarly as heparin [42], we first posed the question whether this effect is solely dependent on the degree of sulfation of the utilized GAG compounds. The use of naturally sulfated GAG chondroitin sulfate (CS) in comparison with sHA and an untreated control disproved this hypothesis, as CS was not able to significantly change Fn conformation, whereas sHA treated sample showed a significant decrease in Fn-FRET ratio compared to the untreated control. As degree of sulfation alone is thus not the driving force of interaction with Fn, the question arises, whether treatment of hBMSC with heparin and sHA, leading to a decrease in Fn-FRET both rely on the same mechanism. Treatment with the cell contractility inhibitor blebbistatin revealed that, while heparin treatment still shows a significant decrease in Fn-FRET, the effect of sHA treatment on Fn-FRET ratio is abrogated. These results give first evidence, that changes of Fn-FRET ratio upon treatment with heparin or sHA likely depend on different mechanisms.

We further found that, as already previously indicated, natural unsulfated HA did not significantly bind to manually pulled Fn fibers, whereas sHA shows specific binding with no preference towards stretched or relaxed strain state. Interestingly, labeled heparin exhibited preferential binding towards stretched Fn fibers compared to relaxed ones. A competitive binding assay between sHA and Hep to relaxed Fn fibers reveals a higher potential of heparin to block sHA binding as vice versa. Binding of FnBPA5 to relaxed Fn fibers preincubated with sHA and HA did not lead to a significant reduction, if compared to control, indicating that sHA is not primarily binding to the HepI domain of Fn. This gets further supported by the evaluation of sHA binding before and after incubation of FnBPA5 which does not show a significant reduction in sHA binding compared to the negative control measured 2 hours after incubation. It was furthermore found that heparin and clinically used low molecular weight heparin derivatives are not capable of sufficiently blocking FnBPA5 binding from Fn fibers.

Arnoldini, S., Vogel, S., Möller, S., Schnabelrauch, M., Hempel, U., Vogel, V., "Influence of glycosaminoglycan sulfation on Fn binding and binding competition with FnBPA5", Manuscript in preparation

Additional scientific contributions

Vogel, S., **Arnoldini, S.**, Möller, S., Schnabelrauch, M., & Hempel, U. Sulfated hyaluronan alters fibronectin matrix assembly and promotes osteogenic differentiation of human bone marrow stromal cells. Scientific Reports, 6 (2016) 36418. http://doi.org/10.1038/srep36418
(manuscript not included in this thesis)

References

[1] H.F. Dvorak, Tumors: wounds that do not heal: similarities between tumor stroma generation and wound healing, N Engl J Med. 315 (1986) 1650–1659.

[2] M. Schäfer, S. Werner, Cancer as an overhealing wound: an old hypothesis revisited, Nat Rev Mol Cell Biol. 9 (2008) 628–638. doi:10.1038/nrm2455.

[3] M. Zeisberg, R. Kalluri, Cellular Mechanisms of Tissue Fibrosis. 1. Common and organ-specific mechanisms associated with tissue fibrosis, AJP: Cell Physiology. 304 (2013) C216–C225. doi:10.1152/ajpcell.00328.2012.

[4] B. Piersma, R.A. Bank, M. Boersema, Signaling in Fibrosis: TGF-β, WNT, and YAP/TAZ Converge, Front. Med. 2 (2015) 1138. doi:10.1101/gad.192856.112.

[5] F.L. Miles, R.A. Sikes, Insidious changes in stromal matrix fuel cancer progression, Mol. Cancer Res. 12 (2014) 297–312. doi:10.1158/1541-7786.MCR-13-0535.

[6] H.E. Barker, T.R. Cox, J.T. Erler, The rationale for targeting the LOX family in cancer, Nat Rev Cancer. 12 (2012) 540–552. doi:10.1038/nrc3319.

[7] R. Kalluri, The biology and function of fibroblasts in cancer, Nat Rev Cancer. 16 (2016) 582–598. doi:doi:10.1038/nrc.2016.73.

[8] M. Allen, J. Louise Jones, Jekyll and Hyde: the role of the microenvironment on the progression of cancer, J. Pathol. 223 (2010) 163–177. doi:10.1002/path.2803.

[9] S. Bhattacharyya, Z. Tamaki, W. Wang, M. Hinchcliff, P. Hoover, S. Getsios, et al., FibronectinEDA promotes chronic cutaneous fibrosis through Toll-like receptor signaling, Sci Transl Med. 6 (2014) 232ra50–232ra50. doi:10.1126/scitranslmed.3008264.

[10] M.A. Travis, D. Sheppard, TGF-β Activation and Function in Immunity, Annu. Rev. Immunol. 32 (2014) 51–82. doi:10.1146/annurev-immunol-032713-120257.

[11] E.S. Wijelath, S. Rahman, M. Namekata, J. Murray, T. Nishimura, Z. Mostafavi-Pour, et al., Heparin-II Domain of Fibronectin Is a Vascular Endothelial Growth Factor-Binding Domain: Enhancement of VEGF Biological Activity by a Singular Growth Factor/Matrix Protein Synergism, Circ. Res. 99 (2006) 853–860. doi:10.1161/01.RES.0000246849.17887.66.

[12] G. Huang, Y. Zhang, B. Kim, G. Ge, D.S. Annis, D.F. Mosher, et al., Fibronectin Binds and Enhances the Activity of Bone Morphogenetic Protein 1, Journal of Biological Chemistry. 284 (2009) 25879–25888. doi:10.1074/jbc.M109.024125.

[13] E.M. Smith, M. Mitsi, M.A. Nugent, K. Symes, PDGF-A interactions with fibronectin reveal a critical role for heparan sulfate in directed cell migration during Xenopus gastrulation, Proc. Natl. Acad. Sci. U.S.a. 106 (2009) 21683–21688. doi:10.1006/dbio.1996.0174.

[14] M. Mitsi, K. Forsten-Williams, M. Gopalakrishnan, M.A. Nugent, A catalytic role of heparin within the extracellular matrix, J. Biol. Chem. 283 (2008) 34796–34807. doi:10.1074/jbc.M806692200.

[15] P.-J. Wipff, D.B. Rifkin, J.-J. Meister, B. Hinz, Myofibroblast contraction activates latent TGF-beta1 from the extracellular matrix, J. Cell Biol. 179 (2007) 1311–1323. doi:10.1083/jcb.200704042.

[16] B. Hinz, The extracellular matrix and transforming growth factor-β1: Tale of a strained relationship, Matrix Biol. 47 (2015) 54–65. doi:10.1016/j.matbio.2015.05.006.

[17] J.-F. Groulx, D. Gagné, Y.D. Benoit, D. Martel, N. Basora, J.-F. Beaulieu, Collagen VI is a basement membrane component that regulates epithelial cell-fibronectin interactions, Matrix Biol. 30 (2011) 195–206. doi:10.1016/j.matbio.2011.03.002.

[18] K.E. Kubow, R. Vukmirovic, L. Zhe, E. Klotzsch, M.L. Smith, D. Gourdon, et al., Mechanical forces regulate the interactions of fibronectin and collagen I in extracellular matrix, Nature Communications. 6 (2015) 1–11. doi:10.1038/ncomms9026.

[19] C.C. DuFort, M.J. Paszek, V.M. Weaver, Balancing forces: architectural control of

mechanotransduction, Nat Rev Mol Cell Biol. 12 (2011) 308–319. doi:10.1038/nrm3112.

[20] F. Kai, H. Laklai, V.M. Weaver, Force Matters: Biomechanical Regulation of Cell Invasion and Migration in Disease, Trends in Cell Biology. (2016) 1–12. doi:10.1016/j.tcb.2016.03.007.

[21] U. Schwarz-Linek, J.M. Werner, A.R. Pickford, S. Gurusiddappa, J.H. Kim, E.S. Pilka, et al., Pathogenic bacteria attach to human fibronectin through a tandem beta-zipper, Nature. 423 (2003) 177–181. doi:10.1038/nature01589.

[22] B. Henderson, S. Nair, J. Pallas, M.A. Williams, Fibronectin: a multidomain host adhesin targeted by bacterial fibronectin-binding proteins, FEMS Microbiology Reviews. 35 (2010) 147–200. doi:10.1111/j.1574-6976.2010.00243.x.

[23] J.L. Astarita, V. Cremasco, J. Fu, M.C. Darnell, J.R. Peck, J.M. Nieves-Bonilla, et al., The CLEC-2–podoplanin axis controls the contractility of fibroblastic reticular cells and lymph node microarchitecture, Nat Immunol. 16 (2014) 75–84. doi:10.1038/ni.3035.

[24] S.E. Acton, A.J. Farrugia, J.L. Astarita, D. Mourão-Sá, R.P. Jenkins, E. Nye, et al., Dendritic cells control fibroblastic reticular network tension and lymph node expansion, Nature. 514 (2015) 498–502. doi:10.1038/nature13814.

[25] M.J. Paszek, N. Zahir, K.R. Johnson, J.N. Lakins, G.I. Rozenberg, A. Gefen, et al., Tensional homeostasis and the malignant phenotype, Cancer Cell. 8 (2005) 241–254. doi:10.1016/j.ccr.2005.08.010.

[26] W.C. Little, M.L. Smith, U. Ebneter, V. Vogel, Assay to mechanically tune and optically probe fibrillar fibronectin conformations from fully relaxed to breakage, Matrix Biology. 27 (2008) 451–461. doi:10.1016/j.matbio.2008.02.003.

[27] G. Baneyx, L. Baugh, V. Vogel, Coexisting conformations of fibronectin in cell culture imaged using fluorescence resonance energy transfer, Proc. Natl. Acad. Sci. U.S.a. 98 (2001) 14464–14468. doi:10.1073/pnas.251422998.

[28] M.L. Smith, D. Gourdon, W.C. Little, K.E. Kubow, R.A. Eguiluz, S. Luna-Morris, et al., Force-Induced Unfolding of Fibronectin in the Extracellular Matrix of Living Cells, Plos Biol. 5 (2007) e268. doi:10.1371/journal.pbio.0050268.sv001.

[29] S. Hertig, M. Chabria, V. Vogel, Engineering mechanosensitive multivalent receptor-ligand interactions: why the nanolinker regions of bacterial adhesins matter, Nano Lett. 12 (2012) 5162–5168. doi:10.1021/nl302153h.

[30] N.A.G. Meenan, L. Visai, V. Valtulina, U. Schwarz-Linek, N.C. Norris, S. Gurusiddappa, et al., The tandem beta-zipper model defines high affinity fibronectin-binding repeats within Staphylococcus aureus FnBPA, J. Biol. Chem. 282 (2007) 25893–25902. doi:10.1074/jbc.M703063200.

[31] F. Spill, D.S. Reynolds, R.D. Kamm, M.H. Zaman, Impact of the physical microenvironment on tumor progression and metastasis, Current Opinion in Biotechnology. 40 (2016) 41–48. doi:10.1016/j.copbio.2016.02.007.

[32] A.L. Fletcher, S.E. Acton, K. Knoblich, Lymph node fibroblastic reticular cells in health and disease, Nat Rev Immunol. 15 (2015) 350–361. doi:10.1038/nri3846.

[33] R. Kalluri, M. Zeisberg, Fibroblasts in cancer, Nat Rev Cancer. 6 (2006) 392–401. doi:10.1038/nrc1877.

[34] E.E. Torr, C.R. Ngam, K. Bernau, B. Tomasini-Johansson, B. Acton, N. Sandbo, Myofibroblasts exhibit enhanced fibronectin assembly that is intrinsic to their contractile phenotype, Journal of Biological Chemistry. 290 (2015) 6951–6961. doi:10.1074/jbc.M114.606186.

[35] E. Scandella, B. Bolinger, E. Lattmann, S. Miller, S. Favre, D.R. Littman, et al., Restoration of lymphoid organ integrity through the interaction of lymphoid tissue-inducer cells with stroma of the T cell zone, Nat Immunol. 9 (2008) 667–675. doi:10.1038/ni.1605.

[36] R.L. Coffman, A. Sher, R.A. Seder, Vaccine Adjuvants: Putting Innate Immunity to Work, Immunity. 33 (2010) 492–503. doi:10.1016/j.immuni.2010.10.002.

[37] M. Mitsi, Z. Hong, C.E. Costello, M.A. Nugent, Heparin-Mediated Conformational Changes in Fibronectin Expose Vascular Endothelial Growth Factor Binding Sites, Biochemistry. 45 (2006) 10319–10328. doi:10.1021/bi060974p.

[38] B. Li, Z. Lin, M. Mitsi, Y. Zhang, V. Vogel, Heparin-induced conformational changes of fibronectin within the extracellular matrix promote hMSC osteogenic differentiation, Biomater. Sci. (2014). doi:10.1039/C3BM60326A.

[39] P. Vaudaux, T. Avramoglou, D. Letourneur, D.P. Lew, J. Jozefonvicz, Inhibition by heparin and derivatized dextrans of Staphylococcus aureus adhesion to fibronectin-coated biomaterials, Journal of Biomaterials Science, Polymer Edition. 4 (1993) 89–97. doi:10.1163/156856292X00321.

[40] P. Francois, D. Letourneur, D.P. Lew, J. Jozefonwicz, P. Vaudaux, Inhibition by heparin and derivatized dextrans of Staphylococcus epidermidis adhesion to in vitro fibronectin-coated or explanted polymer surfaces, Journal of Biomaterials Science, Polymer Edition. 10 (1999) 1207–1221. doi:10.1163/156856299X00027.

[41] M. Chabria, S. Hertig, M.L. Smith, V. Vogel, Stretching fibronectin fibres disrupts binding of bacterial adhesins by physically destroying an epitope, Nature Communications. 1 (2010) 135–9. doi:10.1038/ncomms1135.

[42] S. Vogel, S. Arnoldini, S. Möller, M. Schnabelrauch, U. Hempel, Sulfated hyaluronan alters fibronectin matrix assembly and promotes osteogenic differentiation of human bone marrow stromal cells, Sci. Rep. (2016) 1–13. doi:10.1038/srep36418.

Chapter 2

General introduction

The extracellular matrix (ECM)

Cells organize themselves into different functional tissues, which then together build up the organism. Different kinds of tissue are differently organized being comprised of cells with unique functions embedded in tissue specific niches. Such niches play major roles in tissue homeostasis and tissue function via the interplay of cellular components and the extracellular protein network, commonly referred to as the extracellular matrix (ECM). The ECM serves versatile functions and is composed of several hundred different proteins, glycoproteins and proteoglycans [1,2]. The ECM can be roughly subdivided into two different forms of appearance: first, the basal lamina, a 40-120 nm thick sheet of matrix molecules, which tightly separates the epithelium or endothelium from the surrounding connective tissue. It mainly consists of proteins of the laminin family, collagen IV, nidogen and perlecan. Its main functions are to act as a barrier for unwanted cell migration, to separate different functional tissue compartments and to mechanically support and link different tissues. The second form of ECM appearance is the more abundantly found connective tissue matrix. It lacks the barrier function of the basal lamina but shares the function of giving structural and mechanical support to cells. The connective tissue matrix is excreted by tissue specific fibroblasts and has a huge variability depending on its functional role in the organism [3]. Its most abundant components are collagens, fibronectin, elastin and several glycosaminoglycans and proteoglycans. One major role of this form of the ECM is to provide attachment points and thus mechanical support for cells. The features of the ECM go however far beyond this function as a passive cell anchoring scaffold as cells actively interact with the ECM. Cells can apply mechanical forces to ECM proteins [4,5], they can furthermore sense mechanical stiffness or gradients in matrix composition within the ECM and subsequently react to these changes by translating them into biochemical signals, resulting in a differential expression pattern of matrix molecules, thus generating active feedback loops [5-7]. These so called ECM-cell signaling pathways can influence several cellular properties, as cells show anchorage dependent growth, proliferation and survival [8,9] and imbalances within these pathways have been observed to be hallmarks for different pathologies [2,7,10]. Cells can assemble ECM with a huge variety, therefore the regulation of its secretion, degradation as well as the tight control of its composition and the degree of crosslinking between its components are crucial for normal tissue homeostasis [11-13]. Another key feature of the extracellular matrix network is its role as growth factor reservoir: Several growth factors get immobilized in the ECM therefore reducing diffusive range and accessibility of those molecules [14]. Growth factor activation can then be triggered by different factors, such as enzymatic matrix degradation mediated by MMPs [2,15], or possibly also by mechanical forces exerted by cells, capable of unfolding the latent complex and thus activate transforming growth factor-β (TGF-β) [16,17]. These changes in matrix organization and mechanical forces, can thus ultimately lead to altered cell signaling, as depicted in figure 2.1. The complex interplay between cellular forces and ECM compliance was proposed to be controlled via positive and negative feedback loops, reacting to changed ECM stiffness or changed mechanical

forces with an alternative gene expression program [7,12,13]. In several pathologies accompanied by an abnormal accumulation of ECM molecules, such as cancer or other fibrotic diseases, these normally tightly regulated feedback loops are impaired leading to an imbalance of assembly and degradation of matrix molecules and thus to a shift of the tensional equilibrium (Figure 2.1) [7,12,13]. It remains an open question, which factor stands at the beginning of these events and drives malignant transformations. It however is clear now, that increased tissue stiffness is not only a by-product of tumorigenesis, but actively promoting this process [13].

Signaling molecules linking cells and the ECM: the function of Integrins

Cells attach to the ECM via a family of heterodimeric proteins, called integrins, which span the cell's plasma membrane, connect at the extracellular side with ECM proteins and are linked to the actin cytoskeleton inside the cell [9]. Integrins are composed of one α and one β subunit and combinations of 18 different α and 8 β subunits lead to 24 different types of integrin heterodimers [9]. Different integrin subtypes have different ligands and are of key importance during embryogenesis and development. Mutations in these proteins lead to pathologic phenotypes or are embryonically lethal, thus underlining the importance of integrin-matrix connections [18,19]. Integrins also play a major role in the force transduction from the cell's acto-myosin contractile machinery to the extracellular matrix. In that manner forces generated within the actin cytoskeleton can be transferred via integrins to all integrin ligands, such as fibronectin and collagens and thus induce mechanical strain on those molecules.

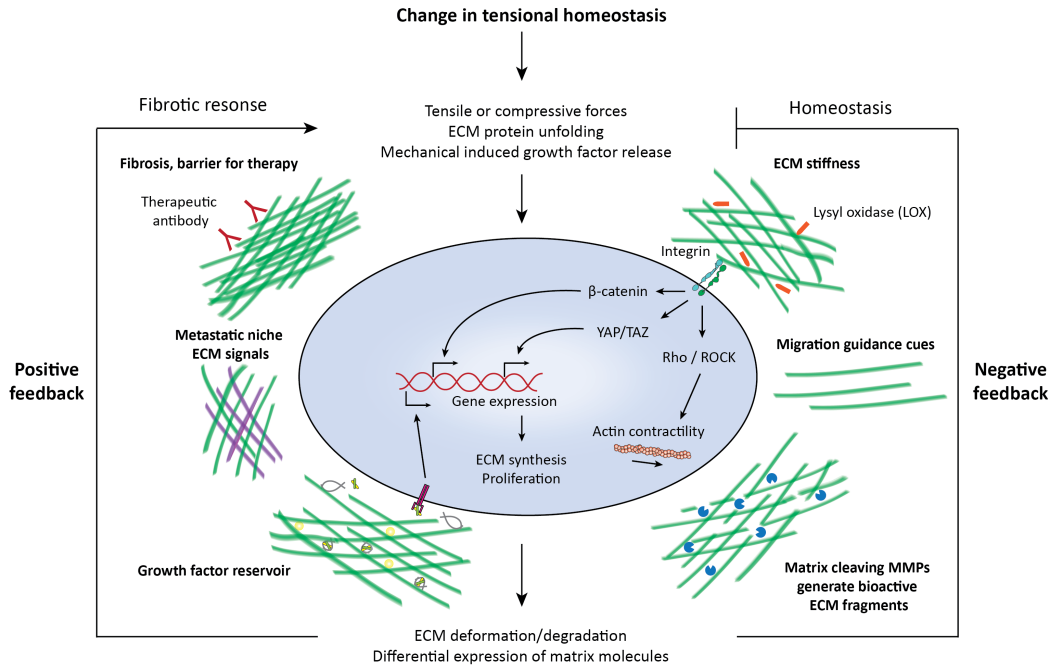

Figure 2.1: The ECM serves different functions: It acts as a mechanical anchorage for cells, as a migration guidance or barrier, as a signal reservoir by immobilizing growth factors or cytokines. Cells interact with the ECM via application of mechanical forces, they can sense ECM stiffness and may change their behavior accordingly [2]. Cell ECM interactions are tightly controlled by positive and negative feedback loops [7]. In pathologies, such as fibrosis these feedback loops are often compromised leading to a constantly active positive feedback loop resulting in an aberrant matrix deposition, ultimately leading to loss of tissue or organ function. Figure adapted from [2] and [7].

A key player within the ECM: Fibronectin

A key ligand of integrins is the ECM protein fibronectin (Fn). Fn is a homodimeric, 440 kDa extracellular glycoprotein. It has a modular structure consisting of three different types of modules (FnI, FnII, FnIII). Its two monomers are linked together near the C-terminus via a pair of disulfide bonds. Fn has multiple binding sites for integrins: the RGD sequence binding a large variety of integrins (e.g: $\alpha_5\beta_1$, $\alpha_v\beta_3$, and other α_v integrins) and the IDAPS sequence binding integrin $\alpha_4\beta_1$ [20]. Apart from the integrin binding sites Fn was also shown to bind different growth factors, such as hepatocyte growth factor (HGF) [21], vascular endothelial growth factor (VEGF) [1,22], fibroblast growth factor (FGF), platelet derived growth factor (PDGF), latent transforming growth factor-β (TGF-β) complex [23], as well as glycosaminoglycans, such as heparin, opening up cryptic binding sites within Fn, thus increasing growth factor binding [22]. Fn is especially important for ECM structure and integrity as it binds to many other ECM proteins including collagens, fibrin, syndecan-4 or tenascin [24], schematically shown in figure 2.2. Different isoforms of Fn exist in the human body: plasma fibronectin (pFn), is a soluble component of blood plasma (at a concentration of approximately 200-300 µg/mL [25]), primarily synthetized by hepatocytes in the liver [26] and cellular fibronectin (cFn), synthesized by fibroblasts containing additional extra domains, not present in plasma Fn [27,28]. The assembly of fibronectin into fibrillar structures is a mechanically induced process, involving cellular forces that lead to a partial unfolding of Fn dimers [26]. Application of cellular forces to Fn is integrin mediated and blocking antibodies against Fn binding integrins were shown to prevent Fn fibrillogenesis [29]. Fibronectin's self-interaction site at $FnI_{1\text{-}5}$, is known to be crucial for fibrillogenesis as Fn

lacking this site is unable to be assembled into fibers. Indeed, a recent study using sub-diffraction fluorescence microscopy revealed a periodic organization of multiple Fn dimers into higher order structures via interaction of FnI_{1-5} and $FnIII_{1-5}$ modules [30]. Fibronectin is required for normal embryonic development [31] and represents a key player in wound healing, as it is the first actively assembled matrix component remodeling the previously assembled provisional fibrin matrix in a wound site [32]. Blood platelets, fibrin and plasma fibronectin build the first provisional matrix before at a later time point myofibroblasts and endothelial cells invade the wound and start to secrete cellular fibronectin, a process governed by cytokines, namely transforming growth factor β (TGF-β) and connective tissue growth factor. This cell invasion was shown to be fibronectin dependent [33]. The newly built fibrillar fibronectin matrix then stimulates deposition of collagens, resulting in wound contraction [32].

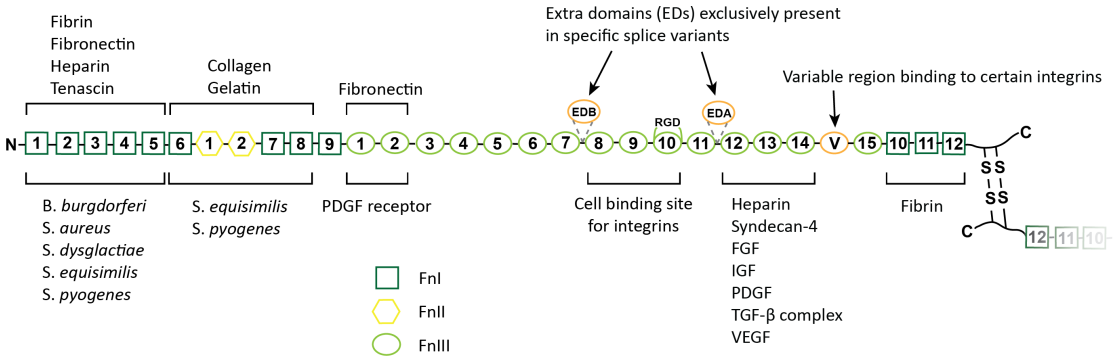

Figure 2.2: Modular structure of a fibronectin monomer showing interaction sites for self-interactions, binding sites for other matrix proteins, RGD peptide sequence and other integrin cell binding sites, attachment sites of bacteria, as well as interaction site of many growth factors and the location of extra domains and disulfide connection to the second monomer.

The role of the extracellular matrix in cancer

A tumor consists of cancer cells being embedded in tumor stroma, which is composed of cancer associated fibroblasts and matrix molecules. Alterations in the ECM composition, crosslinking and especially in cell-matrix interactions have been shown to be important hallmarks of cancer [14]. Cancer associated fibroblast are responsible for tissue stiffening as they have a higher collagen secretion and turnover by matrix metalloproteinases (MMPs) [13,34-36]. Cancerous tissue exhibits an elevated mechanical stiffness compared to healthy tissue and shows altered tissue architecture and growth governed by cytoskeletal tension, boosting the assembly of integrin clusters and focal adhesions, as well as growth factor dependent activation of downstream cell signaling [12,13,17,37,38]. However, apart from changes in matrix composition, such as for instance also the increased presence of tenascin-C [39,40], drastic changes in crosslinking of matrix fibers, especially collagens have been reported to be of crucial importance in preparing the ground for a malignant tissue transformation [13,41]: the collagen crosslinking enzymes of the lysyl oxidase (LOX) family have indeed been shown to be upregulated in several different cancer types [11] and are responsible for crosslinking of collagen fibers and hence leading to an overall stiffening of the respective tissue [41]. Such tissue stiffening has recently been reported to be a driver for epithelial-mesenchymal transition (EMT) and tumor metastasis [12,42-44]. However, despite increasing knowledge on changes in tissue rigidity and matrix crosslinking, still very little is known on

how these changes impact the strain state of individual matrix fibers in these tissues and whether a changed strain state of matrix fibers can lead to a functional display or a destruction of binding sites within the matrix, with potential consequences for individual cell signaling events or cell-matrix interactions.

Tumor tissues exhibit a considerable increase in matrix density as well as a poorly organized vasculature, caused by increased expression of matrix proteins and potentially also by incorporation of Fn and other proteins from blood plasma [45]. This crowded environment leads to a highly heterogeneous distribution of nutrients and oxygen, consequently also resulting in an uneven distribution of a potential therapeutic agent upon intravenous administration (Fig. 2.1). As the drug distribution within the tumor is diffusion limited, the key variables affecting it are tissue density, inhomogeneous vascular architecture as well as the hydrodynamic radius of the respective therapeutic agent [46].

Increased presence of fibronectin in tumors has been reported, especially of its splice variants containing extra domains EDA and EDB, also referred to as cellular or oncofetal fibronectin. Increased presence of fibronectin in breast cancer, but also in several other cancer types, have been linked with poor clinical outcome as it was shown that interaction of epithelial cells with Fn stimulates the epithelial-mesenchymal transition (EMT), thus fueling cancer metastasis [47,48]. The question how increased presence of Fn is promoting metastasis and whether this is due to specific splice variants, due to changed Fn fibrillogenesis or mechanical strain on Fn fibers, still remains open.

The role of the extracellular matrix in fibrosis

In tissue fibrosis, an excessive accumulation of matrix proteins compromises physiological organ function. Fibrotic tissue shows striking similarities with tumor stroma and exhibits a likewise upregulation of collagen I expression [10,49] leading to an overall stiffening of the tissue and an increase in cellular acto-myosin contractility induced by a myofibroblastic phenotype of the tissue-residing fibroblasts. Transforming growth factor-β (TGF-β) represents a key mediator of fibrosis and is immobilized in an inactive latency complex within the ECM. The higher cellular tension forces in fibrosis lead to an increased release of TGF-β from its latency complex enabling it to bind to the TGF-β receptor and can thus lead to downstream signaling [17]. Fibronectin is long known to be a key protein being upregulated by TGF-β signaling during fibrosis [50,51], but current therapeutic approaches in fibrosis treatment mainly focus on inhibition of TGF-β or its receptors, collagen crosslinking or inhibition of other pathways involved in fibrosis, such as Wnt, Notch or Hedgehog signaling [52,53]. Therefore, only little is known about the role of fibronectin in fibrosis and whether its increased presence and possible altered mechanical strain state has a functional role influencing the course of the disease.

Assessing mechanical aspects of the ECM

It is known that the ECM plays a major role in normal tissue homeostasis, as well as in cancer and fibrosis. However, the exact mechanisms how matrix excretion, crosslinking and turnover are controlled or to what extent they can get out of control is up to now only poorly understood. For a better understanding of these processes, several approaches have been made to elucidate, how cells apply forces to the ECM and how these forces get transmitted within the ECM. Cells can sense local forces or ECM protein gradients and translate this information into biochemical signals, a process called mechanotransduction [6]. Most notably, mesenchymal stem cells have been reported to differentiate into different lineages, dependent on certain geometrical cues, such as confined cell spreading area [54,55], substrate stiffness or ligand density effects [56,57]. To measure forces involved in mechanosensing, different approaches have been taken: traction force microscopy measuring cell-force induced bead displacement in gels [58,59], micropillar assays measuring force-induced deflection of pillars [60], atomic force microscopy probing tissue stiffness via indentation or protein unfolding (AFM) [61] or fluorescence resonance energy transfer (FRET) probes [62,63]. FRET uses the effect of non-radiative transfer of excitation energy between a donor and acceptor pair of fluorophores, with donor emission spectrum overlapping with excitation spectrum of acceptor fluorophore [64]. Fluorophore pairs fulfilling this requirement are commonly referred to as FRET pairs. Energy transfer can only occur in case of close spatial proximity (<10 nm distance) of these two fluorophores [64]. It thus requires, that proteins of interest are fluorescently labeled, either through genetic modification or chemical coupling of a FRET fluorophore pair. The development of a FRET probe for fibronectin made it possible to discriminate between compact and more extended conformations of the fibronectin molecule *in vitro* and in cell culture [65,66]. To achieve this, fibronectin was double labeled at amines and cysteines with a pair of fluorophores (Alexa 488 Donor and Alexa 546 Acceptor, respectively) that are able to transfer excitation energy if they are in close spatial proximity. Double-labeled Fn is then exogenously added to the culture medium of cells, which incorporate it into their Fn matrix. This principle has been used in several studies [66-69] and it has thus been shown that mechanical forces can extend Fn and it was proposed that forces can even partially unfold FnIII domains leading to a decrease in FRET ratio also being able to open up cryptic motifs in those modules [66], and to destroy binding sites on the Fn molecule [70]. The Fn-FRET probe however has certain limitations, namely batch-to-batch differences and the necessity of incorporating double-labeled fibronectin into the ECM, which is not possible in fixed samples or in histological tissue sections. These limitations disqualify Fn-FRET as a mechanical sensor for Fn in tissue in a clinical context, because patient samples or biopsies are not amenable to those prerequisites for FRET analysis.

To circumvent those drawbacks of the Fn-FRET probe an attempt has already been done to utilize a high throughput phage-based system to test peptide candidates as mechanical probes for Fn [71]. A phage 6-mer peptide library was screened for candidates that exhibit enhanced binding to stretched, respectively relaxed manually pulled Fn fibers. Candidates from screening were then, without knowledge of binding epitope on Fn, amplified and tested in Fn fibers, different cell-grown Fn matrices treated with blebbistatin or TGF-β, as well as in *ex vivo* tissue sections. This study however gives only little mechanistic insight into the exact location and mechanism of binding, and the respective affinities of these phage based peptides are not known. Furthermore,

phage-peptide complexes as screened in this study have a high molecular weight, which significantly reduces their tissue penetration properties. In another study a monoclonal antibody against fibronectin, binding to an epitope at amino acid residues 526-675 between modules FnI_9 and $FnIII_1$, was reported to exhibit enhanced binding to relaxed Fn fibers compared to stretched ones in a manually pulled Fn fiber assay [72]. It however remains unclear, whether cell-exerted forces are also capable of unfolding and thus destroying this epitope on Fn, as no information or study in a cellular or tissue environment was published so far following up on this. In conclusion, up to now, no mechanical probe with known binding mechanism and binding affinity that could measure the mechanical strain of Fn fibers in histological tissue sections or *in vivo* has been put forward.

Bacterial peptide sequences binding to fibronectin

Within the 30 kDa N-terminal fragment of fibronectin (FnI_1-FnI_5) different gram-positive bacteria, such as S. *aureus*, S. *pyogenes*, S. *equisimilis*, S. *dysgalactiae* and the spirochete B. *burgdorferi* have been reported to attach (Fig. 2.2). The first report of a putative bacterial binding site on fibronectin dates back almost 40 years [73], but only later it got clear how bacteria use Fn as an attachment point to facilitate infection. Magnus Höök and coworkers were able to isolate a cell-wall anchored fibronectin binding protein (FnBP) from S. *aureus* in 1987 and in later years more and more bacteria have been identified to have similar fibronectin binding adhesion proteins [74,75]. It was also discovered that this Fn binding could be attributed to repeating peptide motifs within fibronectin binding proteins (Fig. 2.3 A,B) and that this is a common feature to several gram-positive bacteria [76,77]. Bacterial fibronectin binding peptides were later shown to have no secondary structure in solution and that they only upon binding to fibronectin undergo a disordered-to-ordered transition [78]. This binding of unstructured bacterial peptide adhesins to Fn is multivalent [79], as several binding repeats adhere to consecutive FnI domains via addition of an antiparallel β-sheet to the existing β-sheets of the FnI modules (Fig. 2.3 C) [80]. The multivalent binding complex of a bacterial peptide to several FnI modules via β-sheet addition was thus referred to as a β–zipper [80,81]. Clustering of several Fn N-termini in close proximity, is hypothesized to facilitate bacterial host cell invasion and it was indeed reported that S. *aureus* lacking the fibronectin binding proteins show significantly lower binding to Fn and exhibited lower invasion rates of endothelial cells [82,83], thus indicating that the presence of fibronectin binding proteins renders bacteria more virulent in sepsis.

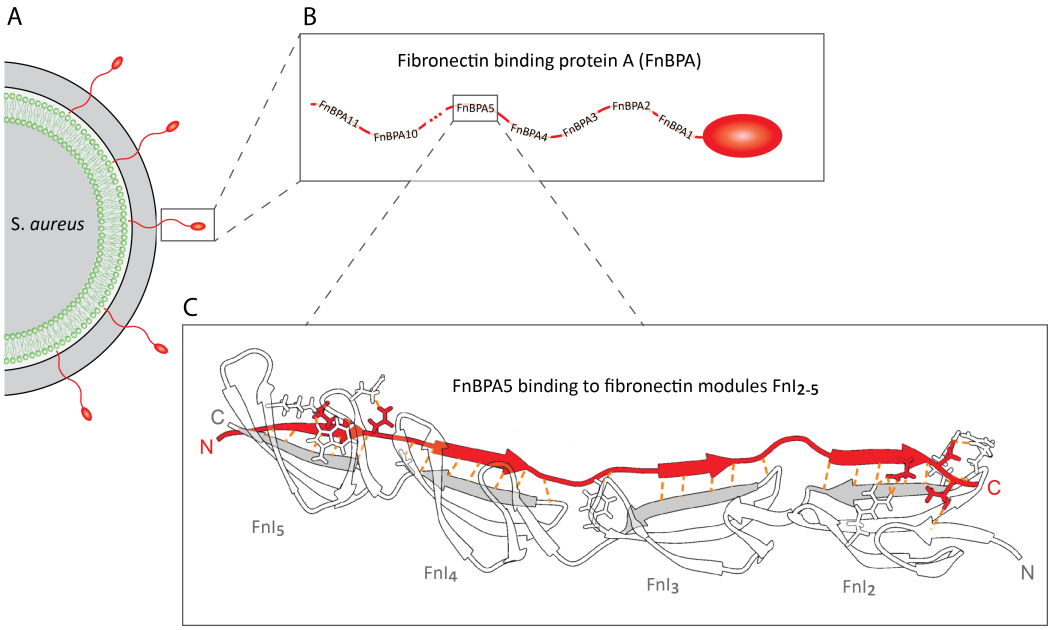

Figure 2.3: Bacterial fibronectin binding protein at different length scales. **(A)** FnBPs protrude from the bacterial cell surface and are important virulence factors of bacteria facilitating bacterial attachment to wound sites. **(B)** FnBPA protein consisting of eleven fibronectin binding repeats all binding several FnI modules. **(C)** Close-up of bacterial Fn binding repeat FnBPA5 binding to four consecutive FnI domains via addition of a beta-sheet to each module thus forming an antiparallel beta-zipper. Figure (A) and (B) adapted from [83] and figure (C) from an illustration of Dr. Samuel Hertig (also shown in figure 3.1).

Bacterial Fn binding peptides can sense the mechanical strain of Fn fibers

As mentioned above several bacteria are known to use Fn binding proteins to facilitate host infection and host cell invasion. Chabria and coworkers discovered, using a combination of steered molecular dynamics (SMD) simulations and an *in vitro* manually pulled Fn fiber assay, that some bacterial Fn binding peptides differentially bind to stretched versus relaxed Fn fibers [70]. They could correlate this changed binding behavior to a mechanical force-induced increase of the intermodular distance of individual FnI domains and thus a partial destruction of the multivalent binding epitope. Multivalent Fn binding peptides have several binding motifs to multiple consecutive FnI domains linked with variable linker regions. If such a linker between two binding motifs within a bacterial peptide is not long enough to be able to bridge the increased intermodular distance between FnI modules, as induced by mechanical stretching, the multivalent binding order will get reduced. This leads to a partial detachment of the bacterial fibronectin binding peptide from Fn, schematically shown in figure 2.4 and an overall decrease of binding affinity. Hertig and coworkers compared binding motifs of several Fn binding peptides from different bacterial species and linker regions between individual binding motifs to FnI modules of these peptides in a sequence alignment [84]. From the linker length between binding motifs they could correctly predict whether some divalent peptides bind in a strain dependent manner to manually pulled Fn fibers or not. They could even show that originally strain sensitive peptides could be rendered non-strain sensitive by artificially enlarging the linker length via insertion of additional amino acids into the linker region [84]. Hence, the linker length between binding motifs was found to represent a conserved mechanism for several bacteria to distinguish between different Fn strain states. The exact physiological reason for this affinity switch between

different mechanical strain states of Fn for some bacterial Fn binding peptides is not fully clear yet. It is hypothesized that stronger binding to relaxed Fn fibers may facilitate attachment to wound sites, as in wounded tissue tensional integrity is compromised leading to relaxed, loose ends of protein fibers representing attractive first attachment points for bacteria upon host infection [70].

The fifth Fn binding peptide of S. *aureus* protein FnBPA as model peptide to target and probe Fn

The fifth binding peptide of the fibronectin binding protein A of S. *aureus* (FnBPA5) (Fig. 2.3 B,C) exhibits one of the shortest linker regions between FnI binding motifs, compared to other Fn binding peptides [84] and was shown in a steered molecular dynamic simulation, to partially unbind from Fn upon application of a force of 400 pN [84]. This is schematically shown in figure 2.4. Because of its four binding motifs to FnI_2-FnI_5 modules this peptide has previously been shown to exhibit a strong affinity to the N-terminus of Fn with a dissociation constant of 44.2 ± 9.7 nM [85]. This high affinity together with its strain sensitive behavior shown in silico were the reasons this specific peptide was chosen as a model peptide to study how bacterial fibronectin binding peptides bind to Fn *in vitro* and *in vivo*.

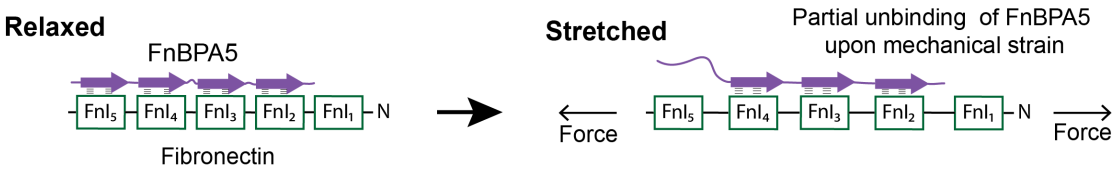

Figure 2.4: Partial unbinding of FnBPA5 from Fn upon force application and induction of a mechanical strain. Stretched state only showing trivalent binding leads to an overall lower affinity of FnBPA5 to stretched Fn compared to the relaxed state.

References

[1] R.O. Hynes, The Extracellular Matrix: Not Just Pretty Fibrils, Science. 326 (2009) 1216–1219. doi:10.1126/science.1176009.

[2] C. Bonnans, J. Chou, Z. Werb, Remodelling the extracellular matrix in development and disease, Nat Rev Mol Cell Biol. 15 (2014) 786–801. doi:10.1038/nrm3904.

[3] B. Alberts, A. Johnson, J. Lewis, M. Raff, K. Roberts, P. Walter, Cell Junctions, Cell Adhesion, and the Extracellular Matrix, in: Molecular Biology of the Cell, 5 ed., Garland Science, 2008: pp. 1131–1202.

[4] J. Eyckmans, R. Pieters, D. Eberli, B.J. Nelson, M.S. Sakar, C.S. Chen, Cellular forces and matrix assembly coordinate fibrous tissue repair, Nature Communications. 7 (2016) 1–8. doi:10.1038/ncomms11036.

[5] A.D. Doyle, K.M. Yamada, Mechanosensing via cell-matrix adhesions in 3D microenvironments, Exp. Cell Res. 343 (2016) 60–66. doi:10.1016/j.yexcr.2015.10.033.

[6] V. Vogel, M. Sheetz, Local force and geometry sensing regulate cell functions, Nat Rev Mol Cell Biol. 7 (2006) 265–275. doi:10.1038/nrm1890.

[7] J.D. Humphrey, E.R. Dufresne, M.A. Schwartz, Mechanotransduction and extracellular matrix homeostasis, Nat Rev Mol Cell Biol. 15 (2014) 802–812. doi:10.1038/nrm3896.

[8] R.K. Assoian, Anchorage-dependent Cell Cycle Progression, J. Cell Biol. 136 (1997) 1–4. doi:10.1083/jcb.136.1.1.

[9] R.O. Hynes, Integrins: bidirectional, allosteric signaling machines, Cell. 110 (2002) 673–687.

[10] M. Zeisberg, R. Kalluri, Cellular Mechanisms of Tissue Fibrosis. 1. Common and organ-specific mechanisms associated with tissue fibrosis, AJP: Cell Physiology. 304 (2013) C216–C225. doi:10.1152/ajpcell.00328.2012.

[11] H.E. Barker, T.R. Cox, J.T. Erler, The rationale for targeting the LOX family in cancer, Nat Rev Cancer. 12 (2012) 540–552. doi:10.1038/nrc3319.

[12] F. Spill, D.S. Reynolds, R.D. Kamm, M.H. Zaman, Impact of the physical microenvironment on tumor progression and metastasis, Current Opinion in Biotechnology. 40 (2016) 41–48. doi:10.1016/j.copbio.2016.02.007.

[13] J.L. Leight, A.P. Drain, V.M. Weaver, Extracellular Matrix Remodeling and Stiffening Modulate Tumor Phenotype and Treatment Response, Annu. Rev. Cancer Biol. 13 (2016) 17.1–17.22. doi:10.1146/annurev-cancerbio-050216-034431.

[14] P. Lu, V.M. Weaver, Z. Werb, The extracellular matrix: a dynamic niche in cancer progression, J. Cell Biol. 196 (2012) 395–406. doi:10.1083/jcb.201102147.

[15] A. Page-McCaw, A.J. Ewald, Z. Werb, Matrix metalloproteinases and the regulation of tissue remodelling, Nat Rev Mol Cell Biol. 8 (2007) 221–233. doi:10.1038/nrm2125.

[16] P.-J. Wipff, D.B. Rifkin, J.-J. Meister, B. Hinz, Myofibroblast contraction activates latent TGF-beta1 from the extracellular matrix, J. Cell Biol. 179 (2007) 1311–1323. doi:10.1083/jcb.200704042.

[17] B. Hinz, The extracellular matrix and transforming growth factor-β1: Tale of a strained relationship, Matrix Biol. 47 (2015) 54–65. doi:10.1016/j.matbio.2015.05.006.

[18] L.E. Stephens, A.E. Sutherland, I.V. Klimanskaya, A. Andrieux, J. Meneses, R.A. Pedersen, et al., Deletion of beta 1 integrins in mice results in inner cell mass failure and peri-implantation lethality, Genes & Development. 9 (1995) 1883–1895. doi:10.1101/gad.9.15.1883.

[19] F. Vidal, D. Aberdam, C. Miquel, A.M. Christiano, L. Pulkkinen, J. Uitto, et al., Integrin β4 mutations associated with junctional epidermolysis bullosa with pyloric atresia, Nat Genet. 10 (1995) 229–234.

[20] A. Sharma, J.A. Askari, M.J. Humphries, E.Y. Jones, D.I. Stuart, Crystal structure of a heparin-and integrin-binding segment of human fibronectin, The EMBO Journal. 18 (1999) 1468–1479. doi:10.1093/emboj/18.6.1468.

[21] S. Rahman, Y. Patel, J. Murray, K.V. Patel, R. Sumathipala, M. Sobel, et al., Novel hepatocyte growth factor (HGF) binding domains on fibronectin and vitronectin coordinate a distinct and amplified Met-integrin induced signalling pathway in endothelial cells, BMC Cell Biology. 6 (2005) 8. doi:10.1186/1471-2121-6-8.

[22] M. Mitsi, K. Forsten-Williams, M. Gopalakrishnan, M.A. Nugent, A catalytic role of heparin within the extracellular matrix, J. Biol. Chem. 283 (2008) 34796–34807. doi:10.1074/jbc.M806692200.

[23] M.M. Martino, J.A. Hubbell, The 12th-14th type III repeats of fibronectin function as a highly promiscuous growth factor-binding domain, The FASEB Journal. 24 (2010) 4711–4721. doi:10.1096/fj.09-151282.

[24] V. Vogel, Mechanotransduction involving multimodular proteins: converting force into biochemical signals, Annu Rev Biophys Biomol Struct. 35 (2006) 459–488. doi:10.1146/annurev.biophys.35.040405.102013.

[25] V. Vadillo-Rodríguez, M.A. Pacha-Olivenza, M.L. Gónzalez-Martín, J.M. Bruque, A.M. Gallardo-Moreno, Adsorption behavior of human plasma fibronectin on hydrophobic and hydrophilic Ti6Al4V substrata and its influence on bacterial adhesion and detachment, J. Biomed. Mater. Res. 101A (2012) 1397–1404. doi:10.1002/jbm.a.34447.

[26] Y. Mao, J.E. Schwarzbauer, Fibronectin fibrillogenesis, a cell-mediated matrix assembly process, Matrix Biology. 24 (2005) 389–399. doi:10.1016/j.matbio.2005.06.008.

[27] R. Pankov, K.M. Yamada, Fibronectin at a glance, Journal of Cell Science. 115 (2002) 3861–3863.

[28] W.S. To, K.S. Midwood, Plasma and cellular fibronectin: distinct and independent functions during tissue repair, Fibrogenesis Tissue Repair. 4 (2011). doi:10.1186/1755-1536-4-21.

[29] F.J. Fogerty, Inhibition of binding of fibronectin to matrix assembly sites by anti- integrin (alpha 5 beta 1) antibodies, J. Cell Biol. 111 (1990) 699–708. doi:10.1083/jcb.111.2.699.

[30] S.M. Früh, I. Schoen, J. Ries, V. Vogel, Molecular architecture of native fibronectin fibrils, Nature Communications. 6:7275 (2015). doi:10.1038/ncomms8275.

[31] E.L. George, E.N. Georges-Labouesse, R.S. Patel-King, H. Rayburn, R.O. Hynes, Defects in mesoderm, neural tube and vascular development in mouse embryos lacking fibronectin, Development. 119 (1993) 1079–1091.

[32] E.A. Lenselink, Role of fibronectin in normal wound healing, Int Wound J. (2013). doi:10.1111/iwj.12109.

[33] D. Greiling, R.A. Clark, Fibronectin provides a conduit for fibroblast transmigration from collagenous stroma into fibrin clot provisional matrix, Journal of Cell Science. 110 (1997) 861–870.

[34] S. Jodele, L. Blavier, J.M. Yoon, Y.A. DeClerck, Modifying the soil to affect the seed: role of stromal-derived matrix metalloproteinases in cancer progression, Cancer Metastasis Rev. 25 (2006) 35–43. doi:10.1007/s10555-006-7887-8.

[35] E. Wieczorek, E. Jablonska, W. Wasowicz, E. Reszka, Matrix metalloproteinases and genetic mouse models in cancer research: a mini-review, Tumour Biol. 36 (2015) 163–175. doi:10.1007/s13277-014-2747-6.

[36] S.I. Fraley, P.-H. Wu, L. He, Y. Feng, R. Krisnamurthy, G.D. Longmore, et al., Three-dimensional matrix fiber alignment modulates cell migration and MT1-MMP utility by spatially and temporally directing protrusions, Sci. Rep. 5 (2015) 598. doi:10.1002/jbm.a.31847.

[37] M.J. Paszek, N. Zahir, K.R. Johnson, J.N. Lakins, G.I. Rozenberg, A. Gefen, et al., Tensional homeostasis and the malignant phenotype, Cancer Cell. 8 (2005) 241–254. doi:10.1016/j.ccr.2005.08.010.

[38] K.R. Levental, H. Yu, L. Kass, J.N. Lakins, M. Egeblad, J.T. Erler, et al., Matrix Crosslinking Forces Tumor Progression by Enhancing Integrin Signaling, Cell. 139 (2009) 891–906. doi:10.1016/j.cell.2009.10.027.

[39] K.S. Midwood, G. Orend, The role of tenascin-C in tissue injury and tumorigenesis, J. Cell Commun.

Signal. 3 (2009) 287–310. doi:10.1007/s12079-009-0075-1.

[40] F. Saupe, A. Schwenzer, Y. Jia, I. Gasser, C. Spenlé, B. Langlois, et al., Tenascin-C Downregulates Wnt Inhibitor Dickkopf-1, Promoting Tumorigenesis in a Neuroendocrine Tumor Model, Cell Reports. 5 (2013) 482–492. doi:10.1016/j.celrep.2013.09.014.

[41] C.C. DuFort, M.J. Paszek, V.M. Weaver, Balancing forces: architectural control of mechanotransduction, Nat Rev Mol Cell Biol. 12 (2011) 308–319. doi:10.1038/nrm3112.

[42] S.C. Wei, L. Fattet, J.H. Tsai, Y. Guo, V.H. Pai, H.E. Majeski, et al., Matrix stiffness drives epithelial–mesenchymal transition and tumour metastasis through a TWIST1–G3BP2 mechanotransduction pathway, Nat. Cell Biol. 17 (2015) 678–688. doi:10.1038/ncb3157.

[43] D. Hanahan, R.A. Weinberg, Hallmarks of cancer: the next generation, Cell. 144 (2011) 646–674. doi:10.1016/j.cell.2011.02.013.

[44] M.W. Pickup, J.K. Mouw, V.M. Weaver, The extracellular matrix modulates the hallmarks of cancer, EMBO Rep. 15 (2014) e201439246–1253. doi:10.15252/embr.201439246.

[45] J.A. Nagy, A.M. Dvorak, H.F. Dvorak, Vascular hyperpermeability, angiogenesis, and stroma generation, Cold Spring Harb Perspect Med. 2 (2012) a006544. doi:10.1101/cshperspect.a006544.

[46] A.I. Minchinton, I.F. Tannock, Drug penetration in solid tumours, Nat Rev Cancer. 6 (2006) 583–592. doi:10.1038/nrc1893.

[47] Y.K. Bae, A. Kim, M.K. Kim, J.E. Choi, S.H. Kang, S.J. Lee, Fibronectin expression in carcinoma cells correlates with tumor aggressiveness and poor clinical outcome in patients with invasive breast cancer, Hum. Pathol. 44 (2013) 2028–2037. doi:10.1016/j.humpath.2013.03.006.

[48] J. Park, J.E. Schwarzbauer, Mammary epithelial cell interactions with fibronectin stimulate epithelial-mesenchymal transition, Oncogene. 33 (2014) 1649–1657. doi:10.1038/onc.2013.118.

[49] D. Duscher, Z.N. Maan, V.W. Wong, R.C. Rennert, M. Januszyk, M. Rodrigues, et al., Mechanotransduction and fibrosis, Journal of Biomechanics. 47 (2014) 1997–2005. doi:10.1016/j.jbiomech.2014.03.031.

[50] R.A. Ignotz, J. Massagué, Transforming growth factor-beta stimulates the expression of fibronectin and collagen and their incorporation into the extracellular matrix, J. Biol. Chem. 261 (1986) 4337–4345.

[51] W.D. Xu, E.C. LeRoy, E.A. Smith, Fibronectin release by systemic sclerosis and normal dermal fibroblasts in response to TGF-beta, The Journal of Rheumatology. 18 (1991) 241–246.

[52] J.H.W. Distler, A. Jüngel, L.C. Huber, U. Schulze-Horsel, J. Zwerina, R.E. Gay, et al., Imatinib mesylate reduces production of extracellular matrix and prevents development of experimental dermal fibrosis, Arthritis Rheum. 56 (2006) 311–322. doi:10.1002/art.22314.

[53] J. Rosenbloom, F.A. Mendoza, S.A. Jimenez, Strategies for anti-fibrotic therapies, Biochim. Biophys. Acta. 1832 (2013) 1088–1103. doi:10.1016/j.bbadis.2012.12.007.

[54] R. McBeath, D.M. Pirone, C.M. Nelson, K. Bhadriraju, C.S. Chen, Cell shape, cytoskeletal tension, and RhoA regulate stem cell lineage commitment, Dev. Cell. 6 (2004) 483–495.

[55] K.A. Kilian, B. Bugarija, B.T. Lahn, M. Mrksich, Geometric cues for directing the differentiation of mesenchymal stem cells, Proc. Natl. Acad. Sci. U.S.a. 107 (2010) 4872–4877. doi:10.1073/pnas.0903269107.

[56] A.J. Engler, S. Sen, H.L. Sweeney, D.E. Discher, Matrix Elasticity Directs Stem Cell Lineage Specification, Cell. 126 (2006) 677–689. doi:10.1016/j.cell.2006.06.044.

[57] B. Trappmann, J.E. Gautrot, J.T. Connelly, D.G.T. Strange, Y. Li, M.L. Oyen, et al., Extracellular-matrix tethering regulates stem-cell fate, Nat Mater. 11 (2012) 642–649. doi:10.1038/nmat3339.

[58] Y. Cho, E.Y. Park, E. Ko, J.-S. Park, J.H. Shin, Recent advances in biological uses of traction force microscopy, Int. J. Precis. Eng. Manuf. 17 (2016) 1401–1412. doi:10.1007/s12541-016-0166-x.

[59] W.J. Polacheck, C.S. Chen, Measuring cell-generated forces: a guide to the available tools, Nat.

Methods. 13 (2016) 415–423. doi:10.1016/j.pmatsci.2007.05.002.

[60] A. Saez, M. Ghibaudo, A. Buguin, P. Silberzan, B. Ladoux, Rigidity-driven growth and migration of epithelial cells on microstructured anisotropic substrates, Proc. Natl. Acad. Sci. U.S.a. 104 (2007) 8281–8286. doi:10.1073/pnas.0702259104.

[61] A.F. Oberhauser, C. Badilla-Fernandez, M. Carrion-Vazquez, J.M. Fernandez, The Mechanical Hierarchies of Fibronectin Observed with Single-molecule AFM, J. Mol. Biol. 319 (2002) 433–447. doi:10.1016/S0022-2836(02)00306-6.

[62] F. Meng, F. Sachs, Visualizing dynamic cytoplasmic forces with a compliance-matched FRET sensor, Journal of Cell Science. 124 (2010) 261–269. doi:10.1242/jcs.071928.

[63] J. Seong, A. Tajik, J. Sun, J.-L. Guan, M.J. Humphries, S.E. Craig, et al., Distinct biophysical mechanisms of focal adhesion kinase mechanoactivation by different extracellular matrix proteins, Proc. Natl. Acad. Sci. U.S.a. 110 (2013) 19372–19377. doi:10.1073/pnas.1307405110.

[64] H.C. Ishikawa-Ankerhold, R. Ankerhold, G.P.C. Drummen, Advanced Fluorescence Microscopy Techniques—FRAP, FLIP, FLAP, FRET and FLIM, Molecules. 17 (2012) 4047–4132. doi:10.3390/molecules17044047.

[65] G. Baneyx, L. Baugh, V. Vogel, Coexisting conformations of fibronectin in cell culture imaged using fluorescence resonance energy transfer, Proc. Natl. Acad. Sci. U.S.a. 98 (2001) 14464–14468. doi:10.1073/pnas.251422998.

[66] M.L. Smith, D. Gourdon, W.C. Little, K.E. Kubow, R.A. Eguiluz, S. Luna-Morris, et al., Force-Induced Unfolding of Fibronectin in the Extracellular Matrix of Living Cells, Plos Biol. 5 (2007) e268. doi:10.1371/journal.pbio.0050268.sv001.

[67] K.E. Kubow, E. Klotzsch, M.L. Smith, D. Gourdon, W.C. Little, V. Vogel, Crosslinking of cell-derived 3D scaffolds up-regulates the stretching and unfolding of new extracellular matrix assembled by reseeded cells, Integr. Biol. 1 (2009) 635. doi:10.1039/b914996a.

[68] W.R. Legant, C.S. Chen, V. Vogel, Force-induced fibronectin assembly and matrix remodeling in a 3D microtissue model of tissue morphogenesis, Integr. Biol. 4 (2012) 1164–1174. doi:10.1039/c2ib20059g.

[69] W.C. Little, M.L. Smith, U. Ebneter, V. Vogel, Assay to mechanically tune and optically probe fibrillar fibronectin conformations from fully relaxed to breakage, Matrix Biology. 27 (2008) 451–461. doi:10.1016/j.matbio.2008.02.003.

[70] M. Chabria, S. Hertig, M.L. Smith, V. Vogel, Stretching fibronectin fibres disrupts binding of bacterial adhesins by physically destroying an epitope, Nature Communications. 1 (2010) 135–9. doi:10.1038/ncomms1135.

[71] L. Cao, M.K. Zeller, V.F. Fiore, P. Strane, H. Bermudez, T.H. Barker, Phage-based molecular probes that discriminate force-induced structural states of fibronectin in vivo, Proc. Natl. Acad. Sci. U.S.a. 109 (2012) 7251–7256. doi:10.1073/pnas.1118088109.

[72] W.C. Little, R. Schwartlander, M.L. Smith, D. Gourdon, V. Vogel, Stretched Extracellular Matrix Proteins Turn Fouling and Are Functionally Rescued by the Chaperones Albumin and Casein, Nano Lett. 9 (2009) 4158–4167. doi:10.1021/nl902365z.

[73] P. Kuusela, Fibronectin binds to Staphylococcus aureus, Nature. 276 (1978) 718–720. doi:10.1038/276718a0.

[74] E. Hanski, M. Caparon, Protein F, a fibronectin-binding protein, is an adhesin of the group A streptococcus Streptococcus pyogenes, Proc. Natl. Acad. Sci. U.S.a. 89 (1992) 6172–6176.

[75] V. Ozeri, A. Tovi, I. Burstein, S. Natanson-Yaron, M.G. Caparon, K.M. Yamada, et al., A two-domain mechanism for group A streptococcal adherence through protein F to the extracellular matrix, The EMBO Journal. 15 (1996) 989–998.

[76] M.J. McGavin, S. Gurusiddappa, P.E. Lindgren, M. Lindberg, G. Raucci, M. Hook, Fibronectin receptors from Streptococcus dysgalactiae and Staphylococcus aureus. Involvement of conserved

residues in ligand binding, J. Biol. Chem. 268 (1993) 23946–23953.

[77] U. Schwarz-Linek, M. Höök, J.R. Potts, Fibronectin-binding proteins of Gram-positive cocci, Microbes and Infection. 8 (2006) 2291–2298. doi:10.1016/j.micinf.2006.03.011.

[78] K. House-Pompeo, Y. Xu, D. Joh, Pietro Speziale, M. Höök, Conformational Changes in the Fibronectin Binding MSCRAMMs Are Induced by Ligand Binding, J. Biol. Chem. 271 (1996) 1379–1384.

[79] U. Schwarz-Linek, M.J. Plevin, A.R. Pickford, M. Hook, I.D. Campbell, J.R. Potts, Binding of a peptide from a Streptococcus dysgalactiae MSCRAMM to the N-terminal F1 module pair of human fibronectin involves both modules, FEBS Lett. 497 (2001) 137–140.

[80] U. Schwarz-Linek, J.M. Werner, A.R. Pickford, S. Gurusiddappa, J.H. Kim, E.S. Pilka, et al., Pathogenic bacteria attach to human fibronectin through a tandem beta-zipper, Nature. 423 (2003) 177–181. doi:10.1038/nature01589.

[81] R.J. Bingham, E. Rudino-Pinera, N.A.G. Meenan, U. Schwarz-Linek, J.P. Turkenburg, M. Hook, et al., Crystal structures of fibronectin-binding sites from Staphylococcus aureus FnBPA in complex with fibronectin domains, Proc. Natl. Acad. Sci. U.S.a. 105 (2008) 12254–12258. doi:10.1073/pnas.0803556105.

[82] A.M. Edwards, J.R. Potts, E. Josefsson, R.C. Massey, Staphylococcus aureus Host Cell Invasion and Virulence in Sepsis Is Facilitated by the Multiple Repeats within FnBPA, PLoS Pathog. 6 (2010) e1000964. doi:10.1371/journal.ppat.1000964.s003.

[83] T.J. Foster, J.A. Geoghegan, V.K. Ganesh, M. Höök, Adhesion, invasion and evasion: the many functions of the surface proteins of Staphylococcus aureus, Nature Reviews Microbiology. 12 (2014) 49–62. doi:10.1038/nrmicro3161.

[84] S. Hertig, M. Chabria, V. Vogel, Engineering mechanosensitive multivalent receptor-ligand interactions: why the nanolinker regions of bacterial adhesins matter, Nano Lett. 12 (2012) 5162–5168. doi:10.1021/nl302153h.

[85] N.A.G. Meenan, L. Visai, V. Valtulina, U. Schwarz-Linek, N.C. Norris, S. Gurusiddappa, et al., The tandem beta-zipper model defines high affinity fibronectin-binding repeats within Staphylococcus aureus FnBPA, J. Biol. Chem. 282 (2007) 25893–25902. doi:10.1074/jbc.M703063200.

Chapter 3

Novel peptide probes to assess the tensional state of fibronectin fibers from cells to cancer

An updated version of the work presented in this chapter was accepted for publication in Nature Communications: Simon Arnoldini, Alessandra Moscaroli, Mamta Chabria, Manuel Hilbert, Samuel Hertig, Roger Schibli, Martin Behe and Viola Vogel are the authors of this manuscript. The application of fibronectin binding peptides for use in tumor or fibrosis diagnosis and therapy was patented by the authors in the European patent application EP16174824 (priority date June 16th 2016) and is related to the work presented in this chapter. Simon Arnoldini conducted all stainings, imaging and analysis within this chapter and Alessandra Moscaroli conducted the *in vivo* work, as well as organ excretion and sectioning, Samuel Hertig created figure 3.1 and Manuel Hilbert did the fluorescence anisotropy measurements. Simon Arnoldini, Alessandra Moscaroli, Martin Behe and Viola Vogel wrote the manuscript.

Abstract

Major transformations of extracellular matrix (ECM) accompany disease progression in cancer, yet how the crosstalk between ECM and cells drives these processes remains unknown. This is partly due to the lack of probes to measure cellular forces or strain of ECM fibers in tissues. As fibronectin (Fn) is a key player within the ECM, we introduce a new probe to assess Fn fiber strain in tissues. The Fn binding peptide FnBPA5 derived from S. aureus, is shown here to bind with nM affinity to relaxed but not stretched Fn fibers, as stretching causes a structural mismatch to its multivalent binding epitope. After validation of the FnBPA5 peptide as mechanical strain probe in fibroblast ECM through a pixel-by-pixel comparison with Fn-FRET, we identified relaxed Fn fibers in tumor cryosections, illustrating the utility of this peptide for histological applications. After verifying adequate plasma stability, radiolabeled ^{111}In-FnBPA5 was injected in a prostate cancer mouse model. SPECT/CT scans and biodistribution analysis revealed specific accumulation of ^{111}In-FnBPA5 in tumor with prolonged retention compared to other organs. The future utilization of this probe may give new insights how changes in Fn strain at the tissue level influence cell signaling and disease progression in different Fn-related diseases.

Introduction

Despite major progress in our understanding how proteins act as mechano-chemical switches [1-3] and how the mechanobiology of cells regulates their fate [4-6], our knowledge about the mechanobiology of tissues in development, under homeostatic conditions and in pathological transformations remains sparse. Even though a large toolbox of technologies to quantify forces and mechanical strains at the molecular and cellular levels is available today [7,8], how to translate these findings to the tissue level is a challenge, since not a single probe to either measure forces or force-induced molecular strains in tissues exists today that is applicable to be used *in vivo* or in histological tissue sections. This prevents a thorough characterization of how changed tensional states in tissue fibers might tune the structure-function relationships of extracellular matrix (ECM) proteins, and how this might ultimately regulate tissue growth, regeneration, homeostasis or disease progression. For cancer [9-11] and fibrotic disorders [12-15], altered cellular forces, changed ECM composition and crosslinking, and thus increased tissue stiffness have been well documented, yet, how this correlates with local strains of ECM fibers and thus the ECM-cell crosstalk remains completely unknown. Availability of novel probes to document and track ECM fiber strain in histological samples and living tissues is thus highly relevant. Fibronectin (Fn) thereby represents one of the most abundant ECM proteins [4,16] with a plethora of binding sites for other ECM proteins, growth factors and cells, and especially its isoforms containing the extra domains A (EDA) and B (EDB), are overexpressed in cancer [17], wound healing and inflammation [18], and serve as biomarkers for metastasis and bad prognosis in many cancer types [19-26]. Fn homes several well-characterized mechanosensitive switches [3,27-31], that can influence ligand binding affinities and thus cell attachment and signaling [28,29,32-35]. This effect is dependent both on cellular force application to individual Fn fibers [36], as well as on the overall composition of the extracellular matrix [37,38]. Even though our focus here is on cancer, the availability of such mechanosensitive strain probes will be equally important to finally uncover how forces regulate tissue growth and regeneration processes, from early development to wound healing, where fibronectin expression and matrix assembly is highly upregulated as well [39-41].

Here we explore whether properly designed peptide probes can be exploited to identify the tensile state of ECM fibers in histological tissue sections, as well as in living animals. Even though we had introduced in 2001 a molecular probe that recognizes the mechanical strain of Fn fibrils based on fluorescence resonance energy transfer (FRET) [36,42,43], quantifying Fn-FRET ratios is more complicated in tissues compared to cell culture experiments. Instead, we asked whether Fn-binding peptides derived from bacterial adhesins can be exploited to distinguish highly stretched from relaxed Fn fibers *in vivo*, as well as to stain the fiber strain of Fn in histological samples. Bacteria evolved adhesins that specifically target fibronectin with high affinity [44]. These Fn-binding peptides (FnBPs) are unstructured in solution and form an antiparallel tandem beta-zipper upon binding in a row to multiple N-terminal fibronectin type I (FnI_{1-5}) modules. The tight binding complex formed with FnI modules is stabilized by backbone hydrogen bonds and is connected via short unstructured peptide loops (Figure 3.1) [45-47]. This multivalent binding to multiple adjacent domains greatly increases the binding affinity to Fn, from the µM to the nM range, if targeting not only FnI_{4-5} but FnI_{2-5}, respectively [47-49]. We could show

previously that the spatial match between this multivalent binding motif of the short peptide fragment STAFF5C targeting FnI_{4-5} derived from *Staphylococcus aureus* (FnBPA5) is destroyed by stretching Fn-fibers[45]. Here, we validate the use of the FnBPA5 peptide which specifically binds to relaxed but not stretched Fn fibrils, as schematically shown in figure 3.1 D,E, for tissue applications.

For the histological tissue stains, as well as for the *in vivo* experiments, a mouse model for human prostate carcinoma was chosen (PC3 xenografts). This type of carcinoma exhibits an extended tumor microenvironment, caused by a dysregulation of the equilibrium between matrix production and turnover, representing an adequate model for the validation of the FnBPA5 peptide probe [50]. To provide a proof of-concept, histological tissue sections of cancer stroma were co-stained with a polyclonal Fn antibody, as well as with the fluorescently labeled FnBPA5 peptide (Fig. 3.1 F), to image the locations of total Fn versus relaxed Fn, respectively. To then investigate its suitability as an *in vivo* probe, the pharmacokinetics of ^{111}In-FnBPA5 and its distribution in various organs was explored in living mice after injection into the tail vein using single photon emission computed tomography (SPECT) analysis.

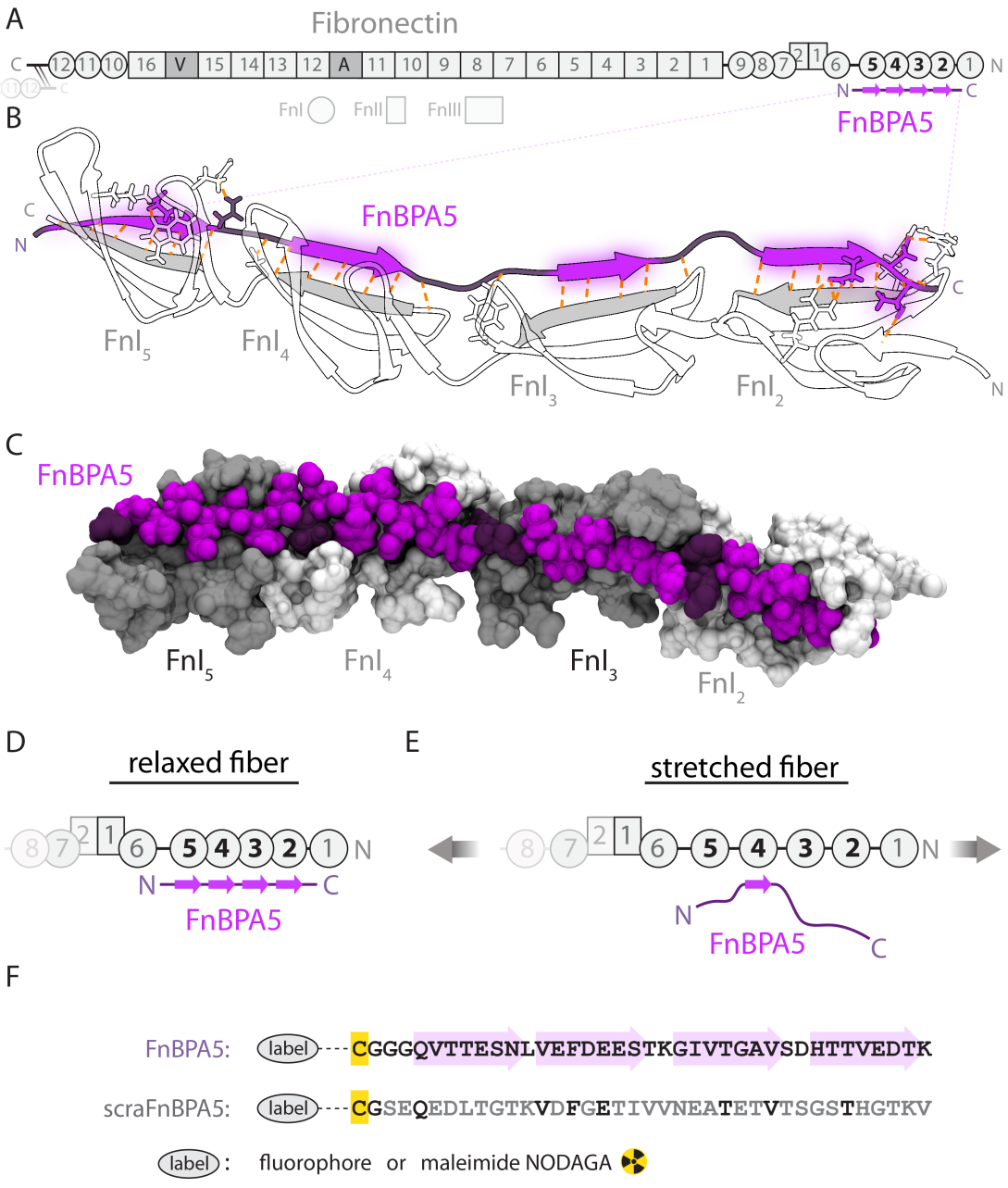

Figure 3.1. Multivalent binding motif by which the bacterial peptide FnBPA5 specifically recognizes fibronectin (Fn). **(A)** Schematic representation of the multidomain protein Fn. The binding epitope for FnBPA5 (purple) is located near the N-terminus of fibronectin (grey). **(B)** FnBPA5 binds to modules $FnI_{2\text{-}5}$ (white, strands forming intermolecular β-sheets in grey) via an antiparallel beta-zipper by forming an extensive network of backbone hydrogen bonds (orange dotted lines). Linker residues of FnBPA5 are shown in darker purple. **(C)** Surface rendering of the complex shown in B), highlighting the snug fit of the interaction. Odd-numbered FnI modules are shown in darker grey for distinction. **(D)** FnBPA5 binds to relaxed, but not to stretched Fn fibers as stretching causes a structural mismatch to its multivalent binding epitope located on the Fn type I domains $FnI_{2\text{-}5}$. **(E)** Mechanically induced strain on Fn molecule leads to a reduction of multivalency and thus an affinity switch in binding of FnBPA5 **(F)** Sequences of the FnBPA5 peptide and its randomly scrambled negative control, scraFnBPA5. Residues in the wild type peptide forming intermolecular betasheets are indicated with light purple arrows, and residues of the scrambled control peptide conserved with respect to the wild type are shown in black. Both peptides were labeled on the N-terminal cysteine residues (yellow) with Alexa488 or Cy5 fluorophores for *in vitro* experiments and NODAGA for *in-vivo* experiments.

Results

To systematically explore whether peptides can be utilized as strain probes to visualize the mechanical tension of ECM fibers in histological sections and in living animals, we tested the synthesized bacterial Fn-binding peptide FnBPA5, together with a scrambled peptide (scraFnBPA5) as negative control having the same amino acid residues, but no affinity to Fn (Figure 3.1 D). For the *in vitro* analysis and physicochemical characterization, the peptides were functionalized with an Alexa 488 or Cy5 fluorophore for immunofluorescence microscopy studies, while they were radiolabeled with ^{111}In for the *in vivo* SPECT/CT imaging and the biodistribution analysis performed in a prostate cancer mouse model.

FnBPA5 targeting FnI_{2-5} preferentially binds to relaxed but not stretched Fn fibers

To confirm strain-dependent binding of the FnBPA5 peptide to fibrillar Fn *in vitro*, since only its shorter fragment STAFF5C was tested earlier [47], single Fn fibers were pulled out of a concentrated Fn solution containing 5% Cy5-labeled Fn and deposited onto a stretchable silicone sheet to adjust a defined mechanical Fn fiber strain (Fig. 3.2) [51]. Representative ratiometric images of fluorescent signal of FnBPA5-Alexa 488 divided by Fn-Cy5 show significantly higher peptide binding of FnBPA5 to relaxed Fn fibers compared to stretched fibers (Figure 3.2 A). The quantification of three independent experiments showed a significant ($p<0.001$) decrease in FnBPA5/Fn ratio for stretched fibers (380% mechanical strain) compared to relaxed ones (7% mechanical strain) (Fig. 3.2 B). This indicates that stretching of individual Fn fibers destroys the multivalent binding motif as stretching causes a structural mismatch between the peptide and its multivalent binding epitope located on the Fn type I domains FnI_{2-5}. This is in line with previously published computational results for FnBPA5, as well as with the experimental binding studies using much shorter fragments of FnBPA5, i.e. bivalent fragment of FnBPA5 STAFF5C binding to FnI_{4-5}, and other bacterial and engineered Fn binding peptides [46,47].

FnBPA5 binds with nM affinity to soluble, as well as to relaxed Fn fibers

Affinity of FnBPA5-Alexa 488 towards relaxed fibrillar and soluble Fn was determined *in vitro* by two independent assays, fluorescent anisotropy titrations and single fiber binding assays. Fluorescence anisotropy titrations with Alexa 488 labeled FnBPA5 revealed a dissociation constant (K_d) of 75 ± 8 nM to soluble Fn. In contrast, the control peptide scraFnBPA5-Alexa 488 did not show any binding (Fig. 3.2 D). Single Fn-fiber assays [51] were then used to quantify the affinity of FnBPA5-Alexa 488 and of its scrambled control peptide to relaxed Fn fibers. The saturation binding curve was derived from a pixel-by-pixel analysis of the intensity ratio of FnBPA5-Alexa 488 and Fn-Cy5 labeled fibers. Fitting of the binding curve revealed a K_d value of 28 ± 6 nM (Fig 3.2 E). Confocal microscopy images of Fn fibers exposed to FnBPA5-Alexa 488 or its scrambled control peptide are shown in Fig. 3.2 F. FnBPA5-Alexa 488 showed significantly higher binding to Fn fibers than the scrambled control peptide, confirming the sequence-specificity of the interaction (Fig. 3.2 G). A displacement assay using ^{nat}In-FnBPA5 (cold labeled) against FnBPA5-Alexa 488 was performed to assess whether radiolabeling impairs FnBPA5

binding to single Fn fibers showing that the radiolabeling process did not affect binding properties of FnBPA5 to Fn (Supplementary fig. 3.1).

The dissociation constants for soluble, full-length Fn and fibrillar fibronectin are close to the affinity reported for FnBPA5 binding to N-terminal Fn fragments in solution (K_d = 44.2 nM) [48]. Most importantly, the affinities of the FnBPA5-Alexa 488 to plasma Fn and to relaxed fibrillar Fn are comparable and of the same order of magnitude as those reported for several clinical antibodies that target ECM proteins [52]. To test if similar tight binding is observed in native extracellular matrix, Fn-rich ECM assembled by human dermal fibroblasts was incubated for 1 hour with FnBPA5-Alexa 488 or scrambled control peptide. Specific binding to fibrillar Fn was only observed for FnBPA5-Alexa 488 (Fig. 3.2 H). To see whether FnBPA5 binding to Fn in cell culture also exhibits strain sensitive behavior, we next compared it with a mechanosensitive Fn-FRET sensor [36,43].

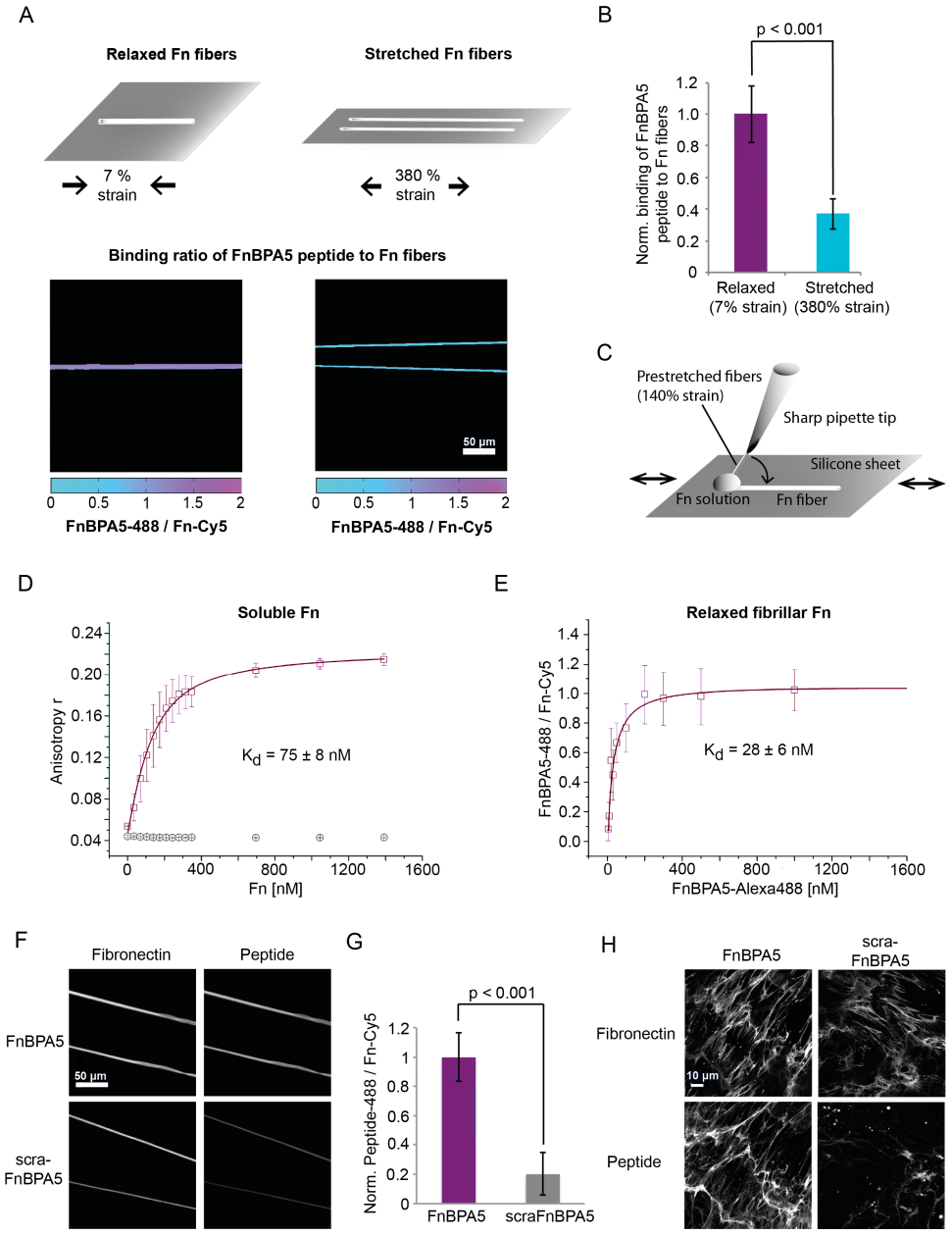

Figure 3.2: *In vitro* binding studies of the peptide FnBPA5-Alexa 488 and the scrambled control (scraFnBPA5-Alexa 488) to soluble and fibrillar Fn. **(A)** Mechanosensitive binding of FnBPA5 was tested using relaxed (7% strain) and stretched (380% strain) fibers. Color-coded intensity ratio images of FnBPA5-Alexa 488 divided by Fn-Cy5 of manually pulled Fn fibers of different mechanical state show higher binding to relaxed fibers than to stretched ones, leading to a higher FnBPA5/Fn ratio (representative images). **(B)** Normalized analysis of relaxed and stretched fibers showing a significant decrease in binding ratio of FnBPA5 from relaxed to stretched fibers. Data from 30 fibers from 3 independent experiments with error bars being standard deviations. P-value was obtained from a student's t-test. **(C)** Schematic of manual fiber pulling, using a sharp pipette tip dipping into a Fn solution and pulling Fn fibers onto a flexible silicone sheet. **(D)** The binding of FnBPA5-Alexa 488 and scraFnBPA5-Alexa 488 to soluble plasma Fn was determined using an anisotropy measurement (see methods). The results show a K_d of 75 ± 8 nM for FnBPA5-Alexa 488 and no specific binding for the scrambled control peptide. **(E)** Measurements of affinity of FnBPA5-Alexa 488 to single relaxed Fn fibers showed a K_d of 28 ± 6 nM. **(F)** Fluorescence images showing the binding of FnBPA5-Alexa 488 and scrambled control peptide to single Fn fibers. For this experiment Cy5-labeled Fn was used (images on the left side). **(G)** The quantification of the fluorescence intensity showed a significant higher binding of FnBPA5-Alexa 488 compared to the control. Data from 30 fibers from three independent experiments were analyzed. Shown error bars represent the standard deviation. **(H)** Human dermal fibroblast ECM was stained for fibronectin and incubated with FnBPA5-Alexa 488 and the scrambled control peptide, respectively. Representative images show specific binding of FnBPA5-Alexa 488 to Fn.

Validation of the FnBPA5 peptide: pixel-by-pixel comparison to Fn-FRET probe

We next asked how FnBPA5 binding behavior to Fn fibrils (Fig. 3.3 A) of the ECM assembled by fibroblasts in cell culture correlates to the Fn fiber strain as probed by a totally different method, i.e. by quantifying the acceptor/donor Fn-FRET ratios. Therefore, we used our previously developed fluorescently double labeled Fn-FRET probe (Fig. 3.3 B) to visualize how cells stretch Fn fibers in 2D cell culture and in cell-derived ECM scaffolds [7,36,53]. Pixel-by-pixel ratiometric analysis of FnBPA5-Cy5 channel divided by directly excited acceptor channel of Fn (peptide binding ratio, Fig. 3.3 C) and acceptor divided by donor channel of double labeled Fn (FRET ratio, Fig. 3.3 D) shows a correlation of areas exhibiting high FRET ratios with areas having high peptide binding (Fig 3.3 C-E), going in line with the hypothesis of an enhanced binding of FnBPA5 to relaxed Fn conformations. This is of particular interest, since FnBPA5 peptide binds to and probes the N-terminal region of Fn, while the acceptors in the Fn-FRET molecules are localized at cryptic cysteines on the Fn type III modules, $FnIII_7$ and $FnIII_{15}$, respectively (Fig. 3.3 A,B). To quantitatively test this correlation of higher FnBPA5 binding to areas of high FRET ratio, the average FnBPA5/Fn ratio for all pixels sharing the same FRET ratio for multiple fields of view ($n > 10$) was plotted in figure 3.3 F with a color-code for the number of pixels used for the averaging. This analysis shows an increase of average FnBPA5-Cy5/Fn-546 ratio with increasing FRET ratio, confirming the first impression of image comparison by eye. In figure 3.3 G probability density functions of FnBPA5/Fn ratios for two different FRET ratios (0.3 in blue, 0.5 in red) are shown with vertical lines representing the arithmetic mean of the individual distribution. The clear shift of the two density functions gives evidence that FnBPA5 binds predominantly to relaxed Fn fibers and can thus be used to visualize relaxed Fn fibrils, offering a new tool to probe the mechanical strain of Fn fibers in settings that are not amenable to currently available methods, such as within histological tissue sections or *in vivo*.

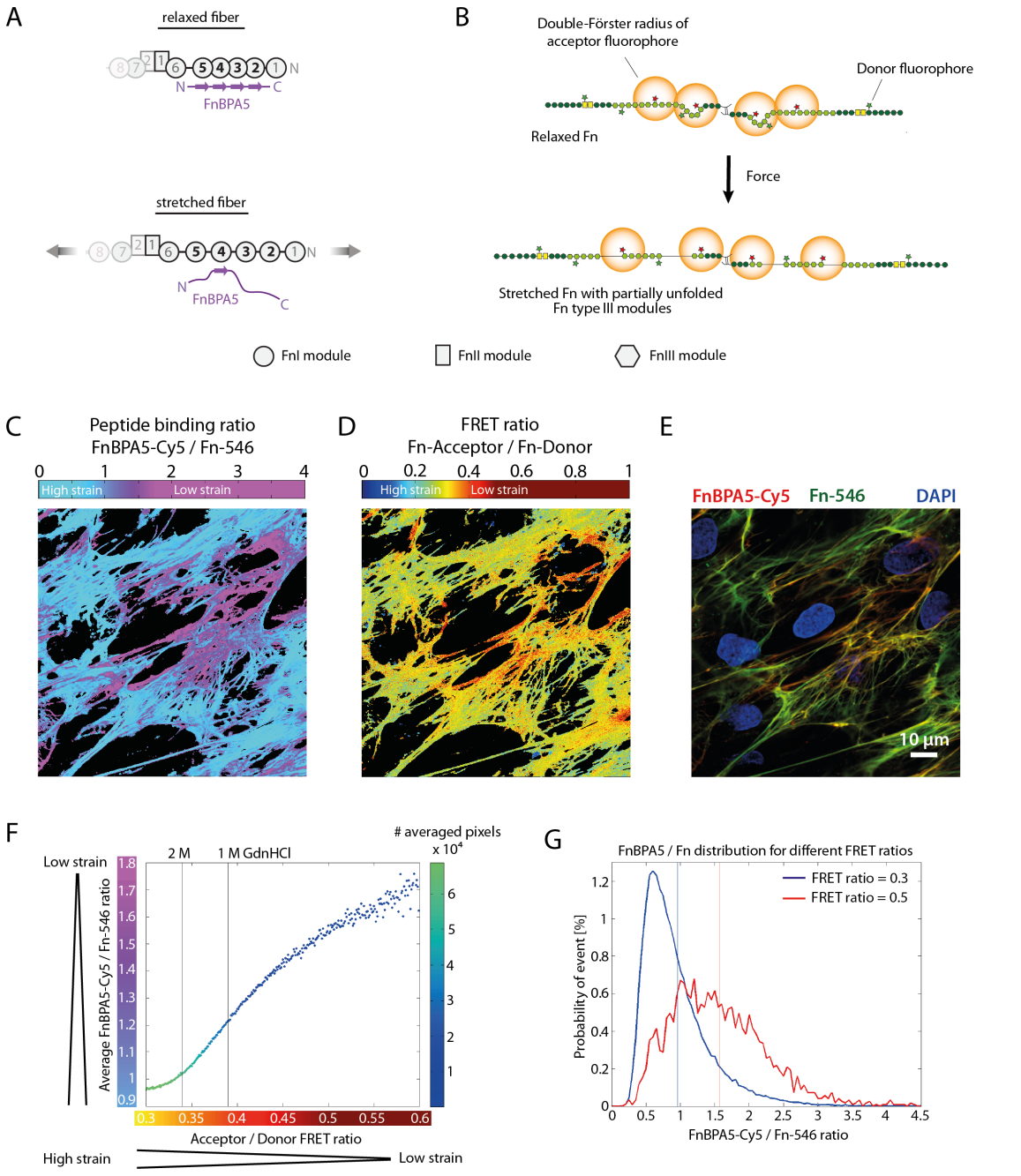

Figure 3.3: Comparison of FnBPA5 binding to a cell-grown Fn matrix with a Fn FRET probe. **(A)** Schematic of strain sensitive binding of FnBPA5 to N-terminal FnI domains of Fn. **(B)** Schematic of Fn-FRET probe with acceptor fluorophores at specified domains and donor fluorophores at random locations, exhibiting a lower energy transfer in stretched state compared to relaxed one **(C)** FnBPA5-Cy5 was normalized with directly excited Fn-546, showing in the false color ratiometric image high FnBPA5 binding in violet areas. **(D)** False color ratiometric image of Fn-Acceptor 546 / Fn-Donor 488 FRET ratio. Red colors represent higher FRET ratios representing more relaxed Fn conformations whereas blue colors show lower FRET ratios corresponding to regions with more stretched Fn. **(E)** Merged fluorescence image of FnBPA5-Cy5 (red), Fn-546 (green) and DAPI (blue). **(F)** Quantitative analysis of mean FnBPA5 binding ratios for given FRET ratios for all images (n>10) of an experiment shows an increase in FnBPA5 binding for higher FRET ratios. Number of pixels used for averaging is given in the color code. **(G)** Distribution of FnBPA5-Cy5 / Fn-546 ratio for two given FRET ratios (0.3 and 0.5) showed in probability density functions for FnBPA5 binding ratios. Vertical lines represent the arithmetic mean of the distributions. Shift of distribution of FnBPA5/Fn for the FRET value of 0.5 (red) indicates a higher overall binding compared to distribution for FRET value of 0.3 (blue).

Cryosections of tumor stroma contain large regions of relaxed Fn-fibers

To gain insights into the mechanical strain of Fn fibers in tumor tissue, *post-mortem* tumor cryosections from human prostate cancer (PC-3) xenografts were co-stained with FnBPA5-Alexa 488 and with various antibodies. Staining with a polyclonal Fn antibody to visualize the overall Fn distribution over the whole tissue section (Fig. 3.4 A) revealed that Fn is abundantly present, as expected [54,55]. In contrast, the FnBPA5-Alexa 488 stain reveals that FnBPA5 specifically accumulated in certain regions of the tumor. To address whether the FnBPA5 peptide is mostly found around the tumor vasculature, the endothelial cells were stained using a CD-31 (PECAM-1) antibody. In agreement with the literature, regions of high and poor vascularization are seen. Significantly though, highly vascularized regions do not typically co-localize in these sections with the regions rich in FnBPA5 peptide as seen in the overview image (Fig.3.4 A) and in the high-resolution zoomed-in images (Fig. 3.4 B). Finally, with a further analysis of the tumour sections, we could show a co-localization of FnBPA5 with Fn (Fig. 3.4 B,D).

In a previous work we demonstrated that relaxed but not stretched Fn fibers serve as template for early collagen I fiber growth in cell culture and that Fn fibrils subsequently partially relax in the presence of a collagen-I rich ECM [38]. We , therefore, analyzed whether FnBPA5 peptide preferentially co-localizes with regions rich in mature collagen fibrils as quantified by second harmonic generation (SHG). The SHG signals from the same representative regions show indeed some overlap between collagen rich and FnBPA5 peptide-rich regions. A spatial proximity analysis revealed that 87% of all collagen (SHG) pixels are in close spatial proximity to one or more pixels of FnBPA5 above a threshold. The obtained results are shown in figure 3.4 C and D, together with a schematic representation of this analysis.

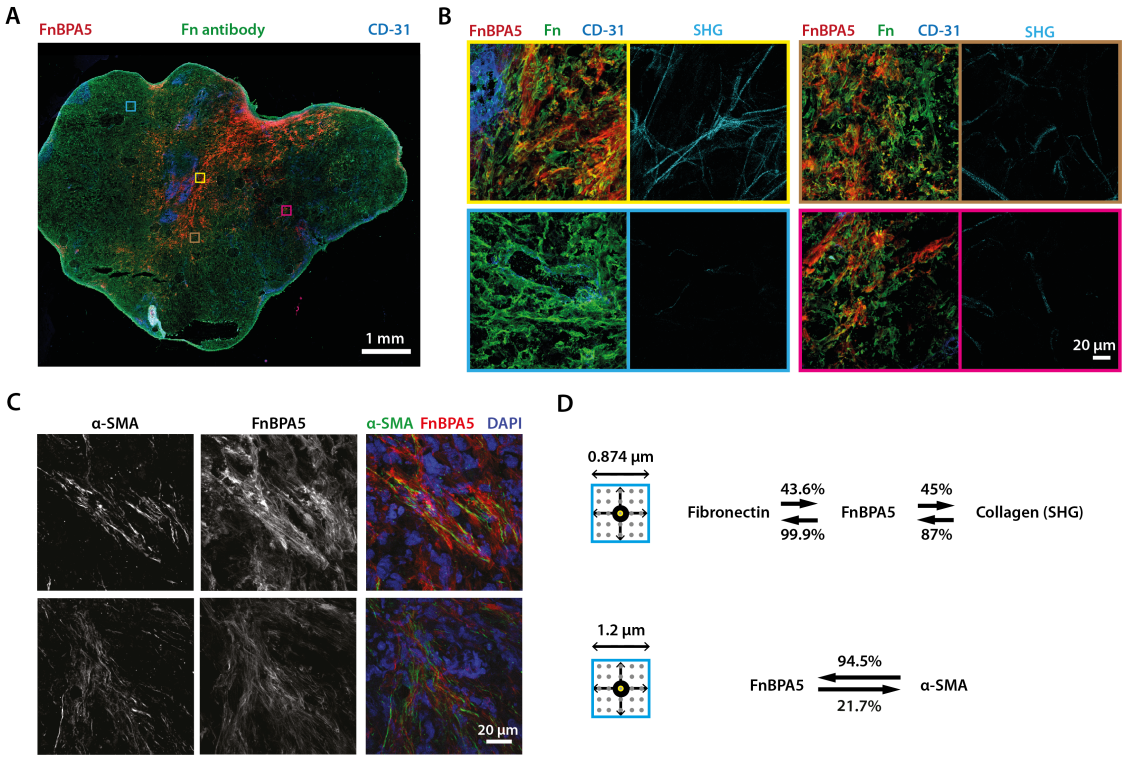

Figure 3.4: *Post-mortem* tumor cryosections from prostate cancer (PC-3) xenografts. **(A)** Overview mosaic image of a whole PC-3 tumor tissue section co-stained with the peptide FnBPA5-Alexa-488 (red), together with antibodies against Fn (green) and endothelial cell marker CD-31 (PECAM-1) (blue). **(B)** Zoomed-in high resolution images of different indicated regions showing superpositions of the stains FnBPA5 (red), fibronectin (green) and CD-31 (blue), as well as the mature collagen fibers in the same regions as visualized by SHG (cyan). **(C)** Representative images of PC-3 tumor tissue section staining of α-SMA and FnBPA5 and merge with nuclei staining using DAPI. **(D)** Respective results for fibronectin, FnBPA5 and Collagen (SHG) and FnBPA5, data analyzed from 19 images and from FnBPA5 and α-SMA, data analyzed from 60 images.

To elucidate the mechanismsm of FnBPA5 binding to Fn in tissues, PC-3 tumor sections were co-stained with FnBPA5-Cy5 and anti-alpha smooth muscle actin (α-SMA), a marker for upregulated cell contractility (Fig. 3.4 C). Surprisingly, we could observe a higher binding of FnBPA5 peptide to regions within the tissue sections adjacent to α-SMA expressing cells (Fig. 3.4 C,D). Increased cellular contractility is generally believed to be mostly triggered by myofibroblastic activation induced by transforming growth factor-β (TGF-β). Interestingly, we could show *in vitro* that human dermal fibroblasts samples stimulated with TGF-β showed significantly higher binding of FnBPA5 (Supplemenatry fig. 3.2 A) but also an overall increase in fibronectin protein level, as observed by Western Blotting, if compared to the untreated control (Supplemenatry fig. 3.2 B), as also previously reported in the literature [56]. Densitometric quantification of blots from 3 independent experiments showed indeed a significant 2.3-fold increase in fibronectin normalized to loading control GAPDH (Supplemenatry fig. 3.2 C), similar to the increase of FnBPA5 binding observed via fluorescence measurement by plate reader. Stimulation to myofibroblastic lineage was controlled for in the α-SMA staining of the blot (Supplemenatry fig. 3.2 B).

FnBPA5 exhibits high plasma stability and can be used for in vivo applications

Peptides usually show low stability to different catalytic enzymes found in tissue and blood, resulting in a short biological half-life, which could significantly limit their *in vivo* application [57]. To show that FnBPA5 can be used *in vivo,* and is not rapidly cleaved by enzymes in the blood plasma, we next performed a plasma stability test. The metabolic stability of the peptide radiotracer ^{111}In-FnBPA5 was tested *in vitro*, in which the radiolabeled FnBPA5 was incubated at 37°C with human blood plasma, or water as control. At different determined time points (0, 1, 24, 48 and 72 hours) the unbound peptide fraction was separated from the plasma proteins and analyzed by reversed-phase high-pressure liquid chromatography (RP-HPLC). Approximately 80% of ^{111}In-FnBPA5 resulted still intact after 72 hours (Supplementary figure 3.3), thus verifying that the radiotracer ^{111}In-FnBPA5 has sufficient plasma stability to be used for *in vivo* applications.

^{111}In-FnBPA5 shows prolonged accumulation in prostate tumor xenografts in vivo

In vivo SPECT/CT analysis was conducted to monitor the distribution of ^{111}In-FnBPA5 up to 96 hours post injection (p.i.). PC-3-bearing mice, a subcutaneous model for human prostate carcinoma, were injected with approximately 15 MBq ^{111}In-FnBPA5 and ^{111}In-scraFnBPA5 (2.4 nmol, 100µL PBS), respectively. ^{111}In-FnBPA5 (Fig. 3.5 A) and the scrambled control peptide (Fig. 3.5 B) mainly accumulated in the kidneys. High renal uptake is a common observation in targeted radionuclide therapy with small peptides (e.g. somatostatin analogues) [58-60]. In the present case, using the scambled control peptide, we excluded a Fn-specific binding in the kidneys. The high renal uptake observed could be related to megalin-mediated endocytosis in the proximal tubules, which is a physiological mechanism ensuring the re-uptake of valuable nutrients [59].

To visualize additional binding of the radiotracers throughout the body, the kidneys were subsequently removed from the sacrificed mice and the scan was repeated. Mice injected with ^{111}In-FnBPA5 showed activity in different organs, with a predominant uptake in tumor, liver and spleen (Figure 3.5 C). In contrast, for mice injected with ^{111}In-scraFnBPA5 no uptake was visible after kidney dissection (Fig. 3.5 D).

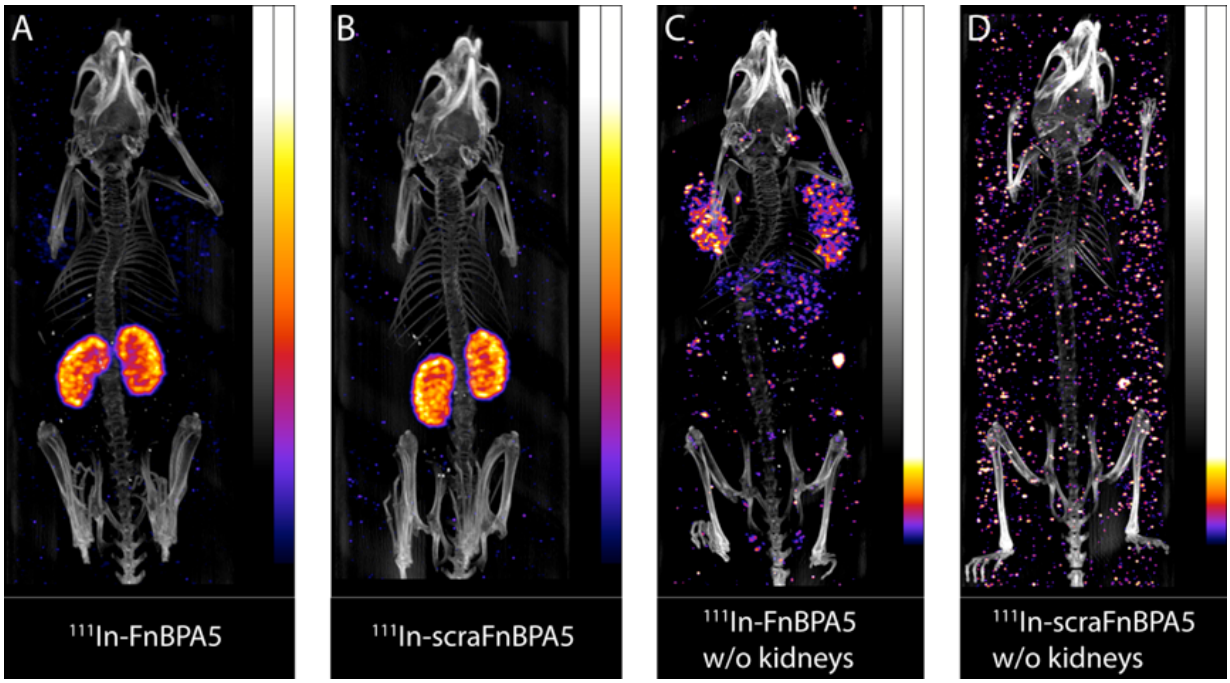

Figure 3.5: SPECT/CT images of mice bearing PC-3 xenografts 96 hours post injection. Mice were injected with 15 MBq ^{111}In-FnBPA5 **(A)** and **C**) ^{111}In-scraFnBPA5 **(B)** and **(D)**, respectively. Images were acquired *post- mortem* 96 hours post injection. In **(A)** and **(B)** dominant kidney uptake of both ^{111}In-FnBPA5 and scrambled control peptide indicate unspecific clearance via the kidney. To assess additional information on peptide distribution within the body kidneys were removed in **(C)** and **(D)** and show uptake in tumors and liver for ^{111}In-FnBPA5, whereas the ^{111}In-scraFnBPA5 control does not show any specific uptake in other organs.

To gain insights into tissue-specific peptide pharmacokinetics, groups of four PC-3-bearing mice were injected with approximately 150 kBq ^{111}In-FnBPA5 and ^{111}In-scraFnBPA5 (2.4 nmol/100µL PBS), respectively. The biodistribution of both tracers was analyzed at determined time points (1, 4, 24 and 96 hours p.i.) by means of percentage of injected activity per gram tissue (% IA / g). An equal accumulation of both peptides was observed in the kidneys (Fig. 3.6 A,B), confirming the findings obtained from SPECT imaging. In both cases, maximal activity was seen at 1 hour p.i. (140 ± 18 % IA / g for ^{111}In-FnBPA5 and 163 ± 18 % IA / g for ^{111}In-scraFnBPA5). In contrast to the scrambled control peptide, ^{111}In-FnBPA5 showed additional accumulation in all other examined organs (Fig. 3.6 A), in particular, in the tumor, the liver and the spleen. These results are in accordance with the SPECT analysis shown in figure 3.5, and illustrate that the organ uptake of ^{111}In-FnBPA5 is, apart from the kidneys, dependent on the peptide's ability to bind Fn. The values were significantly higher compared to the scrambled control peptide at all time points: the tumor uptake was significantly higher with a maximum at 1 h p.i. (4.74 ± 0.77 % IA / g). Interestingly, the tumor-to-blood ratio increased from 3.05 ± 1.66 at 1 h p.i. to 34.03 ± 18.36 at 96 h p.i. and the tumor-to-liver ratio increased from 0.66 ± 0.22 at 1 h p.i. to 2.11 ± 0.82 at 96 h p.i. (Figure 3.6 D and supplementary table 3.1). This indicates that the retention of ^{111}In-FnBPA5 in the tumor was longer compared to other tissue (Figure 3.6 A).

To further confirm the Fn specificity of ^{111}In-FnBPA5, *in vivo* blocking experiments were performed. A 10-fold excess of unlabeled FnBPA5 (24 nmol) was pre-injected directly before ^{111}In-FnBPA5 to saturate binding sites (Fig. 3.6 C and supplementary tables 3.3 and 3.4). The pre-injection of unlabeled FnBPA5 caused a significant

reduction ($p < 0.05$) of ^{111}In-FnBPA5 accumulation in all examined organs with exception of the kidneys and the pancreas (supplementary table 3.3). Furthermore, the blocking effect was less pronounced for the tumor tissue (- 35.6%) than to the liver (- 58.2%). In contrast, no significant differences were seen for ^{111}In-scraFnBPA5 (supplementary table 3.4).

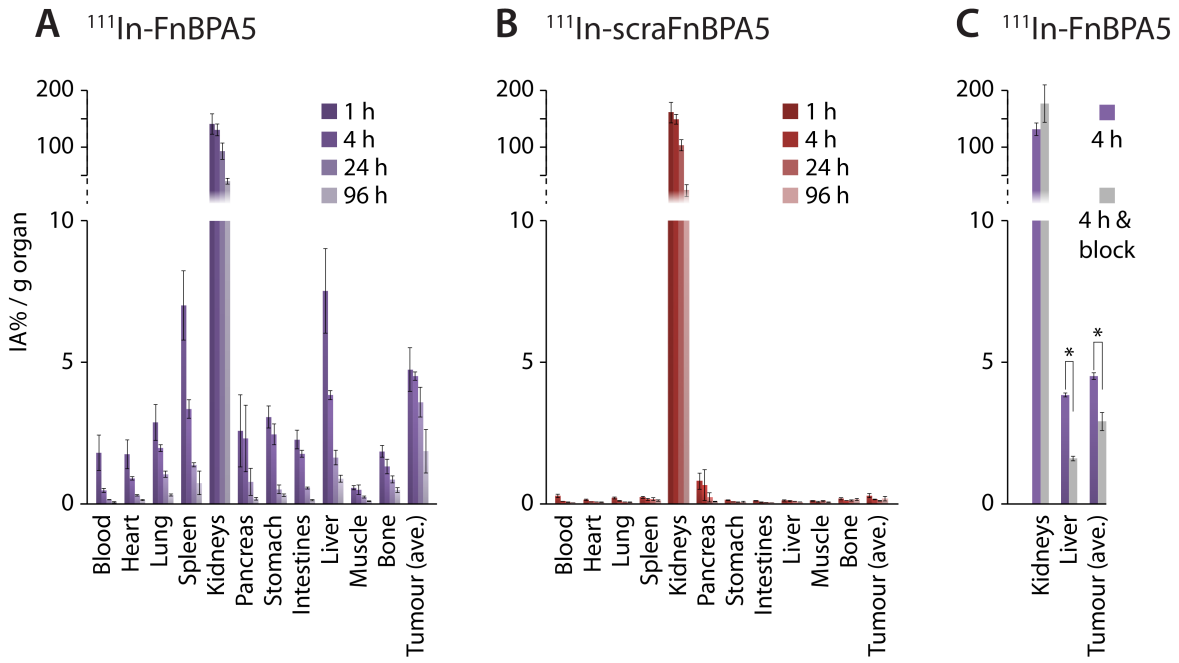

D

^{111}In-FnBPA5	1h p.i	4h p.i	24h p.i	96h p.i
Tumour-to-blood	3.05 ± 1.65	9.68 ± 1.83	23.93 ± 2.52	34.03 ± 18.36
Tumour-to-liver	0.66 ± 0.22	1.18 ± 0.08	2.21 ± 0.25	2.11 ± 0.82

Figure 3.6: Biodistribution and blocking study of radiolabeled ^{111}In-FnBPA5 and ^{111}In-scraFnBPA5. **(A)** The biodistribution of ^{111}In-FnBPA5 in PC-3 bearing mice was monitored at different time points in various organs. **(B)** The biodistribution of ^{111}In-scraFnBPA5 was monitored in the same way. ^{111}In-FnBPA5 (violet) showed a significantly higher uptake than ^{111}In-scraFnBPA5 (red) in all organs except for the kidneys, confirming the Fn-specificity of the accumulation. **(C)** Blocking studies were performed and the uptake was analyzed 4 hour p.i. The blocking of the binding sites via the pre-injection of unlabeled FnBPA5 caused a significant reduction in the uptake of ^{111}In-FnBPA5 in both liver and tumor (*$p < 0.05$) whereas it did not change the uptake in kidneys. The blocking showed a higher influence on ^{111}In-FnBPA5 uptake in the liver than in the tumor, suggesting the presence of a higher amount of binding sites (fibronectin) in the tumor. **(D)** The higher retention time of ^{111}In-FnBPA5 in the tumor is reflected in increasing tumor-to-blood and tumor-to-liver ratios with increasing time.

Discussion

Major transformations of extracellular matrix accompany tumor progression, yet how the crosstalk between extracellular matrix and cells drive these processes remains unknown, at least in part due to the lack of probes to either measure cell traction forces in living tissues or the mechanical strain of extracellular matrix fibers. Fn is a key player within the extracellular matrix [4,16] with Fn fiber assembly and affinities of several binding partners changed by mechanical forces [29,30]. We introduce here the bacterial derived peptide nanoprobe FnBPA5 [47] to assess strain state of Fn fibers in histological tissue sections (Fig. 3.4) and in a living mouse model (Fig. 3.5). In particular, we exploited FnBPA5 as nanoprobe to visualize regions rich in mechanically relaxed Fn fibers in cancer stroma (Fig. 3.4, 3.6).

FnBPA5-Alexa 488 shows strong binding affinity with a K_d in the low nanomolar range to both plasma (Fig. 3.2 D) and to relaxed (Fig. 3.2 E), but not stretched Fn-fibers (Fig. 3.2 B), confirming previously predicted binding behavior from computational steered molecular dynamic simulations [46,47] and *in vitro* binding measurements of native FnBPA5 to N-terminal Fn fragments in solution [48]. The comparision between FnBPA5 and a FRET based strain-sensitive probe for Fn [36,43] demonstreated the strain-sensitive binding of FnBPA5 to Fn in cellular environment. (Fig. 3.3). Staining tissue sections of the PC-3 tumor stroma with a polyclonal Fn-antibody and FnBPA5 (Fig. 3.4) showed that Fn is abundant in tumor tissue, as expected [54,55] and that FnBPA5 binds to specific fractions of Fn within the tissue section. Mature collagen fibers as visualized by SHG tend to colocalize with relaxed Fn-fibers, as 87% of all collagen pixels above a threshold were proximal to FnBPA5 positive pixels (Fig. 3.4 D). Interestingly, co-staining of alpha smooth muscle actin and FnBPA5 shown in figure 3.4 C,D showed a correlation of higher FnBPA5 binding adjacent to α-SMA expressing cells in tumor tissue, it is however not yet fully clear whether this is observed due to relaxation of Fn in these areas, or because of an overall increased presence of Fn in myofibroblasts, as shown *in vitro* for TGF-β stimulated fibroblasts (Supplementary figure 3.2) and reported in the literature [56,61].

Peptides to be used for *in vivo* applications require sufficient plasma stability, which often prohibited their use previously [62-64]. In contrast, our findings show that ^{111}In-FnBPA5 is not rapidly degraded by enzymes in human blood plasma (Supplementary figure 3.3), as 80 % of ^{111}In-FnBPA5 was still intact after 72 hours exposure to plasma *in vitro*. ^{111}In-FnBPA5 thus has adequate serum stability for *in vivo* usage and a superior plasma stability compared to many other radiotracers [62-64]. Upon intravenous injection, SPECT/CT imaging revealed a Fn-specific uptake of ^{111}In-FnBPA5 in PC-3 tumor stroma with an enhanced retention time in tumor tissue compared to other analyzed organs (Fig. 3.5, 3.6). Considerable accumulation of peptides in the kidneys was observed (Fig. 3.5, 3.6), as also typically seen for other peptide radiotracers [58,59]. Kidney uptake was not Fn-specific, as the accumulation was also seen for the scrambled peptide. For possible future *in vivo* applications, different strategies could reduce the renal uptake and thus possible related nephrotoxicity [65]. Uptake in liver, spleen and tumor of ^{111}In-FnBPA5 as revealed by *in vivo* SPECT images and *post-mortem* biodistribution experiments was attributed to the specific binding properties of the FnBPA5 peptide to Fn, in contrast to the scrambled control. Indeed, liver and spleen uptake could be attributed to the intrinsic function of these organs as plasma

Fn excreting organ [66] and as organ for blood filtering from pathogens [67] respectively, with the peptide being cargoed while bound to plasma Fn, as previously reported for other Fn binding peptides [68]. The relatively fast clearance, evidence of liver and spleen uptake of plasma Fn from previous reports [69] as well as the *in vitro* binding studies presented herein (Fig. 3.2 D) further support this notion.
After 24 hours post injection, 3.6 % of the initially injected activity of ^{111}In-FnBPA5 was detected per gram of tumor (Supplementary table 3.1), which is comparable to *in vivo* uptake values of Fn targeting antibodies [70]. The clearance of ^{111}In-FnBPA5 from the tumor was considerably delayed compared to the other organs (Fig 3.6). In particular, the tumor-to-background ratio progressively shifted towards higher values at later time points (Fig. 3.6 and supplementary table 3.1). This prolonged retention of ^{111}In-FnBPA5 in cancerous tissue can be explained by a higher proportion of relaxed Fn fibers, an elevated level of total Fn or a higher amount of uptake of plasma Fn from the bloodstream, and thus an overall increase of available binding sites in the tumor microenvironment. Indeed, additional blocking experiments performed *in vivo* (Fig 3.6 C, Supplementary table 3.3 and 3.4) support this hypothesis as the blocking effect was less pronounced in the tumor compared to the liver.

Taken together, our data suggest that the FnBPA5 peptide can be utilized as probe in histological sections and *in vivo* to actively identify relaxed Fn fibers as illustrated here in tumor tissue. We therefore provide a proof-of-concept that properly engineered peptides can be exploited to probe the mechanical strain of tissue fibers in histological organ sections and in living animals, and that regions dense in relaxed Fn fibers are rather heterogeneously distributed in cancer stroma. This represents a significant advance in this field of research, as previous attempts to probe Fn fiber strain using phage probes did not prove successful *in vivo* and only gave little mechanistic insights [71]. Having a new tool at hand capable of probing ECM fiber tension in tissues may thus facilitate to link previous findings of biochemical alterations in diverse physiological and pathological processes with mechanical aspects inherent to these processes [11,14,20].

While we exploited here the high affinity adhesin FnBPA5 from *S.aureus*, many other bacteria evolved adhesins that target the same N-terminal region on fibronectin. Their sensitivity to the mechanical strain of Fn fibers can easily be adjusted by tuning the linker length between individual binding motifs to FnI modules to either unbind or compensate for the structural mismatch caused by stretching Fn-fibers, which increases the distances between FnI modules [47]. In addition to their high affinity and good plasma stability as illustrated here (Supplementary figure 3.3), peptides are expected to penetrate significantly better into dense stromal tissue structures compared to antibodies because of their smaller size [72,73]. Compared to antibodies and since we had identified one antibody that binds preferentially to stretched Fn fibrils in a stretch assay [3], peptides typically show much lower immunogenicity and solid-phase technology permits to chemically synthesize different ligands with a remarkable low production time and costs [74].

The biomedical implications are highly significant, as the availability of peptides that can probe the tensional state of ECM fibers in tissues, either to stain histological samples (Fig. 3.4) or in living animals (Fig. 3.5), opens up completely new frontiers in mechanobiology, particularly the mechanobiology of cancer and other diseases.

Both tumorigenesis as well as the physiological process of lymph node swelling have been reported to be accompanied by changed cellular contractility of inherent fibroblasts, being upregulated in tumors [61] and downregulated upon lymph node expansion [75-77]. Availability of strain sensitive peptides are essential as first step to carry these large insights obtained at both the molecular and cellular levels towards the tissue level. Since nothing is known at the tissue level regarding the tensional state of Fn in healthy and diseased organs, nor during early development and ageing, the availability of probes that can map the strain of ECM fibrils is crucial to learn how the mechanical strain correlates with cell signaling events and disease progression. Such knowledge is required to finally decipher how the crosstalk between cells and their extracellular matrix is regulated by fiber tension and how the concepts developed regarding ECM proteins acting as mechano-chemical switches [5,78,79] co-regulate tissue growth, homeostasis and pathologies. For a wide range of diagnostic purposes, these newly introduced peptides can easily be adopted to a range of specific biomedical needs by linking them to other labels, custom-built and adapted to case-specific requirements. In our case, the addition of a glycine spacer with an N-terminal cysteine rendered the bacterial Fn-targeting peptides FnBPA5 tunable to be linked to an additional signaling molecule such as an Alexa fluorophore or a chelator for radiolabeling (e.g. NODAGA), without changing its optimized binding properties. We thus anticipate that these and other strain sensitive peptides, perhaps even targeting other extracellular matrix proteins, can be linked to radioisotopes or to other contrast agents allowing to image their distributions by different imaging modalities. Equally well, novel therapeutic approaches are feasible where relaxed Fn fibrils within extracellular matrix are specifically targeted, for example by linking such peptides to drugs or drug carrier systems to be used as therapeutic agents. Finally, these strain sensitive peptides provide new tools for the design of *in vivo* pathology tests to assess whether and to what extent the tensional state of Fn within a tissue is altered. Using high affinity peptides to specifically target and visualize relaxed Fn in tissues, thus also opens the door for understanding the *in vivo* pathology of cancer and potentially many other diseases.

Materials and Methods

Fn isolation and labelling

Fn was isolated from human plasma (Zürcher Blutspendedienst SRK, Switzerland) using gelatin sepharose chromatography, as previously described [80]. Plasma was thawed and passed through a PD-10 column (GE Healthcare, Germany) to remove aggregates. Effluent was collected and run through a gelatin sepharose column. After washing the column Fn was eluted from the gelatin column with a 6M urea solution. Fn was then re-buffered to PBS before usage. For the labelling, Fn was denatured in a 4M guanidinium hydrochloride (GdnHCl) solution to open up cryptic cysteines at $FnIII_7$ and $FnIII_{15}$. The denatured fibronectin was incubated with a 30-fold molar excess of Alexa Fluor 546 C5 maleimide (Invitrogen), for 1 hour at room temperature. Labeled protein was then separated from free dye by passing it through a size-exclusion PD-10 column (GE Healthcare, Germany) into a 0.1 M $NaHCO_3$ solution in PBS. For the second labeling step the protein was incubated for 1 hour with a 70-fold molar excess of Alexa Fluor 488 carboxylic acid succinimidyl ester (Invitrogen) to label free amines. Protein was then separated from dye using a PD-10 column and analyzed for concentration and donor to acceptor labeling ratio by measuring absorption at 280 and 488 and 546 nm. Single labeled Fn was labeled as described above, but only involving the first labeling step using Cy5-maleimide (GE Healthcare).

Chemical denaturation curve of FRET-Fn

For measurement of chemical denaturation curve of double-labeled Fn different denaturation mixtures with increasing concentration of denaturant guanidinium hydrochloride (GdnHCl) was used to extend Fn in solution. To measure the denaturation curve an 8-well LabTek slide was covered with 2% BSA for 1 hour rinsed with water, air-dried and denaturation mixtures were added to the individual wells. The corresponding denaturation curve were measured using an Olympus FV 1000 confocal microscope with a PMT voltage of 550 V for both PMTs and can be found in supplementary figure 3.4.

Synthesis and labelling of FnBPA5 and scrambled FnBPA5

The modified FnBPA5 and scrambled FnBPA5, shown in figure 3.1 D, were commercially synthesised (Peptide Specialty Laboratories GmbH, Heidelberg, Germany, or Pichem GmbH, Graz, Austria). A spacer of three glycines and a cysteine residue at the N-terminus of the original peptide sequence from *S. aureus* were introduced. The cysteine was introduced for further modifications with fluorescent dye (Alexa 488 or Cy5) or with 1-(1,3-caroxypropyl)-1,4,7-triazacyclononane-4,7-diacetic acid (NODAGA), for radiolabeling with ^{111}In. Lyophilized peptides were dissolved in water (TraceSELECT® quality, Sigma-Adrich, Buchs, Switzerland) with 10% DMF and stored at -20°C for further usage.

Fn fiber assay for measurement of affinity and strain-sensitive binding behavior

Fn fibers were manually pulled from a concentrated droplet of Fn in PBS (95% unlabeled and 5% Cy5-labeled protein) using a sharp pipette tip and deposited onto a flexible silicone sheet (SMI, USA), as previously described [51], rinsed and rehydrated in PBS (schematically shown in figure 3.2 C). For affinity measurement Fn fibers were deposited onto a pre-stretched sheet and subsequently relaxed (about 7% strain as defined earlier [31]). For measurement of strain-sensitive binding behavior fibers were either relaxed or stretched (about 380% strain). After a blocking step with bovine serum albumin (BSA, Sigma-Aldrich, Buchs, Switzerland) to avoid unspecific attachment of binding ligands to fibers or silicone sheet the fibers were incubated with varying concentrations of FnBPA5-Alexa 488 or scrambled FnBPA5-Alexa 488 for 1 hour and after a washing step imaged by means of confocal microscopy.

Cell culturing and immunofluorescence staining

Normal human dermal fibroblasts (PromoCell, Vitaris AG, Switzerland) were cultured in alpha minimum essential medium (α-MEM) with 10% foetal bovine serum (FBS) from BioWest (Nuaillé, France), and split before reaching confluence. Cells were seeded onto Fn-coated 8-well chambered cover glasses (Nunc^{TM} Lab-Tek^{TM} Chambered Coverglass, Thermo Fisher Scientific, Reinach, Switzerland) at a density of 50 x 10^3 cells per cm^2 and allowed to attach to the surface before medium exchange to medium containing 50 μg/ml Fn. Dependent on the experiment a fraction of 10% of exogenous Fn was double-labeled for FRET analysis. Cells in figure 3.2 H were cultured for 48 hours. Fibronectin was stained using a rabbit polyclonal anti-fibronectin antibody (1:100 diluted, ab23750, Abcam, Switzerland) and 5 μg/ml FnBPA5-Alexa488 respectively scrambled FnBPA5-Alexa488 peptide for 1 hour. After fixation with a 4% paraformaldehyde solution in PBS the samples were blocked in 4% donkey serum (Abcam, Switzerland) for 1 hour at room temperature. Samples were then incubated for 1 hour with a donkey anti-rabbit Alexa 546 secondary antibody (Invitrogen^{TM}, Thermo Fisher Scientific, Switzerland). Samples in figure 3.3 were fixed similarly and cell nuclei were stained using DAPI (Invitrogen^{TM}, Thermo Fisher Scientific, Switzerland).

FRET analysis

Fn was exogenously added to the cell culture medium at a concentration of 50 μg/ml with a 10 % fraction of double labeled Fn. Fn is then incorporated by the cells into their matrix. FnBPA5-Cy5 was added one hour prior to fixation. For FRET analysis acceptor fluorescence intensity was divided by donor intensity pixel by pixel, to get a FRET ratio at a single-pixel resolution. More stretched Fn conformations exhibited lower fluorescence energy transfer between donors and acceptors and hence a lower acceptor/donor ratio. FnBPA5 binding was quantified in a similar way, by normalizing FnBPA5-Cy5 signal with directly excited acceptor signal of Fn.

Confocal microscopy

Single Fn fiber samples were imaged with an Olympus FV1000 confocal microscope (Olympus AG, Switzerland) using a 40x water immersion objective with a numerical aperture of 0.9. FnBPA5-Alexa 488 and Fn-Cy5 channels were imaged with a 512x512 pixel resolution and photomultiplier tube voltage and laser powers were kept constant within an experiment. Fibroblast ECM samples (Fig. 3.2 E) and FRET samples (Fig. 3.3) were acquired with the same microscope using an oil immersion 1.45 NA 60x objective with a pixel resolution of 1024x1024. Images were acquired with the pinhole diameter fixed at 200 µm and pixel dwell time at 8 µs/pixel. FRET images were acquired as described previously [36]. Briefly, images were taken from fixed matrices using a 50/50 beam splitter. Samples were excited with a 488 nm laser and acceptor (Alexa 546) and donor (Alexa 488) signal was detected in two PMTs using a 12 nm detection bandwidth for donor (514-526 nm) and acceptor (566-578 nm). PMT voltage for FRET imaging was kept constant at 550 V for donor and acceptor PMT. Laser transmissivity was adjusted in order to achieve high detection sensitivity while minimizing photobleaching of samples.

Image analysis

Images were analyzed using Fiji-ImageJ and Matlab (MathWorks, Switzerland). For the Fn fiber affinity study, the pixel-wise ratio of FnBPA5-Alexa 488 signal intensity divided by Fn-Cy5 intensity was calculated for each fiber, if intensities were above a cut-off threshold and below saturation. A mean of 10 fibers was imaged per experiment and each concentration was done in triplicate. Binding ratio of 10 µM FnBPA5-Alexa 488 concentration was set to 1 and all other points were normalized to this reference, fitted and plot using Origin 7 (OriginLab Corp., Northampton, USA). Statistical analysis was performed using two-tailed type 3 student t-test, (Microsoft Excel). The analyses were considered as type 3 (two sample unequal variance) and statistical significance was assumed for p-values smaller than 0.05. For ratiometric analysis of fibroblast matrices (Fig. 3.3) images were smoothed using a 2x2 pixel-averaging filter dark current values were subtracted from images and non-realistic extremes and background were excluded from the analysis. Correction factors for donor bleed through and direct activation of the aceptor used for the analysis were experimentally assessed as shown in supplementary figure 3.4 B,C The ratios of individual channels were then calculated and displayed alongside with a color code for colorimetric illustration of the ratio range of interest. FRET acceptor channel was corrected for donor bleed through which was measured to be approximately 20% of the acceptor intensity (Supplementary figure 3.4 B). Further analysis such as FRET-Fn-FnBPA5/Fn ratio quantification were carried out in MatLab.

Fluorescence polarization experiments

The binding affinities of Fn to FnBPA5-Alexa 488 were determined in three independent measurements by anisotropy titrations in a Cary Eclipse Fluorescence Spectrophotometer (Agilent Technologies, Santa Clara, USA) equipped with automated polarizers. FnBPA5 and the scrambled control peptide were synthesised with an N-terminal Alexa-488 dye (piCHEM GmbH, Graz, Austria). The anisotropy of 100 nM Alexa-488 labeled FnBPA5 was measured in PBS at Fn concentrations ranging from 0 to 1.4 µM. Excitation and emission were at λ_{ex} 480nm and λ_{em} 520nm respectively with both slit 10 nm, 20 °C, 5 s signal acquisition and g=1.4. The K_d values were

determined by fitting the data to a one-site-binding model using Origin 7 (OriginLab Corporation, Northampton, USA).

Preparation and staining of histological tissue sections

5 weeks-old female CD1 nude mice were purchased from Charles River (Germany). After 5 days acclimatisation period, the PC-3 tumour cells (human prostate cancer cell line, ACC-465, DSMZ, Braunschweig, Germany) were subcutaneously inoculated in both shoulders of the mice (5 Mio. cells in 100 µL PBS per side). After 4 weeks inoculation, the mice were sacrificed and frozen tumour tissue was cut into 3 µm sections (Microm Cryo-Star HM 560 M, Walldorf, Germany). Non-fixed tissue sections were thawed, washed with PBS, blocked for 30 min with 4% BSA in PBS and incubated for 60 minutes with 5 µg/ml FnBPA5-Alexa488 or FnBPA5-Cy5. After a washing step the tissues were fixed in 4% paraformaldehyde in PBS for 10 minutes. Samples were blocked in PBS with 5% goat serum for 60 minutes and incubated with polyclonal rabbit anti fibronectin antibody (ab23750, abcam) or rat anti CD-31 antibody (ab7388, abcam) or rabbit anti alpha smooth muscle actin antibody (ab5694, abcam) overnight at 4°C. Primary antibody solution was removed and samples were washed before incubation with secondary goat anti rabbit Alexa 633 (Invitrogen) or goat anti rat Alexa 546 (Invitrogen) or goat anti rabbit Alexa 488 (Invitrogen) antibody solution for 45 minutes. After another washing step samples were mounted using Prolong Antifade Gold with or without DAPI (Invitrogen). Overview mosaic image in figure 3.6 A was acquired using a Nikon TE2000-E epifluorescence microscope equipped with a 10x air objective. Whole tissue section was visualized by stitching together individual fields of view using the grid/collection stitching plugin in Fiji [81].
Images presented in figure 3.6 B were acquired using a Leica SP8 MP microscope. Fn, CD-31 and FnBPA5 were acquired via direct excitation of fluorophores with one photon, whereas second harmonic signal was generated using a 900 nm laser and detecting scattered light in a bandwidth around half the incident wavelength (445-460 nm) with an opened pinhole. Images presented in figure 3.4 C were acquired using a Leica SP-4 confocal microscope with a 63x oil immersion objective.

Evaluation of colocalization of two channels of histological tissue section images

Evaluation of colocalization of two channels as shown in figure 3.4 D was carried out using a custom made Matlab script (MathWorks, Switzerland). High resolution images as shown in figure 3.4 B and 3.4 C were used, images were smoothed using a 2x2 pixel-averaging filter, saturated pixels and background below a specific threshold were furthermore excluded from the analysis. For each pixel in the first channel with an intensity above a lower threshold, a 5x5 surrounding evaluation matrix is created looking for proximal pixels in the second channel above a threshold value. In case of one or more pixels in the second channel being above the threshold, the evaluated pixel from the first channel counts as a pixel proximal to the second channel. The values presented in figure 3.4 D represents the percentage of all pixels of a given channel in proximity to pixels above a threshold of a second channel of the overall number of pixels.

Radiolabelling of FnBPA5-NODAGA and scrambled control peptide scraFnBPA5-NODAGA

The fibronectin binding peptide (FnBPA5) and its scrambled control peptide (scrambled FnBPA5) were purchased from Peptide Specialty Laboratories GmbH (Heidelberg, Germany) conjugated with a maleimide NODAGA. The compounds were dissolved in TraceSELECT® Water (Sigma-Aldrich, Buchs, Switzerland) to a final concentration of 0.25 mM. For the labeling 14 nmol of each peptide were radiolabelled in 0.5 M ammonium acetate pH 5.5 by adding 80 MBq $^{111}InCl_3$ (Mallinckrodt, Wollerau, Switzerland) followed by a 30 minute incubation step at 50° C. Quality control was performed by reversed-phase HPLC (Varian Prostar HPLC System, SpectraLab Scientific Inc., Canada); column Dr.Maisch Reprospher 300 C18-TN, 4.6cm x 150mm; 5µm The column was eluted with acetonitrile containing 0.1 % TFA and Ultrapure water containing 0.1 % TFA and a linear gradient starting with 15 % acetonitrile up to 95 % over 15 minutes with a flow rate of 1 mL/min

In vitro plasma stability

To assess *in vitro* plasma stability 12 MBq ^{111}In-FnBPA5 resp. ^{111}In-scrambled FnBPA5 were incubated with filtered fresh human blood plasma at 37°C. At different time points (0, 0.25, 0.5, 1, 2, 48 and 72 hours) plasma samples were taken out and precipitated by the addition of a solution containing 50% ethanol, 50% acetonitrile and 0.1% TFA. After, the sampled were filtrated using a Thomson Single StEP Filter vial 0.45µm PVDF (Thomson Instrument Company, Oceanside, USA) and the supernatant was analyzed by reversed phase HPLC (Varian Prostar HPLC System, SpectraLab Scientific Inc., Canada) using a D-Bio Discovery Wide Pore C18 column (25 cm x 4.6 mm; 5µm). The column was eluted with acetonitrile containing 0.1 % TFA and Ultrapure water containing 0.1 % TFA and a linear gradient starting with 5 % acetonitrile up to 95 % over 30 minutes with a flow rate of 1 mL/min.

Tumor Model

All the animal experiments were approved by the cantonal authorities (permission number 75531) and conducted in accordance with the Swiss law for animal protection. PC-3 cells (human prostate carcinoma cell line, ACC-465, DSMZ, Braunschweig, Germany) were cultured in RPMI 1640 medium (Roswell Park Memorial Institute 1640 medium, Amimed, Bioconcept, Switzerland). Cells were cultured as monolayers at 37°C in a humidified atmosphere containing 5% CO_2. The 4-5 weeks-old female CD1 nude mice were purchased from Charles River (Sulzfled, Germany). After 5-7 days acclimatization period, the tumor cells were subcutaneously inoculated in both shoulders of the mice ($3*10^6$ – $1*10^7$ cells in 100-150 µL PBS per side). Experiments were performed 3-4 weeks after inoculation.

SPECT/CT imaging and biodistribution studies

SPECT/CT experiments were performed using a 4-head multiplexing multi-pinhole camera (NanoSPECT/CT^{plus}, Bioscan Inc., Washington DC, USA). 33 days from the inoculation of the tumor cells, the mice were intravenously injected with approximately 15 MBq ^{111}In-FnBPA5 resp. ^{111}In-scrambled FnBPA5-NODAGA (2.4 nmol, 100 µL PBS)

into the tail vein. The specific activity of both peptides was 6.2 MBq/ nmol. CT scans were performed with a tube voltage of 45 kV and a tube current of 145 µA. SPECT scans at 96 hours post injection were obtained *postmortem* with an acquisition time of 20-90 sec. per view resulting in a total scanning time of 20-45 min per mouse. SPECT/CT images after kidney removal were obtained with an acquisition time of approximately 20 seconds (^{111}In-FnBPA5) and 200 seconds (^{111}In-scrambled FnBPA5) resulting in a total scanning time of 2.5 h for ^{111}In-scrambled FnBPA5. SPECT images were reconstructed using HiSPECT software (Scivis GmbH, Goettingen, Germany). The images were reconstituted and processed with InVivoScope® software (Bioscan Inc., Washington DC, USA).

For the biodistribution experiments, PC-3 tumor grafted mice were injected into the tail vein with 150 kBq ^{111}In-FnBPA5 or ^{111}In-scrambled FnBPA5 (2.4 nmol, 100 µL PBS). For each peptide, groups of four mice were sacrificed at 1, 4, 24 and 96 hours post injection. Blocking experiment (n=4) was performed by injection of an excess of peptide (100 µg, 24 nmol in 100 µL PBS) directly before the administration of the corresponding radiolabelled peptide. The organs were collected, weighed and counted for activity with a γ counter (Packard Cobra II Auto, Gamma, PerkinElmer AG, Schwerzenbach, Switzerland) 4 hours p.i. The results were expressed as a percentage of injected activity per gram of tissue (%IA / g tissue). The analyses were considered as type 3 (two sample unequal variance) and statistical significance was assumed for p-values smaller than 0.05.

References

[1] E.A. Evans, D.A. Calderwood, Forces and bond dynamics in cell adhesion, Science. 316 (2007) 1148–1153. doi:10.1126/science.1137592.

[2] C.P. Johnson, H.Y. Tang, C. Carag, D.W. Speicher, D.E. Discher, Forced Unfolding of Proteins Within Cells, Science. 317 (2007) 663–666. doi:10.1126/science.1139857.

[3] W.C. Little, R. Schwartlander, M.L. Smith, D. Gourdon, V. Vogel, Stretched Extracellular Matrix Proteins Turn Fouling and Are Functionally Rescued by the Chaperones Albumin and Casein, Nano Lett. 9 (2009) 4158–4167. doi:10.1021/nl902365z.

[4] R.O. Hynes, The Extracellular Matrix: Not Just Pretty Fibrils, Science. 326 (2009) 1216–1219. doi:10.1126/science.1176009.

[5] D.E. Discher, D.J. Mooney, P.W. Zandstra, Growth Factors, Matrices, and Forces Combine and Control Stem Cells, Science. 324 (2009) 1673–1677. doi:10.1126/science.1171643.

[6] M.A. Wozniak, C.S. Chen, Mechanotransduction in development: a growing role for contractility, Nat Rev Mol Cell Biol. 10 (2009) 34–43. doi:10.1038/nrm2592.

[7] I. Schoen, B.L. Pruitt, V. Vogel, The Yin-Yang of Rigidity Sensing: How Forces and Mechanical Properties Regulate the Cellular Response to Materials, Annu. Rev. Mater. Res. 43 (2013) 589–618. doi:10.1146/annurev-matsci-062910-100407.

[8] T. Iskratsch, H. Wolfenson, M.P. Sheetz, Appreciating force and shape — the rise of mechanotransduction in cell biology, Nat Rev Mol Cell Biol. 15 (2014) 825–833. doi:10.1038/nrm3903.

[9] M.J. Paszek, N. Zahir, K.R. Johnson, J.N. Lakins, G.I. Rozenberg, A. Gefen, et al., Tensional homeostasis and the malignant phenotype, Cancer Cell. 8 (2005) 241–254. doi:10.1016/j.ccr.2005.08.010.

[10] P.P. Provenzano, D.R. Inman, K.W. Eliceiri, P.J. Keely, Matrix density-induced mechanoregulation of breast cell phenotype, signaling and gene expression through a FAK–ERK linkage, Oncogene. 28 (2009) 4326–4343. doi:10.1038/onc.2009.299.

[11] J.L. Leight, M.A. Wozniak, S. Chen, M.L. Lynch, C.S. Chen, Matrix rigidity regulates a switch between TGF-β1-induced apoptosis and epithelial-mesenchymal transition, Mol. Biol. Cell. 23 (2012) 781–791. doi:10.1091/mbc.E11-06-0537.

[12] D. Duscher, Z.N. Maan, V.W. Wong, R.C. Rennert, M. Januszyk, M. Rodrigues, et al., Mechanotransduction and fibrosis, Journal of Biomechanics. 47 (2014) 1997–2005. doi:10.1016/j.jbiomech.2014.03.031.

[13] H.B. Schiller, M.-R. Hermann, J. Polleux, T. Vignaud, S. Zanivan, C.C. Friedel, et al., β1- and αv-class integrins cooperate to regulate myosin II during rigidity sensing of fibronectin-based microenvironments, Nature. 15 (2013) 625–636. doi:10.1038/ncb2747.

[14] C.C. DuFort, M.J. Paszek, V.M. Weaver, Balancing forces: architectural control of mechanotransduction, Nat Rev Mol Cell Biol. 12 (2011) 308–319. doi:10.1038/nrm3112.

[15] J.D. Humphrey, E.R. Dufresne, M.A. Schwartz, Mechanotransduction and extracellular matrix homeostasis, Nat Rev Mol Cell Biol. 15 (2014) 802–812. doi:10.1038/nrm3896.

[16] R. Pankov, K.M. Yamada, Fibronectin at a glance, Journal of Cell Science. 115 (2002) 3861–3863.

[17] F. Oyama, S. Hirohashi, Y. Shimosato, K. Titani, K. Sekiguchi, Deregulation of alternative splicing of fibronectin pre-mRNA in malignant human liver tumors, J. Biol. Chem. 264 (1989) 10331–10334.

[18] C. Ffrench-Constant, Reappearance of an embryonic pattern of fibronectin splicing during wound healing in the adult rat, J. Cell Biol. 109 (1989) 903–914. doi:10.1083/jcb.109.2.903.

[19] K.L. Gutbrodt, C. Schliemann, L. Giovannoni, K. Frey, T. Pabst, W. Klapper, et al., Antibody-based delivery of interleukin-2 to neovasculature has potent activity against acute myeloid leukemia, Sci Transl Med. 5 (2013) 201ra118. doi:10.1126/scitranslmed.3006221.

[20] J. Park, J.E. Schwarzbauer, Mammary epithelial cell interactions with fibronectin stimulate epithelial-mesenchymal transition, Oncogene. 33 (2014) 1649–1657. doi:10.1038/onc.2013.118.

[21] C. Ricciardelli, R.J. Rodgers, Extracellular matrix of ovarian tumors, Seminars in Reproductive Medicine. 24 (2006) 270–282.

[22] E. Ruoslahti, Fibronectin and its integrin receptors in cancer, Adv. Cancer Res. 76 (1999) 1–20.

[23] Y.K. Bae, A. Kim, M.K. Kim, J.E. Choi, S.H. Kang, S.J. Lee, Fibronectin expression in carcinoma cells correlates with tumor aggressiveness and poor clinical outcome in patients with invasive breast cancer, Hum. Pathol. 44 (2013) 2028–2037. doi:10.1016/j.humpath.2013.03.006.

[24] M.V. Gulubova, T.I. Vlaykova, Significance of tenascin-C, fibronectin, laminin, collagen IV, alpha5beta1 and alpha9beta1 integrins and fibrotic capsule formation around liver metastases originating from cancers of the digestive tract, Neoplasma. 53 (2006) 372–383.

[25] H. Sil, T. Sen, A. Chatterjee, Fibronectin-Integrin (α5β1) Modulates Migration and Invasion of Murine Melanoma Cell Line B16F10 by Involving MMP-9, Oncol Res. 19 (2011) 335–348. doi:10.3727/096504011X13079697132925.

[26] D.J. O'Shannessy, E.B. Somers, L.K. Chandrasekaran, N.C. Nicolaides, J. Bordeaux, M.D. Gustavson, Influence of tumor microenvironment on prognosis in colorectal cancer: Tissue architecture-dependent signature of endosialin (TEM-1) and associated proteins, Oncotarget. 5 (2014) 3983–3995.

[27] M.J. Bradshaw, M.L. Smith, Multiscale relationships between fibronectin structure and functional properties, Acta Biomaterialia. (2013) 1–8. doi:10.1016/j.actbio.2013.08.027.

[28] E.S. Wijelath, S. Rahman, M. Namekata, J. Murray, T. Nishimura, Z. Mostafavi-Pour, et al., Heparin-II Domain of Fibronectin Is a Vascular Endothelial Growth Factor-Binding Domain: Enhancement of VEGF Biological Activity by a Singular Growth Factor/Matrix Protein Synergism, Circ. Res. 99 (2006) 853–860. doi:10.1161/01.RES.0000246849.17887.66.

[29] C. Zhong, M. Chrzanowska-Wodnicka, J. Brown, A. Shaub, A.M. Belkin, K. Burridge, Rho-mediated contractility exposes a cryptic site in fibronectin and induces fibronectin matrix assembly, J. Cell Biol. 141 (1998) 539–551.

[30] T. Ohashi, H.P. Erickson, Fibronectin Aggregation and Assembly: The unfolding of the second Fibronectin type III domain, Journal of Biological Chemistry. 286 (2011) 39188–39199. doi:10.1074/jbc.M111.262337.

[31] E. Klotzsch, M.L. Smith, K.E. Kubow, S. Muntwyler, W.C. Little, F. Beyeler, et al., Fibronectin forms the most extensible biological fibers displaying switchable force-exposed cryptic binding sites, Proc. Natl. Acad. Sci. U.S.a. 106 (2009) 18267–18272.

[32] M. Mitsi, K. Forsten-Williams, M. Gopalakrishnan, M.A. Nugent, A catalytic role of heparin within the extracellular matrix, J. Biol. Chem. 283 (2008) 34796–34807. doi:10.1074/jbc.M806692200.

[33] A.M.D. Wan, E.M. Chandler, M. Madhavan, D.W. Infanger, C.K. Ober, D. Gourdon, et al., Fibronectin conformation regulates the proangiogenic capability of tumor-associated adipogenic stromal cells, BBA - General Subjects. 1830 (2013) 4314–4320. doi:10.1016/j.bbagen.2013.03.033.

[34] B. Hinz, The extracellular matrix and transforming growth factor-β1: Tale of a strained relationship, Matrix Biol. 47 (2015) 54–65. doi:10.1016/j.matbio.2015.05.006.

[35] S. Vogel, S. Arnoldini, S. Möller, M. Schnabelrauch, U. Hempel, Sulfated hyaluronan alters fibronectin matrix assembly and promotes osteogenic differentiation of human bone marrow stromal cells, Sci. Rep. (2016) 1–13. doi:10.1038/srep36418.

[36] M.L. Smith, D. Gourdon, W.C. Little, K.E. Kubow, R.A. Eguiluz, S. Luna-Morris, et al., Force-Induced Unfolding of Fibronectin in the Extracellular Matrix of Living Cells, Plos Biol. 5 (2007) e268. doi:10.1371/journal.pbio.0050268.sv001.

[37] Y. Zhang, Z. Lin, J. Foolen, I. Schoen, A. Santoro, M. Zenobi-Wong, et al., Disentangling the multifactorial contributions of fibronectin, collagen and cyclic strain on MMP expression and

extracellular matrix remodeling by fibroblasts, Matrix Biol. 40 (2014) 62–72. doi:10.1016/j.matbio.2014.09.001.

[38] K.E. Kubow, R. Vukmirovic, L. Zhe, E. Klotzsch, M.L. Smith, D. Gourdon, et al., Mechanical forces regulate the interactions of fibronectin and collagen I in extracellular matrix, Nature Communications. 6 (2015) 1–11. doi:10.1038/ncomms9026.

[39] E.L. George, E.N. Georges-Labouesse, R.S. Patel-King, H. Rayburn, R.O. Hynes, Defects in mesoderm, neural tube and vascular development in mouse embryos lacking fibronectin, Development. 119 (1993) 1079–1091.

[40] E.A. Lenselink, Role of fibronectin in normal wound healing, Int Wound J. (2013). doi:10.1111/iwj.12109.

[41] D. Greiling, R.A. Clark, Fibronectin provides a conduit for fibroblast transmigration from collagenous stroma into fibrin clot provisional matrix, Journal of Cell Science. 110 (1997) 861–870.

[42] G. Baneyx, L. Baugh, V. Vogel, Coexisting conformations of fibronectin in cell culture imaged using fluorescence resonance energy transfer, Proc. Natl. Acad. Sci. U.S.a. 98 (2001) 14464–14468. doi:10.1073/pnas.251422998.

[43] G. Baneyx, L. Baugh, V. Vogel, Fibronectin extension and unfolding within cell matrix fibrils controlled by cytoskeletal tension, Proc. Natl. Acad. Sci. U.S.a. 99 (2002) 5139–5143. doi:10.1073/pnas.072650799.

[44] B. Henderson, S. Nair, J. Pallas, M.A. Williams, Fibronectin: a multidomain host adhesin targeted by bacterial fibronectin-binding proteins, FEMS Microbiology Reviews. 35 (2010) 147–200. doi:10.1111/j.1574-6976.2010.00243.x.

[45] U. Schwarz-Linek, M. Höök, J.R. Potts, Fibronectin-binding proteins of Gram-positive cocci, Microbes and Infection. 8 (2006) 2291–2298. doi:10.1016/j.micinf.2006.03.011.

[46] M. Chabria, S. Hertig, M.L. Smith, V. Vogel, Stretching fibronectin fibres disrupts binding of bacterial adhesins by physically destroying an epitope, Nature Communications. 1 (2010) 135–9. doi:10.1038/ncomms1135.

[47] S. Hertig, M. Chabria, V. Vogel, Engineering mechanosensitive multivalent receptor-ligand interactions: why the nanolinker regions of bacterial adhesins matter, Nano Lett. 12 (2012) 5162–5168. doi:10.1021/nl302153h.

[48] N.A.G. Meenan, L. Visai, V. Valtulina, U. Schwarz-Linek, N.C. Norris, S. Gurusiddappa, et al., The tandem beta-zipper model defines high affinity fibronectin-binding repeats within Staphylococcus aureus FnBPA, J. Biol. Chem. 282 (2007) 25893–25902. doi:10.1074/jbc.M703063200.

[49] U. Schwarz-Linek, J.M. Werner, A.R. Pickford, S. Gurusiddappa, J.H. Kim, E.S. Pilka, et al., Pathogenic bacteria attach to human fibronectin through a tandem beta-zipper, Nature. 423 (2003) 177–181. doi:10.1038/nature01589.

[50] O.E. Franco, S.W. Hayward, Targeting the Tumor Stroma as a Novel Therapeutic Approach for Prostate Cancer, Advances in Pharmacology, 2012. doi:10.1016/B978-0-12-397927-8.00009-9.

[51] W.C. Little, M.L. Smith, U. Ebneter, V. Vogel, Assay to mechanically tune and optically probe fibrillar fibronectin conformations from fully relaxed to breakage, Matrix Biology. 27 (2008) 451–461. doi:10.1016/j.matbio.2008.02.003.

[52] F. Viti, L. Tarli, L. Giovannoni, L. Zardi, D. Neri, Increased binding affinity and valence of recombinant antibody fragments lead to improved targeting of tumoral angiogenesis, Cancer Research. 59 (1999) 347–352.

[53] W.R. Legant, C.S. Chen, V. Vogel, Force-induced fibronectin assembly and matrix remodeling in a 3D microtissue model of tissue morphogenesis, Integr. Biol. 4 (2012) 1164–1174. doi:10.1039/c2ib20059g.

[54] F.L. Miles, R.A. Sikes, Insidious changes in stromal matrix fuel cancer progression, Mol. Cancer Res. 12 (2014) 297–312. doi:10.1158/1541-7786.MCR-13-0535.

[55] H. Kumra, D.P. Reinhardt, Fibronectin-targeted drug delivery in cancer, Adv. Drug Deliv. Rev. 97 (2016) 101–110. doi:10.1016/j.addr.2015.11.014.

[56] W.D. Xu, E.C. LeRoy, E.A. Smith, Fibronectin release by systemic sclerosis and normal dermal fibroblasts in response to TGF-beta, The Journal of Rheumatology. 18 (1991) 241–246.

[57] M. Fani, H.R. Maecke, Radiopharmaceutical development of radiolabelled peptides, Eur J Nucl Med Mol Imaging. 39 Suppl 1 (2012) S11–30. doi:10.1007/s00259-011-2001-z.

[58] M. Gotthardt, J. van Eerd-Vismale, W.J.G. Oyen, M. de Jong, H. Zhang, E. Rolleman, et al., Indication for different mechanisms of kidney uptake of radiolabeled peptides, Journal of Nuclear Medicine. 48 (2007) 596–601.

[59] E. Vegt, M. Melis, A. Eek, M. Visser, M. Brom, W.J.G. Oyen, et al., Renal uptake of different radiolabelled peptides is mediated by megalin: SPECT and biodistribution studies in megalin-deficient mice, Eur J Nucl Med Mol Imaging. 38 (2010) 623–632. doi:10.1007/s00259-010-1685-9.

[60] M. Béhé, G. Kluge, W. Becker, M. Gotthardt, T.M. Behr, Use of polyglutamic acids to reduce uptake of radiometal-labeled minigastrin in the kidneys, Journal of Nuclear Medicine. 46 (2005) 1012–1015.

[61] R. Kalluri, The biology and function of fibroblasts in cancer, Nat Rev Cancer. 16 (2016) 582–598. doi:doi:10.1038/nrc.2016.73.

[62] F. Nilsson, L. Tarli, F. Viti, D. Neri, The use of phage display for the development of tumour targeting agents, Adv. Drug Deliv. Rev. 43 (2000) 165–196.

[63] S. Zitzmann, W. Mier, A. Schad, R. Kinscherf, V. Askoxylakis, S. Krämer, et al., A new prostate carcinoma binding peptide (DUP-1) for tumor imaging and therapy, Clin. Cancer Res. 11 (2005) 139–146.

[64] C.L. Charron, J.L. Hickey, T.K. Nsiama, D.R. Cruickshank, W.L. Turnbull, L.G. Luyt, Molecular imaging probes derived from natural peptides, Nat Prod Rep. 33 (2016) 761–800. doi:10.1039/c5np00083a.

[65] M. Melis, M. Bijster, M. de Visser, M.W. Konijnenberg, J. de Swart, E.J. Rolleman, et al., Dose-response effect of Gelofusine on renal uptake and retention of radiolabelled octreotate in rats with CA20948 tumours, Eur J Nucl Med Mol Imaging. 36 (2009) 1968–1976. doi:10.1007/s00259-009-1196-8.

[66] J.W. Tamkun, R.O. Hynes, Plasma fibronectin is synthesized and secreted by hepatocytes, J. Biol. Chem. 258 (1983) 4641–4647.

[67] R.E. Mebius, G. Kraal, Structure and function of the spleen, Nat Rev Immunol. 5 (2005) 606–616. doi:10.1093/emboj/19.9.2015.

[68] M.E. Akerman, J. Pilch, D. Peters, E. Ruoslahti, Angiostatic peptides use plasma fibronectin to home to angiogenic vasculature, Proc. Natl. Acad. Sci. U.S.a. 102 (2005) 2040–2045. doi:10.1073/pnas.0409844102.

[69] D.C. Deno, T.M. Saba, E.P. Lewis, Kinetics of endogenously labeled plasma fibronectin: incorporation into tissues, Am. J. Physiol. 245 (1983) R564–75.

[70] L. Borsi, E. Balza, M. Bestagno, P. Castellani, B. Carnemolla, A. Biro, et al., Selective targeting of tumoral vasculature: Comparison of different formats of an antibody (L19) to the ED-B domain of fibronectin, Int. J. Cancer. 102 (2002) 75–85. doi:10.1002/ijc.10662.

[71] L. Cao, M.K. Zeller, V.F. Fiore, P. Strane, H. Bermudez, T.H. Barker, Phage-based molecular probes that discriminate force-induced structural states of fibronectin in vivo, Proc. Natl. Acad. Sci. U.S.a. 109 (2012) 7251–7256. doi:10.1073/pnas.1118088109.

[72] A.I. Minchinton, I.F. Tannock, Drug penetration in solid tumours, Nat Rev Cancer. 6 (2006) 583–592. doi:10.1038/nrc1893.

[73] N. Bertrand, J. Wu, X. Xu, N. Kamaly, O.C. Farokhzad, Cancer nanotechnology: The impact of passive and active targeting in the era of modern cancer biology, Adv. Drug Deliv. Rev. 66 (2014) 2–25. doi:10.1016/j.addr.2013.11.009.

[74] N. Sewald, H.D. Jakubke, Peptides: Chemistry and Biology, Second Edition, Chapter 4: Peptide Synthesis, in: Peptides: Chemistry and Biology, Second Edition, 2nd ed., Wiley-VCH, 2009: pp. 175–315.

[75] J.L. Astarita, V. Cremasco, J. Fu, M.C. Darnell, J.R. Peck, J.M. Nieves-Bonilla, et al., The CLEC-2–podoplanin axis controls the contractility of fibroblastic reticular cells and lymph node microarchitecture, Nat Immunol. 16 (2014) 75–84. doi:10.1038/ni.3035.

[76] S.E. Acton, A.J. Farrugia, J.L. Astarita, D. Mourão-Sá, R.P. Jenkins, E. Nye, et al., Dendritic cells control fibroblastic reticular network tension and lymph node expansion, Nature. 514 (2015) 498–502. doi:10.1038/nature13814.

[77] A.L. Fletcher, S.E. Acton, K. Knoblich, Lymph node fibroblastic reticular cells in health and disease, Nat Rev Immunol. 15 (2015) 350–361. doi:10.1038/nri3846.

[78] O. Peleg, T. Savin, G.V. Kolmakov, I.G. Salib, A.C. Balazs, M. Kröger, et al., Fibers with Integrated Mechanochemical Switches: Minimalistic Design Principles Derived from Fibronectin, Biophys. J. 103 (2012) 1909–1918. doi:10.1016/j.bpj.2012.09.028.

[79] J. Seong, A. Tajik, J. Sun, J.-L. Guan, M.J. Humphries, S.E. Craig, et al., Distinct biophysical mechanisms of focal adhesion kinase mechanoactivation by different extracellular matrix proteins, Proc. Natl. Acad. Sci. U.S.a. 110 (2013) 19372–19377. doi:10.1073/pnas.1307405110.

[80] E. Engvall, E. Ruoslahti, Binding of soluble form of fibroblast surface protein, fibronectin, to collagen, Int. J. Cancer. 20 (1977) 1–5. doi:10.1002/ijc.2910200102.

[81] S. Preibisch, S. Saalfeld, P. Tomancak, Globally optimal stitching of tiled 3D microscopic image acquisitions, Bioinformatics. 25 (2009) 1463–1465. doi:10.1093/bioinformatics/btp184.

Acknowledgements

The authors thank Chantel Spencer and Dr. Isabel Gerber at ETH and Alain Blanc, Christine De Pasquale and Olga Gasser at PSI for technical support, as well as Dr. Ingmar Schoen for the microscopy scripts for mosaic imaging and Dr. Silvia Daniela Jaramillo for helpful discussion. The authors furthermore acknowledge support of the Scientific Center for Optical and Electron Microscopy ScopeM of ETH Zurich.

Supplementary Materials:

Fitting of binding curves in Fig. 3.2 D,E and Supplementary Fig. 3.1

Fitting assumption was a noncooperative binding of our ligand. It was furthermore assumed that free ligand concentration is the same as the initial ligand concentration ([L] = $[L]_0$).

$$\theta = \frac{[L]}{K_d + [L]}$$

θ … Ratio of occupied binding sites divided by total binding sites
[L]… Free (unbound) ligand concentration
K_d … Dissociation constant

Measurement of IC_{50} of ^{nat}In-FnBPA5 upon FnBPA5-488 binding to fibrillar Fn

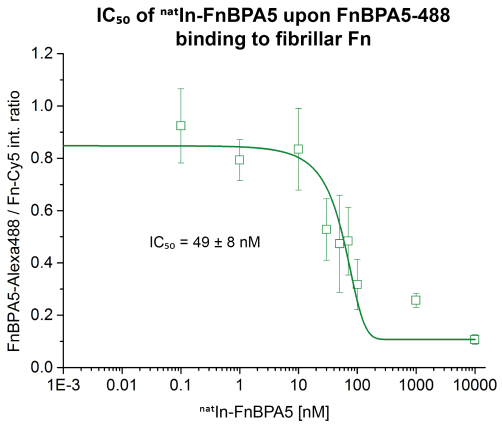

Supplementary figure 3.1: IC_{50} measurement of ^{nat}In-FnBPA5 binding to single Fn fibers. Relaxed Fn fibers were incubated with FnBPA5-Alexa488 peptide, washed and then incubated with different concentrations of In-FnBPA5 to measure the concentration of competitor. At the midpoint between high and low plateau of the curve is the IC_{50} value at 49 ± 8 nM.

Materials and Methods for supplementary figure 3.2

Human dermal fibroblasts were cultured as described in the main text method section and seeded into 12-well plates (TPP, Switzerland) with a density of 50000 cells/well. Cells were allowed to attach for 3 hours before medium change to medium with or without 40 pM TGF-β (Peprotech, Switzerland). Medium was changed every second day and cells were stimulated with TGF-β for 5 days. At day 5 samples were incubated with 5 μg/ml FnBPA5-Alexa488 in serum free medium for 1 hour. After incubation cells were washed in PBS and FnBPA5-Alexa488 fluorescence was immediately afterwards measured using a plate reader (Tecan Infinite M200). One sample always acted as negative control and value was subtracted from samples to be analyzed. After plate reader measurement, cells were scraped off and lyzed using a lysis buffer (20mM TRIS (pH 7.5), 150mM NaCl, 1mM EGTA, 1 mM EDTA, 1% Triton-X-100 in PBS) with protease inhibitor cocktail (Roche, Switzerland). Total protein concentration of individual samples was measured by means of BCA protein assay (Thermo Scientific, Switzerland) and plate reader signal was normalized with overall protein concentration. Loading buffer (5x protein loading buffer with 100 mM dithiothreitol) was added to the lysate and protein concentration was adjusted for even loading and heated to 100°C for 5 minutes. Protein samples were then run on a 4-20% gradient polyacrylamide gel (Bio-Rad, Switzerland). Standard running buffer was used (25 mM Tris, 192 mM Glycine, 0.1% SDS). After protein separation by means of SDS-PAGE, the proteins were transferred on to a nitrocellulose membrane (Amersham Biosciences) using standard transfer buffer (25 mM Tris, 192 mM glycine, 20% methanol) and after transfer blocked in Tris buffered saline (25 mM Tris, 150 mM NaCl) with 4% mild powder. Primary antibodies mouse anti fibronectin antibody clone 10 (BD biosciences, 610077) and rabbit anti GAPDH (Sigma, G9545) were incubated overnight at 4° C. Secondary donkey anti mouse or donkey anti rabbit antibodies conjugated with HRP (Jackson) were incubated for 1 hour and washed before applying Pierce ECL Western Blotting Substrate (Thermo Scientific) and imaging using Hyperfilm ECL (Amersham Biosciences). Densitometric analysis was carried out using Fiji/ImageJ and subsequently Fn bands were normalized with loading control (GAPDH). After initial membrane staining, membranes were stripped using Restore Western Blot Stripping Buffer (Thermo Scientific) for 10 minutes and stained for mouse anti alpha smooth muscle actin antibody clone 1A4 (Sigma, A5228) and developed as described above. Statistical analysis was performed using two-tailed type 3 student t-test, (Microsoft Excel). The analyses were considered as type 3 (two sample unequal variance).

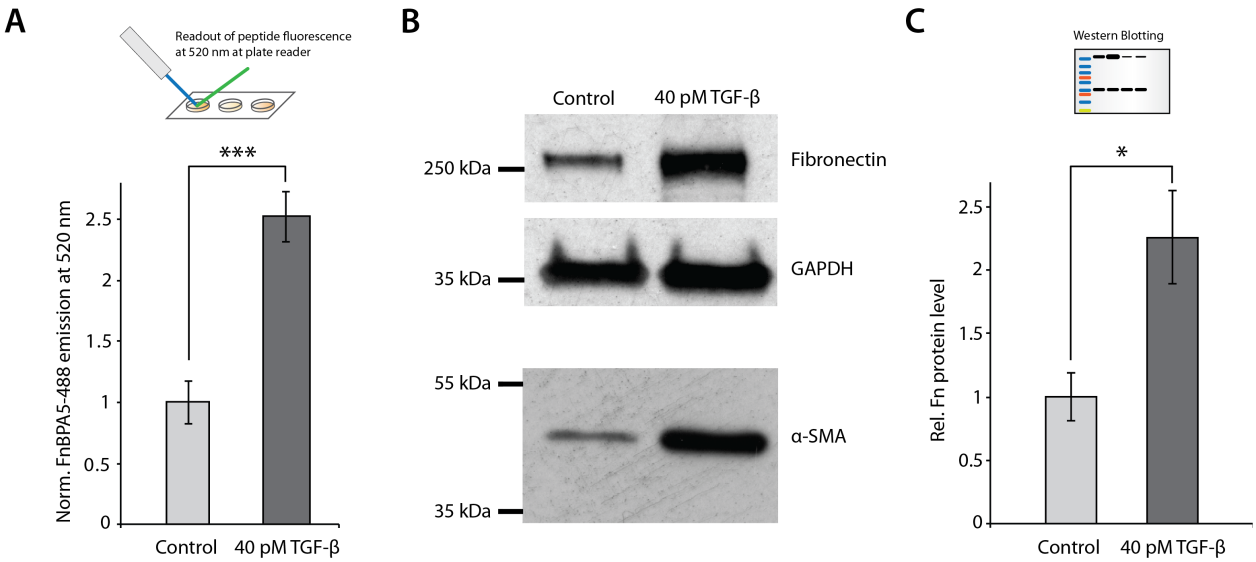

Supplementary figure 3.2: Stimulation of human dermal fibroblasts with TGF-β, measurement of FnBPA5 binding via fluorescence readout using a plate reader and subsequent lysis of cells for quantification of total Fn protein level using Western Blotting. **(A)** TGF-β treated and control samples were incubated with FnBPA5-488, washed and fluorescence of bound FnBPA5 was measured using a plate reader. TGF-β treated samples exhibited a significant 2.5-fold increase in fluorescence signal from FnBPA5-488 ($p<0.001$). After measurement, cells were scraped off the surface and lysed and total protein content was evaluated using a BCA assay. **(B)** Western blotting was carried out with respective protein lysates, revealing a significant higher protein level of Fn in the TGF-β treated sample, compared to the control. GAPDH was used as a loading control to normalize for eventual uneven loading of individual wells. Protein levels of alpha smooth muscle actin indicate that TGF-β treatment indeed worked and led to an increase in expression of myofibroblastic marker. **(C)** Quantification of Western Blots from 3 independent experiments reveal a 2.3-fold, significant increase of Fn protein level normalized with loading control ($p<0.05$), a similar increase in Fn protein level as the increase in FnBPA5 binding, as observed via plate reader measurements.

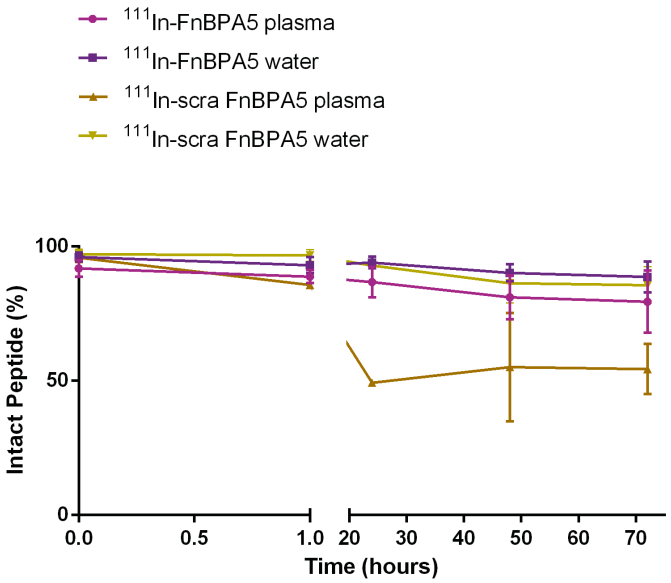

Supplementary figure 3.3: Plasma stability of ^{111}In-FnBPA5 and ^{111}In-scrambled FnBPA5 measured at 37°C at different time points in blood plasma and water. Both ^{111}In-FnBPA5 and ^{111}In-scraFnBPA5 show high stability at 1 hour time point.

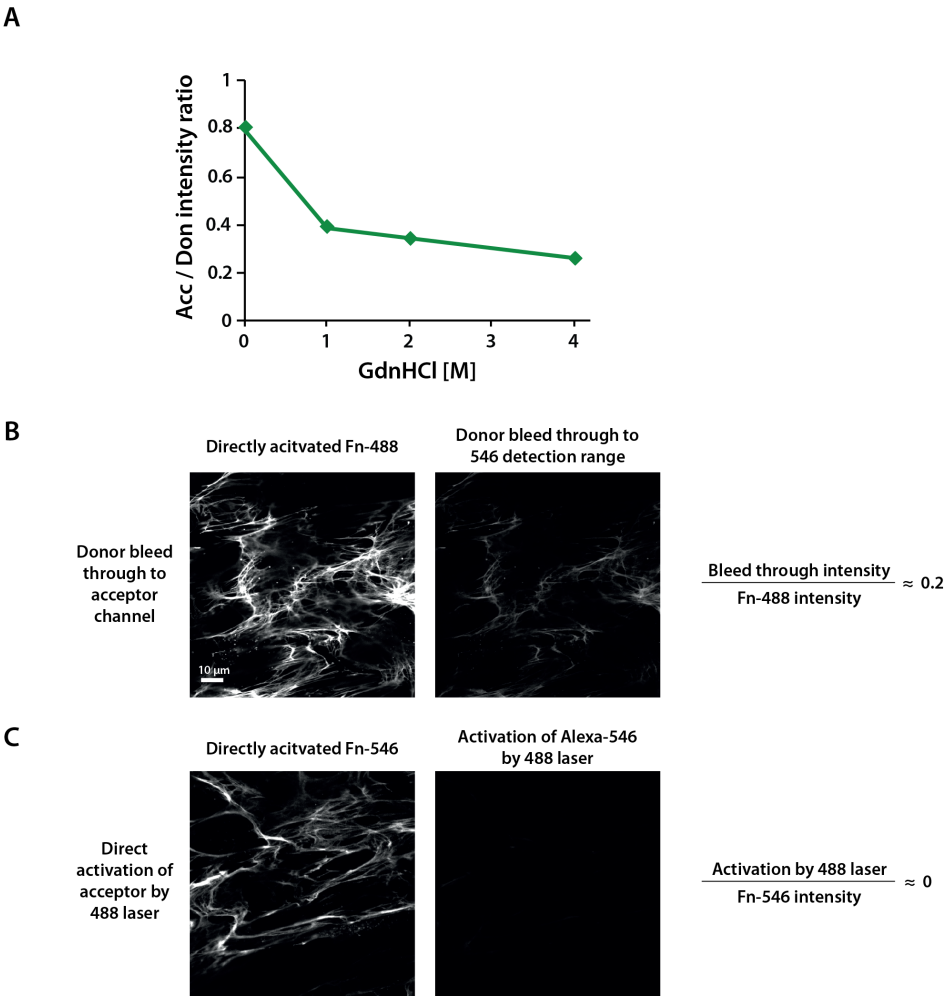

Supplementary figure 3.4: Controls for Fn-FRET experiments. **(A)** Measurement of acceptor/donor intensity ratio of double-labeled Fn in solution under chemical denaturation using increasing concentrations of guanidinium hydrochloride (GdnHCl). Acceptor/donor ratio decreases with increasing concentration of GdnHCl corresponding to an increased opening of the globular structure of plasma Fn and therefore an increase in average distance between donor-acceptor FRET pair. Acceptor channel has been corrected for donor bleed through before calculation of FRET ratio. **(B)** Quantification of donor bleed through to acceptor channel. Donor bleed through to acceptor channel was quantified using a two-day matrix of normal human dermal fibroblasts with exogenous addition of fibronectin to the growth medium (50 µg/ml Fn with 10% single labeled Fn-Alexa 488, randomly labeled at lysines). Quantification of 20 images from 3 different samples showed a 20% bleed through of the donor into the acceptor detection band. The acceptor channel has therefore been corrected in all experiments before calculation of FRET ratio**. (C)** Direct acceptor activation by 488 laser was quantified similarly, but using single-labeled Fn-Alexa 546 labeled at cysteines. Direct activation of acceptor by 488 laser was insignificant and neglected in further quantifications.

Supplementary table 3.1: Biodistribution data of ^{111}In-FnBPA5 in PC-3 grafted mice

^{111}In-FnBPA5, mean IA% / g ± SD (n = 4)				
Dissection time	1 h p.i.	4 h p.i.	24 h p.i.	96 h p.i.
Blood	1.81 ± 0.62	0.48 ± 0.08	0.15 ± 0.008	0.06 ± 0.027
Heart	1.76 ± 0.51	0.91 ± 0.06	0.31 ± 0.025	0.14 ± 0.017
Lung	2.88 ± 0.64	1.98 ± 0.12	1.05 ± 0.11	0.32 ± 0.038
Spleen	7.01 ± 1.23	3.35 ± 0.33	1.38 ± 0.068	0.73 ± 0.417
Kidneys	140.58 ± 18.10	130.66 ± 10.32	92.36 ± 14.25	39.69 ± 4.79
Pancreas	2.58 ± 1.27	2.31 ± 1.18	0.78 ± 0.47	0.18 ± 0.046
Stomach	3.07 ± 0.39	2.46 ± 0.36	0.51 ± 0.15	0.31 ± 0.052
Intestines	2.27 ± 0.33	1.77 ± 0.12	0.57 ± 0.039	0.13 ± 0.02
Liver	7.52 ± 1.50	3.85 ± 0.16	1.64 ± 0.26	0.89 ± 0.12
Muscle	0.57 ± 0.07	0.50 ± 0.17	0.24 ± 0.034	0.095 ± 0.02
Bone	1.85 ± 0.21	1.32 ± 0.26	0.86 ± 0.117	0.50 ± 0.09
Tumor	4.74 ± 0.77	4.51 ± 0.15	3.59 ± 0.53	1.87 ± 0.773
Tumor-to-blood	3.05 ± 1.65	9.68 ± 1.834	23.93 ± 2.52	34.03 ± 18.36
Tumor-to-liver	0.66 ± 0.22	1.18 ± 0.08	2.21 ± 0.25	2.11 ± 0.82
Tumor-to-kidney	0.03 ± 0.00	0.03 ± 0.00	0.04 ± 0.00	0.05 ± 0.02

Supplementary table 3.2: Biodistribution data of the control peptide ^{111}In-scrambled FnBPA5 in PC-3 grafted mice.

	^{111}In-scrambled FnBPA5, mean IA% / g ± SD (n = 4)			
Dissection time	1 h p.i.	4 h p.i.	24 h p.i.	96 h p.i.
Blood	0.26 ± 0.064	0.07 ± 0.008	0.04 ± 0.005	0.02 ± 0.005
Heart	0.12 ± 0.03	0.06 ± 0.006	0.04 ± 0.005	0.04 ± 0.005
Lung	0.19 ± 0.03	0.08 ± 0.005	0.05 ± 0.006	0.04 ± 0.014
Spleen	0.21 ± 0.039	0.13 ± 0.036	0.14 ± 0.048	0.10 ± 0.029
Kidneys	163.70 ± 18.90	151.43 ± 9.056	104.62 ± 9.412	23.63 ± 9.883
Pancreas	0.78 ± 0.295	0.64 ± 0.549	0.21 ± 0.162	0.06 ± 0.016
Stomach	0.12 ± 0.013	0.06 ± 0.006	0.04 ± 0.017	0.04 ± 0.029
Intestines	0.09 ± 0.01	0.04 ± 0.012	0.03 ± 0.00	0.02 ± 0.010
Liver	0.10 ± 0.02	0.08 ± 0.026	0.07 ± 0.010	0.05 ± 0.005
Muscle	0.09 ± 0.025	0.04 ± 0.019	0.08 ± 0.026	0.04 ± 0.013
Bone	0.15 ± 0.035	0.10 ± 0.01	0.09 ± 0.021	0.13 ± 0.036
Tumor	0.27 ± 0.08	0.14 ± 0.02	0.09 ± 0.01	0.16 ± 0.08

Supplementary table 3.3: Blocking experiment: unlabeled FnBPA5 (24 nmol) was intravenously injected directly before ^{111}In-FnBPA5. The analysis was performed 4 hours p.i. * Significance $p < 0.05$.

^{111}In-labelled FnBPA5, mean IA% / g ± SD (n = 4), blocking experiment		
Dissection time	4 h p.i.	4h p.i. blocking
Blood	0.48 ± 0.08	0.29 ± 0.074*
Heart	0.91 ± 0.06	0.37 ± 0.080*
Lung	1.98 ± 0.12	0.95 ± 0.317*
Spleen	3.35 ± 0.33	1.33 ± 0.402*
Kidneys	130.66 ± 10.32	175.80 ± 32.48
Pancreas	2.31 ± 1.18	0.96 ± 0.384
Stomach	2.46 ± 0.36	1.13 ± 0.14*
Intestines	1.77 ± 0.12	0.53 ± 0.137*
Liver	3.85 ± 0.16	1.61 ± 0.56*
Muscle	0.50 ± 0.17	0.20 ± 0.12*
Bone	1.32 ± 0.26	0.73 ± 0.31*
Tumor	4.51 ± 0.15	2.91 ± 0.70*

Supplementary table 3.4: Blocking experiment: unlabeled scrambled FnBPA5 (24 nmol) was intravenously injected directly before ^{111}In-scrambled FnBPA5. The analysis was performed 4 hours p.i., no significant differences were observed

^{111}In-labelled scrambled FnBPA5, mean IA% / g ± SD (n = 4), blocking experiment		
Dissection time	4 h p.i.	4h p.i. blocking
Blood	0.07 ± 0.01	0.07 ± 0.01
Heart	0.05 ± 0.00	0.05 ± 0.01
Lung	0.08 ± 0.01	0.10 ±0.03
Spleen	0.13 ± 0.03	0.18 ± 0.03
Kidneys	151.43 ± 9.06	128.81 ± 17.44
Pancreas	0.64 ± 0.55	1.41 ±1.25
Stomach	0.05 ± 0.01	0.08 ± 0.04
Intestines	0.04 ± 0.01	0.07 ± 0.05
Liver	0.08 ± 0.03	0.08 ± 0.01
Muscle	0.04 ± 0.02	0.04 ± 0.00
Bone	0.09 ± 0.01	0.09 ± 0.01
Tumor	0.14 ± 0.02	0.14 ± 0.04

Chapter 4

Fibronectin fiber strain visualized with a mechanosensitive peptide probe in healthy and tumour tissue and during lymph node swelling

The work presented in this chapter is in preparation for submission:
Simon Arnoldini, Daniela Jaramillo, Alessandra Moscaroli, Annette Oxenius, Martin Behe and Viola Vogel are the authors of this manuscript. Simon Arnoldini conducted all stainings, imaging and analysis within this chapter and Daniela Jaramillo conducted the *in vivo* work, as well as organ excretion of lymph nodes. Alessandra Moscaroli conducted the *in vivo* work, as well as organ excretion and sectioning for the tumor sections. Simon Arnoldini weighed and sectioned the lymph nodes. Simon Arnoldini and Viola Vogel wrote the manuscript.

Abstract

Changes in tensional homeostasis are a driving force of several pathological and physiological tissue changes. However, nothing is known how these changes impact mechanical strain of individual extracellular matrix (ECM) protein fibers within these tissues and thus potentially also the functional display or destruction of binding sites for a plethora of growth factors, cytokines or cells within the ECM. The herein presented utilization of a mechanical probe based on peptide sequences of bacterial origin, specifically binding to relaxed protein fibers of the ECM protein fibronectin (Fn) and not to stretched ones, represents a novel approach to assess the mechanical strain of Fn in tissue sections. Here we show that the Fn binding peptide FnBPA5 can be used to visualize relaxed Fn fibers in tissue and can be exploited to uncover changes in tensional homeostasis in different settings. While tissue sections from healthy organs (lung, liver, heart and kidney) exhibit a stretched state of Fn fibers showing no binding of FnBPA5, tissue section stainings of tumor tissue showed increased binding of FnBPA5 with enhanced signal at Fn fibers adjacent to alpha smooth muscle actin expressing cells. These results indicate that FnBPA5 specifically binds to relaxed Fn not being present in healthy tissue. Binding of FnBPA5 close to alpha smooth muscle actin expressing cells challenges the current dogma stating the existence of a linear relationship between high contractility and stretched ECM proteins. In a model investigating tissue changes during lymph node swelling, FnBPA5 showed increased binding to Fn fibers in virus infected lymph nodes compared to sections from healthy control. Interestingly, treatment with an adjuvant led to lymph node swelling, but did not impact strain state of Fn fibers as peptide binding was in the same range as control tissue. We thus conclude that relaxation of Fn fibers needs an active disorganization of tissue, as occurring in cancer and in viral infection attacking fibroblastic cells within the lymph node. We anticipate that our assay of probing tissue with strain sensitive peptides for Fn represents a novel innovative approach for the better characterization of histological tissue, offering the community a new tool to assess whether a change in Fn fiber strain in a tissue has occurred, and to ultimately link such alterations to changes in cell signaling.

Introduction

In spite of all findings substantiating the importance of mechanoregulated events and their versatile effects on cells [1-3], still only very little is known on how these changes accompany or even trigger homeostatic or pathologic transformations on the tissue level. Changes in cellular forces and extracellular matrix (ECM) stiffness, have been reported for cancer [4-7], different fibrotic disorders [8-11], but also for lymph node swelling as response to acute inflammation [12-14]. As nothing is known about how these changes impact the tensional state of ECM fibers in tissues and since no adequate probes to measure mechanical forces or strains of matrix proteins applicable to 3D tissues exist, no information on these important factors is available so far, thus representing an open field of investigation.

Our focus here is on fibronectin (Fn), representing one of the most abundant ECM proteins with attachment sites for cells, bacteria and a plethora of growth factors, cytokines and matrix molecules [15]. As several binding sites on Fn have been documented to be switched on or off by mechanical forces acting on the molecule, thus changing binding behavior of ligands [16-19] the question arises, whether an upregulated expression and a changed tensional state of Fn in certain settings has an impact on binding and availability of matrix-bound growth factors or cytokines. This is of special interest considering the fact, that increased presence of Fn has been reported in many cancer types [20-24], and is majorly upregulated in tissue and organ fibrosis [3,25].

The recent introduction of new peptide based probes [17,18], measuring strain state of Fn fibers *in vitro*, also being capable of probing tissue sections, offers a unique and novel approach to characterize differences in the tensional state in specific tissues of interest, not possible with other strain probes for Fn such as the previously presented Fn-FRET sensor [26-28]. The utilized peptide sequence was derived from bacterial cell-wall anchored proteins specifically binding to the N-terminus of Fn with high affinity [29]. The herein used peptide FnBPA5 was derived from S. *aureus* and exhibited strain-sensitive binding with high affinity to relaxed Fn fibers, no binding to stretched Fn fibers, and good tissue penetration properties, thus offering significantly more insight as previously presented phage based probes, for which neither exact binding mechanism nor binding affinities are known [30].

Increased presence of fibronectin in many cancer types [20-24], increased cell contractility due to activation of fibroblasts to myofibroblastic phenotype [31], and altered composition and crosslinking of matrix have been identified to be hallmarks for increased tissue rigidity in cancer [6]. These known factors and the complete lack of knowledge regarding the tensional state of ECM fibers in tissues motivated us to firstly investigate healthy and cancerous murine tissue sections. We therefore stained healthy (lung, heart, liver, kidney) and tumor tissue sections of mice with a subcutaneously injected prostate cancer (PC-3) tumor xenograft. Staining for fibronectin and FnBPA5 was carried out to investigate both Fn expression and Fn fiber strain in those tissues. Alpha smooth muscle actin (α-SMA) staining was furthermore carried out to better understand, whether myofibroblastic

differentiation, as previously reported for fibroblasts in cancer [31], might be an influencing factor altering Fn fiber strain and thus FnBPA5 binding to tissue sections from different organs.
Upon immunological challenge lymph nodes drastically increase in size, weight and cellularity and altered cell contractility is an important step in this physiological process [12,13]. It however remains unclear whether and how the strain state of Fn fibers within the reticular fiber network built up by fibroblastic reticular cells (FRCs) in the lymph node's T cell zone [14] is affected by this swelling. To this end we investigated tissue sections from naïve lymph nodes and compared them to sections from mice infected with lymphocytic choriomeningitis virus (LCMV) and with CpG oligodeoxynucleotide adjuvants [32,33]. LCMV infection is an established model system for acute viral infections, with well-characterized properties, known to directly attack FRCs within lymph nodes, thus leading to a depletion of these contractile cells within infected lymph nodes [32]. Adjuvants, such as the CpG oligodeoxynucleotide are biologically inert material that enhance immunity by a variety of mechanisms, lead to lymph node swelling, but do not compromise specific cellular subsets of the immune system [33].

In both of the herein presented model systems, drastic differences in Fn fiber strain were found, observed by different binding of fluorescently labeled FnBPA5 to tissue sections. It was tried to set these differences in relation to Fn content and other known markers for the respective tissues. This study thus presents a first characterization of *in vivo* processes involving changes in tensional homeostasis and could indeed show that FnBPA5 is an adequate tool, capable of visualizing changes in Fn fiber strain between different tissue sections.

Results

To assess whether measurable changes in mechanical strain of Fn fibers within tissue exist, we systematically test two different systems with reported changes in tensional homeostasis between cellular forces and ECM compliance. We therefore probed tissue sections from adult mice of tumors and several healthy organs to determine whether tumorigenesis leads to changed Fn fiber strain in cancerous tissue compared to healthy organ tissue sections. Furthermore, tissue sections from swollen lymph nodes of immunologically challenged mice were stained and compared to sections from naïve lymph nodes with a Fn antibody and fluorescently labeled bacterial Fn binding peptide FnBPA5 selectively attaching to relaxed Fn fibers, using a scrambled peptide derivative as negative control.

FnBPA5 shows no binding to healthy organs but significantly binds to tumor tissue

To assess the tensional state of Fn matrix fibers in different organs we stained tissue sections from lung, heart, liver, kidney and tumor with a polyclonal anti-fibronectin antibody, FnBPA5-Cy5 and DAPI. Representative images of different organs are shown in figure 4.1, giving a first of its kind evidence that Fn fibers in lung, heart, liver and kidney exhibit high mechanical strain, as no specific binding of FnBPA5 peptide was observed (Fig 4.1 B-E). Fn within this homeostatic tissues is more stretched, thus not offering high affinity binding sites for FnBPA5. Quite strikingly, and in contrast to the healthy tissue sections, tumor tissue exhibited high FnBPA5 binding (Fig. 4.1 A), indicating a higher proportion of relaxed Fn fibers within tumor tissue. Binding within tumor tissue however also showed differences dependent on the region within the tissue section. Images from mouse kidney (Fig. 4.1 E) generally show no specific binding of FnBPA5, however binding could be observed in glomerular structures within the kidney tissue. Mouse glomeruli have been reported to have a diameter of around 80 μm [34], and thus correspond to the size of the structure observable in the third image of figure 4.1 E. From figure 4.1 we could see that different tissues are organized differently and that tumor tissue shows drastic increase in FnBPA5 binding, indicating a more relaxed Fn strain state within the tissue. We next asked whether we can correlate increased binding of FnBPA5 to tumor tissue with markers of myofibroblastic differentiation, known to be upregulated in tumor tissue [35].

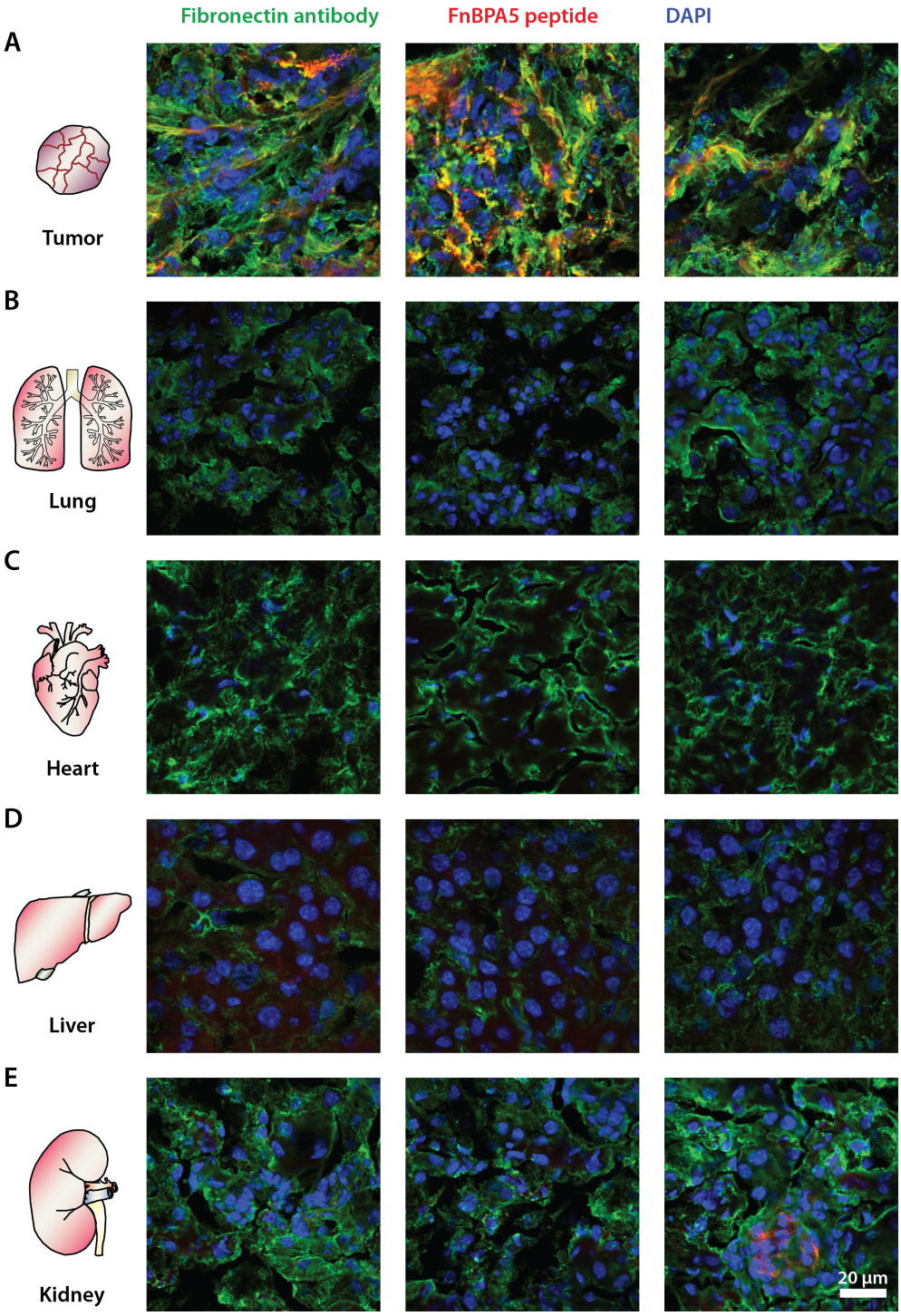

Figure 4.1: Stainings of tissue sections from PC-3 tumor, lung, heart, liver and kidney with Fn antibody (green), FnBPA5-Cy5 (red) and DAPI (blue). **(A)** Tumor tissue shows clear signal from FnBPA5-Cy5 heterogeneously binding to Fn. **(B)** Lung tissue shows Fn, but no binding of FnBPA5-Cy5 indicating stretched conformation of Fn fibers within lung tissue. **(C)** Similar observations were made in heart tissue showing clear presence of Fn, but no binding of FnBPA5-Cy5. **(D)** Liver tissue and **(E)** kidney tissue both show Fn, but little to no binding of FnBPA5. Kidney glomeruli, interestingly show increased binding of FnBPA5-Cy5, as observed in the third image.

FnBPA5 binding to tumor tissue is increased around α-SMA positive cells

As in tumor and fibrotic tissue disorders cellular contractility and ECM production is upregulated [8,36], we next asked whether there is a possible influence of α-SMA expressing cells on Fn fiber strain state in tumor tissue and tissue sections of healthy organs, as visualized using FnBPA5 binding. As α-SMA expression is a well-documented marker for myofibroblasts and has been linked with increased cell contractility and an overall stiffened tissue [35,37], information on the strain state of Fn at and around these cells is especially interesting. While it is generally assumed that higher contractility leads to more stretched ECM fibers, the herein presented results suggest that, at least for Fn, this seems not to be the case. In figure 4.2 representative images of PC-3 cancer tissue sections, as well as tissue sections from lung, heart and liver are stained for anti-alpha smooth muscle actin and FnBPA5. Binding of FnBPA5 around α-SMA expressing cells in tumor sections is clearly visible, and no specific FnBPA5 binding in other organs could be observed. Lung tissue sections show cells expressing α-SMA, however no binding of FnBPA5 could be observed in lung tissue. Interestingly also, areas in tumor sections without myofibroblasts do not show any FnBPA5 binding, similar as observed in healthy tissue sections from lung, liver and heart (Figure 4.2). These data suggest that myofibroblastic lineage induced changes in the ECM of tumor tissue lead to a relaxation of Fn fibers rather than stretching them.

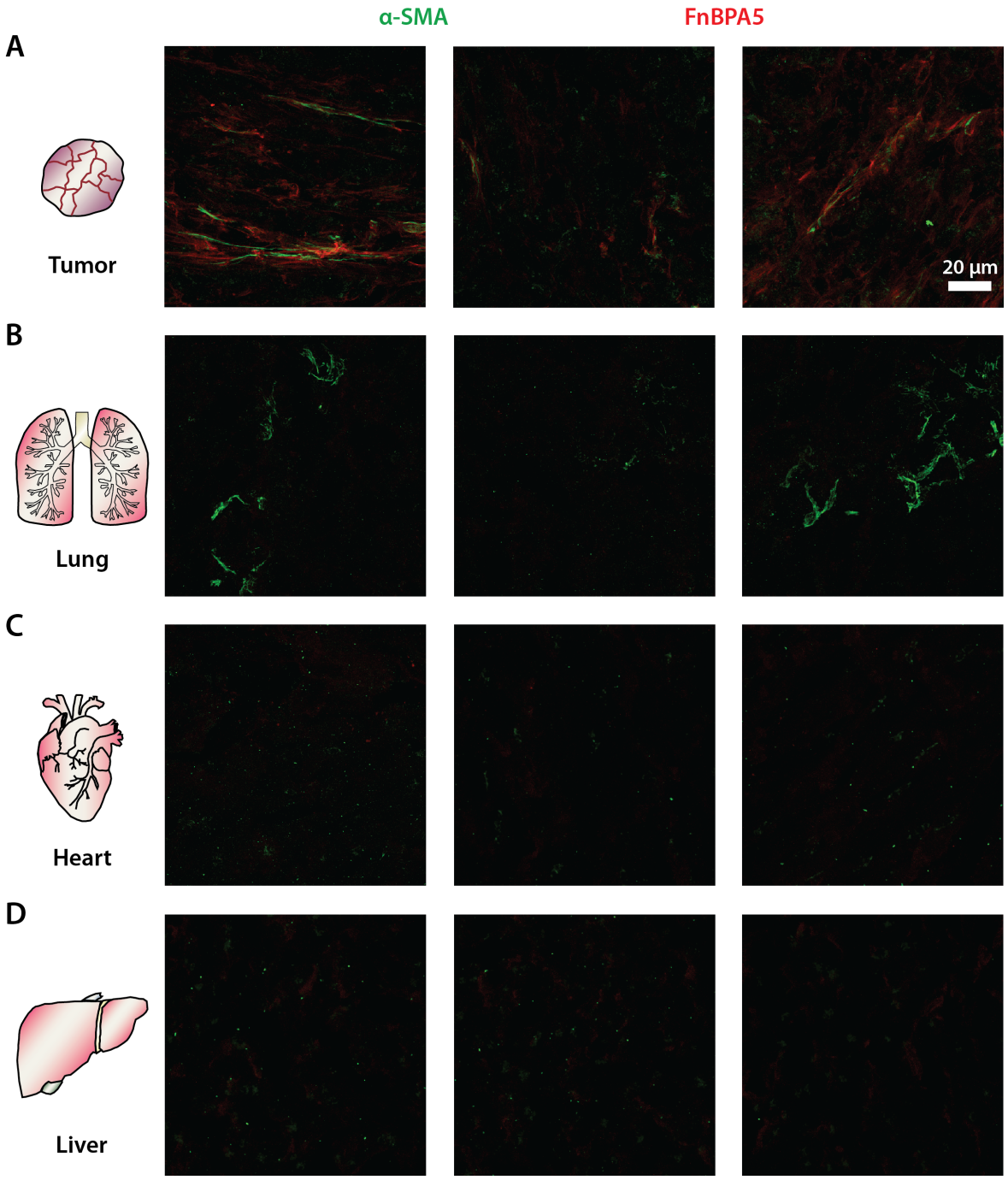

Figure 4.2: Staining of tissue sections from PC-3 tumor xenograft, lung, heart and liver with FnBPA5 and anti-alpha smooth muscle actin (α-SMA) antibody. **(A)** Representative images of PC-3 tumor tissue sections show a clear tendency of higher binding of FnBPA5 adjacent to α-SMA expressing cells within the tissue. **(B)** Tissue sections from lung show expression of α-SMA in a fraction of the cells, however do not show any specific binding of FnBPA5. **(C)**,**(D)** Neither FnBPA5 binding nor α-SMA expressing cells could be observed in heart and liver.

Viral infection but not inflammation leads to differences in Fn strain within lymph nodes

Swollen lymph nodes have long been recognized to be a hallmark for infection and resulting specific immune response. The exact mechanism on the tissue level governing this drastic tissue expansion, have however only recently been discovered [12,13]. A net influx of immune cells presenting antigens to cells within the lymph node for the induction of a specific immune response leads to a fast increase in cellularity within the lymph node. Resident lymph node fibroblasts responsible for the lymph node reticular fiber network have been reported to lose contractility during an infection, thus permitting lymph node expansion. To test the impact of lymph node expansion on Fn strain within lymph node reticular fibers we used lymph nodes from mice being treated with lymphocytic choriomeningitis virus (LCMV) or the adjuvant CpG and compared these treatments to tissue sections from naïve lymph node. For this, groups of 3 mice were injected into the right footpad with PBS, 200 PFU of LCMV or 5 μg CpG and sacrificed 8 days after injection, schematically shown in figure 4.3 A. Schematic lymph node architecture showing B cell follicles and T cell zone with reticular network assembled by fibroblastic reticular cells is shown in figure 4.3 B. Popliteal lymph nodes as draining lymph nodes of the injection site were extracted and weighed to quantify total weight difference between treatments (Fig. 4.3 C). LCMV treated lymph nodes exhibited a significant weight increase ($p<0.01$) if compared to the naïve control lymph nodes. CpG treated lymph nodes also showed a weight increase, due to low sample size of CpG treated mice ($n=3$) this trend was not significant ($p=0.123$). After weighing lymph nodes were embedded in cryomedium frozen and cut into thin sections and subsequently stained with FnBPA5-Cy5 and different antibodies. In figure 4.3 D, 4.3 E and 4.3 F representative sections are shown. Reticular network as visualized by fibronectin antibody staining is clearly visible in all samples, however, binding of FnBPA5 was exclusively seen for lymph node sections from mice treated with LCMV (Fig. 4.3 E). Additionally, co-stainings for collagen-I and FnBPA5 are presented in supplementary figure 4.2 confirming the binding of FnBPA5 to swollen lymph nodes of LCMV treated mice and furthermore show presence of collagen-I in the lymph node's reticular network as previously reported [38]. These findings from the whole tissue section level were confirmed with zoom-in images at different spots within the lymph node sections, only showing binding on FnBPA5 to lymph nodes from LCMV treated mice with heterogeneities in binding between different lymph node zones (Fig. 4.3 G,H,I). Reticular cell and fiber marker ER-TR7 was stained as a control to visualize the reticular fiber network.

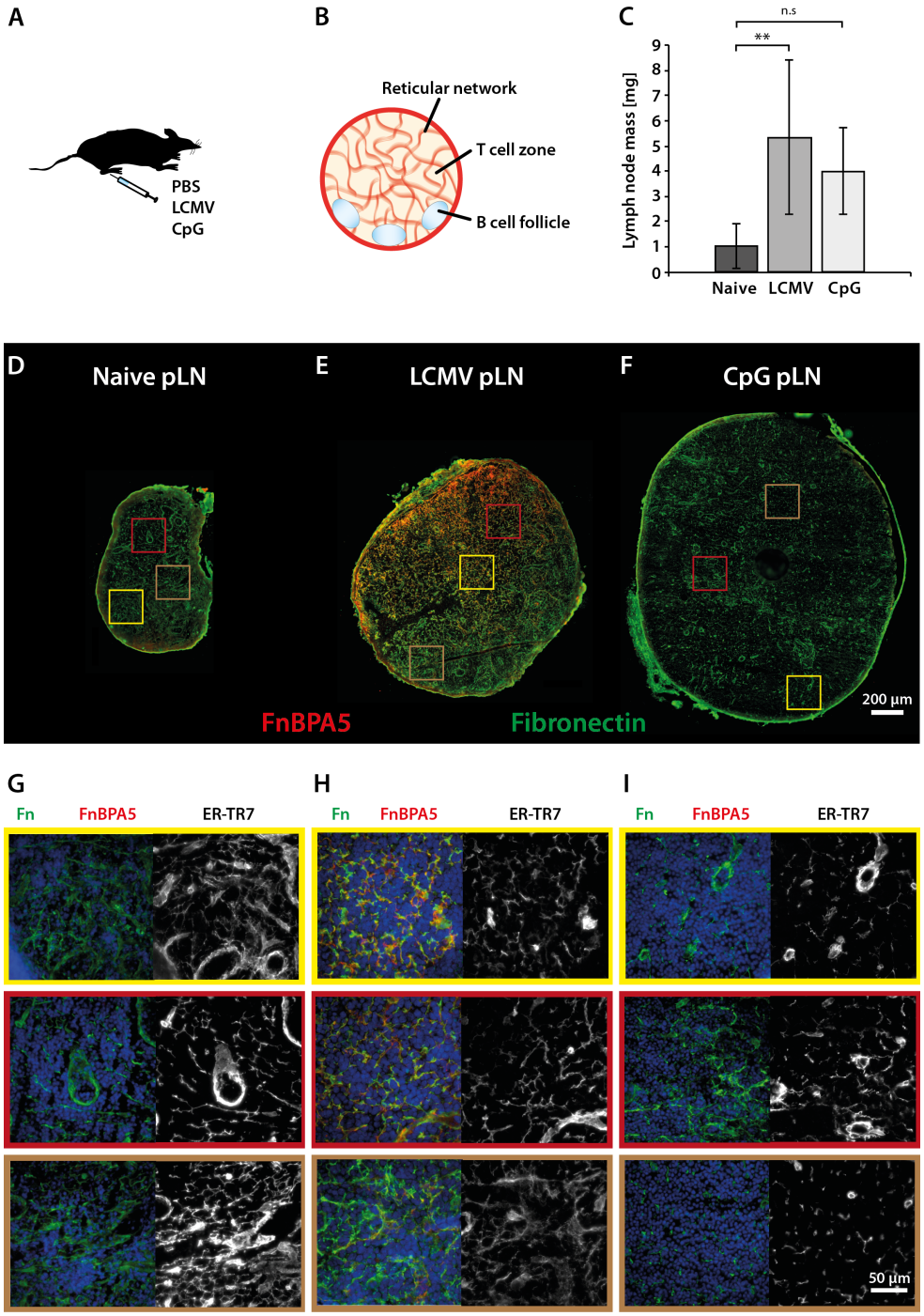

Figure 4.3: Stainings of tissue sections from popliteal lymph nodes from differently treated mice with Fn antibody (green), FnBPA5-Cy5 (red) and DAPI (blue). **(A)** Schematic of experimental setup: Mice were injected intra footpad with PBS, LCMV virus or CpG adjuvant solution. **(B)** Lymph node scheme showing different zones within a lymph node consisting of T-cell and B-cell zone. **(C)** Weight of popliteal lymph nodes 8 days after treatment show significant increase in lymph node mass in LCMV ($p<0.01$) and a non-significant weight increase in CpG treated mice ($p=0.123$). **(D)** Full tissue section image of naïve popliteal lymph node section showing presence of Fn in the reticular network, but no binding of FnBPA5. **(E)** Full tissue section of popliteal lymph node of a LCMV treated mouse showing clear binding of FnBPA5 (red) colocalizing with Fn in the reticular fibers. **(F)** Full tissue section of a popliteal lymph node of a CpG treated mouse showing no binding of FnBPA5 and a drastic decrease in density of reticular fibers due to lymph node swelling. In **(G)**, **(H)**, **(I)** higher resolution zoom-in images of respective areas in (D), (E), (F) are shown together with DAPI staining (blue) alongside with staining from reticular fiber marker ER-TR7.

Discussion

Importance of mechanoregulated processes in homeostasis and different pathologic settings are well characterized [6,8,14,19], however only little is known whether changed cellular forces and tissue rigidity are capable of altering mechanical strain of individual protein fibers within the ECM of the respective tissue, and if this process is capable of inducing long-lasting changes in tissue organization and cell signaling events. Here, two distinctly different models are presented to illustrate that such pathologic transformations within the extracellular matrix are indeed capable of changing Fn fiber strain within tissue. Healthy organs from lung, heart, liver and kidney as well as tumor tissue were probed with the Fn strain probe FnBPA5. Data presented in figure 4.1 reveal for the first time, that Fn within all probed healthy organs is in a relatively high stretch state prohibiting high affinity binding of FnBPA5 and only showed unspecific binding comparable to the scrambled negative control (Supplementary figure 4.1 A). High binding of FnBPA5 and consequent relaxed state of Fn fibers is notably only observed within certain regions of tumor tissue (Fig. 4.1 A). In order to establish an understanding of the underlying mechanisms of tissue change and the selective binding of FnBPA5 peptide to tumor tissue and the absence of binding to healthy organ sections, we costained tissue sections with anti-alpha smooth muscle actin antibody, a marker for myofibroblastic differentiation [35]. As shown in figure 4.2 FnBPA5 showed higher binding in the vicinity of α-SMA expressing cells in tumor tissue and no binding could be observed in regions within the tumor tissue section with no α-SMA positive cells being present. Additionally, no binding of FnBPA5 could be observed to tissue sections from lung, liver and heart, as shown in figure 4.2 B-D. Interestingly though, tissue sections from lung showed α-SMA positive cells, most probably due to the high amount of vascular smooth muscle cells and the overall higher expression level of α-SMA in lung fibroblasts as previously observed [39].

As we hypothesize that Fn relaxation is not only involved in cancer, but also in other processes involving a fast tissue or organ expansion, we investigated different models for lymph node swelling (Fig. 4.3). Lymph node swelling is a process that is well documented and involves relaxation of lymph node fibroblasts [12-14]. Here, we could show that lymph node swelling does not in all cases alter Fn fiber strain within lymph nodes (Fig. 4.3), but is only notably altered in case of an active viral infection with LCMV virus, where a significantly higher binding of FnBPA5 could be observed (Fig. 4.3 E,H), indicating a more relaxed Fn fiber strain, compared to sections from the untreated control (Fig. 4.3 D,G). Interestingly, immunization with the adjuvant CpG led to an increase in lymph node weight (Fig. 4.3 C), but did not lead to an increase of FnBPA5 binding, indicating that Fn fiber strain remains unchanged compared to the naïve control (Fig 4.3 F,I). This gives evidence, that swelling of lymph nodes alone is not enough to change the strain of Fn fibers within the reticular matrix network of lymph nodes. Previous reports from literature indicating that LCMV strongly affected fibroblastic reticular cells through immunopathological mechanisms point out that loss of fibroblasts within the infected lymph node leads to a disruption of the lymphoid architecture especially in the T cell zone [32] that thus may lead to decreased cellular forces and a relaxation of the reticular fiber network.

In summary, our herein presented data indicate, that the well-characterized changes in the tensional equilibrium between cellular forces and extracellular matrix rigidity [4,36,40,41] in tumors and swelling of lymph nodes upon LCMV infections, lead to a relaxation of part of the Fn fibers within the ECM. While in current literature it is generally believed, that increased tissue stiffness and upregulation of cellular contractility in cancer associated fibroblasts, as observed via α-SMA expression and other measures [35,41,42], goes along with more stretched protein fibers within the cancer microenvironment our herein presented data suggest a different interpretation. Enhanced binding of FnBPA5 peptide adjacent to α-SMA expressing cells in tumor tissue sections, as observed in figure 4.2, indicates that fibronectin, or at least the N-terminal region, where FnBPA5 is binding in a strain-sensitive manner, is mechanically relaxed. This relaxation of fibronectin in these specific regions may be caused by well-known alterations in cancer, namely increased presence of specific splice variants of Fn [43-45] and upregulation of collagen content and crosslinking [3,6,46]. Indeed, indications exist that increased presence of collagen fibers lead to a relaxation of Fn fibers, as collagen fibers gradually take over the force-bearing part of the tissue, thus effectively shielding Fn fibers from mechanical forces [47-49]. Another influencing factor could be increased presence and activity of matrix metalloproteinases, known to efficiently disturb the mechanical continuum of ECM fibers in tumor tissue and thus inhibiting propagation of mechanical forces [50,51]. Although the exact mechanism of Fn relaxation in tumors is not given a final explanation in this study, our current results point out, that FnBPA5 could be used as novel tool for the diagnosis of matrix changes in cancer with wide ranging applications for *in vitro* and *in vivo* pathology, which could ultimately be of use for diagnostic purposes and subsequent patient treatment stratification.

We hypothesize here, that a swelling lymph node equilibrates the increase in interstitial tension due to cellular influx with a decrease in FRC contractility [52], thus ending up in having an unchanged strain state of lymph node conduits, as observed in adjuvant treatment as shown here using CpG (Fig. 4.3 F,I). In contrast however, infection with LCMV that directly infects fibroblastic reticular cells within lymph nodes leads to a partial destruction of these cells and thus to a more drastic decrease in cellular forces or even a partial destruction of the continuum of lymph node conduits [14]. This results in a measurable relaxation of the reticular fiber network in the draining lymph nodes at day 8 after infection as visualized in figure 4.3 E,H using bacterial Fn binding peptide FnBPA5. It however remains unclear how the situation in chronic inflammation is comparable to our observation in the LCMV model and how chronic inflammation will influence the mechanical state of the reticular lymph node network, as FRCs are known to be damaged in chronic inflammation as well and lymph node function is drastically compromised due to aberrant accumulation of matrix molecules preventing direct contact of naïve lymphocytes with FRCs and FRC-secreted factors, such as Interleukin-7 crucial for lymph node recovery from infections [14]. As Interleukin-7 is known to bind to fibronectin in the extracellular space and to induce T cell adhesion to fibronectin [53] mechanical alterations of Fn could have mechanistic consequences in either the release of IL-7 or the masking of IL-7-T cell binding sites, thus potentially contributing to T cell loss or T cell exhaustion, as observed during lymph node fibrosis.

Although we see Fn fiber relaxation in both models presented here the exact mechanism how Fn gets mechanically relaxed are likely to be different and remain partially unclear. Different possible scenarios, such as ECM cleaving, cell death, changed cell contractility, or changed matrix composition and crosslinking as well as alterations in the cell-ECM interlinks have been discussed to be responsible for a relaxation of Fn within the ECM. To elucidate the exact mechanisms in different pathologic scenarios the herein used peptide probe could be very valuable as measurement and visualization tool for mechanical changes rather than expression levels of proteins or alterations in certain cell types and may facilitate a deeper understanding of mechanically triggered cell signaling events in these settings.

In conclusion it can be said that the use of FnBPA5 to probe Fn fiber strain in tissue in different settings offers considerable new insight in how Fn fiber strain changes during the course of processes such as tumorigenesis or viral host infection. In contrast to previous phage-based probes introduced to measure Fn strain in a previous study [30], for the herein used peptide probe exact location of binding, binding affinity and mechanism of strain-sensitive affinity switch are known. Usage of this novel probe could deepen and expand current knowledge of mechano regulated processes. Giving special attention to strain state of fibronectin is important, as it has binding sites for a great diversity of growth factors and cytokines, such as Interleukin-7 (IL-7) in lymph nodes [53], or the latent complex of transforming growth factor-beta (TGF-β) [42,54,55], with possible structure function changes upon force application on Fn fibers. As nothing is known on this matter, this study presents a first broad mapping of Fn fiber strain in different organs and different systems, showing clear indications that FnBPA5 can be readily utilized in the future for strain measurement of Fn fibers in different physiological and pathological settings, thus offering a novel diagnostic tool capable of linking changed protein expression levels and cell signaling events with alterations in Fn fiber strain within tissue sections of interest.

Materials and Methods

Synthesis and labelling of FnBPA5 and scrambled FnBPA5

FnBPA5 (CGGGQVTTESNLVEFDEESTKGIVTGAVSDHTTVEDTK) and scrambled FnBPA5 (CGSEQEDLTGTKVDFGETIVVNEATETVTSGSTHGTKV) were commercially synthesized (Pichem GmbH, Graz, Austria). The N-terminal cysteine was used for further modifications with Cy5-maleimide fluorescent dye. Lyophilized peptides were dissolved in phosphate buffered saline (PBS) and stored at -20°C for further usage.

Preparation of PC-3 xenograft mice

5 weeks-old female CD1 nude mice were purchased from Charles River (Germany). All the animal experiments were approved by the cantonal authorities and conducted in accordance with the Swiss law for animal protection. PC-3 tumor cells (human prostate cancer cell line, ACC-465, DSMZ, Braunschweig, Germany) were subcutaneously inoculated in both shoulders of the mice (5 Mio. cells in 100 µL PBS per side) after a 5 days acclimatization period. After 4 weeks inoculation, the mice were sacrificed and organs were extracted, embedded in cryomedium, frozen and cut into 3 µm sections (Microm Cryo-Star HM 560 M, Walldorf, Germany) and placed on Superfrost Plus microscopy slides (Thermo Scientific, USA) and stored at -80°C until further usage.

Preparation of naïve, LCMV and CpG infected murine lymph node tissue sections

Wild-type C57BL/6 mice were purchased from Janvier Elevage (Le Genest St. Isle, France) and bred under pathogen free conditions. Mice used for the experiments were 6-12 weeks of age and sex-matched. All the animal experiments were approved by the cantonal authorities and conducted in accordance with the Swiss law for animal protection. LCMV-WE was obtained from Dr. R.M Zinkernagel (University Hospital Zurich) and propagated in L929 fibroblast cells. CpG oligonucleotide 1668 (TCCATGACGTTCCTGATGCT, phosphorothioate backbone) was synthesized by Mycrosynth (Balgach, Switzerland). Mice were injected with 200 PFU LCMW WE in 50 µL sterile PBS, 5 µg CpG in 50 µL sterile PBS or only 50 µL PBS (control). Mice were sacrificed 8 days after injection and left and right popliteal and inguinal lymph nodes were extracted, weighed and subsequently embedded in Tissue-Tek O.C.T. compound (Sakura, Tokyo, Japan) in Tissue-Tek 4565 disposable vinyl specimen molds (Cryomold Biopsy, Sakura, Tokyo, Japan), frozen and stored at -80°C before sectioning. Lymph nodes were sectioned using a histology cryotome (Thermo Fisher CryoStar NX70, Thermo Scientific, USA) and placed on Superfrost Plus microscopy slides (Thermo Scientific, USA). 8 µm thick cut sections were then stored at -80°C until further usage.

Staining of histological tissue sections

Non-fixed tissue sections were thawed, washed with PBS, and after a small circle with a hydrophobic DAKO pen (DAKO, Denmark) was drawn, blocked for 30 min with 4% BSA in PBS and subsequently incubated for 60 minutes with 5 µg/ml FnBPA5-Cy5 or scra-FnBPA5-Cy5. After a washing step the tissues were fixed in 4% paraformaldehyde in PBS for 10 minutes. Samples were blocked in PBS with 5% goat serum for 60 minutes and incubated with polyclonal rabbit anti fibronectin antibody (ab23750, abcam, Cambridge, UK), or polyclonal rabbit anti alpha smooth muscle actin antibody (ab5694, abcam, Cambridge, UK), or monoclonal rat anti reticular fibroblasts and reticular fibers (ER-TR7) antibody (ab51824, abcam, Cambridge, UK) overnight at 4°C. Primary antibody solution was removed and samples were washed before incubation with secondary goat anti rabbit Alexa 488 (Invitrogen) or goat anti rat Alexa 546 (Invitrogen) antibody solution for 45 minutes. After another washing step samples were mounted using Prolong Antifade Gold mounting medium with DAPI (Invitrogen) and glass coverslips were sealed with transparent nail polish. After a two day curing period of the mounting medium the samples were imaged.

Imaging of histological tissue sections

Images presented in figure 4.1 were acquired using an Olympus FV-1000 confocal microscope with a 60x oil immersion objective. Images presented in figure 4.2 were acquired using a Leica SP-4 confocal microscope with a 63x oil immersion objective. Images in figures 4.3 showing whole tissue sections were acquired using a Nikon TE2000-E epifluorescence microscope equipped with a 40x air objective. Whole tissue sections were visualized by stitching together individual fields of view using the grid/collection stitching plugin in Fiji [56].

References

[1] D.E. Discher, D.J. Mooney, P.W. Zandstra, Growth Factors, Matrices, and Forces Combine and Control Stem Cells, Science. 324 (2009) 1673–1677. doi:10.1126/science.1171643.

[2] J.D. Humphrey, E.R. Dufresne, M.A. Schwartz, Mechanotransduction and extracellular matrix homeostasis, Nat Rev Mol Cell Biol. 15 (2014) 802–812. doi:10.1038/nrm3896.

[3] C. Bonnans, J. Chou, Z. Werb, Remodelling the extracellular matrix in development and disease, Nat Rev Mol Cell Biol. 15 (2014) 786–801. doi:10.1038/nrm3904.

[4] M.J. Paszek, N. Zahir, K.R. Johnson, J.N. Lakins, G.I. Rozenberg, A. Gefen, et al., Tensional homeostasis and the malignant phenotype, Cancer Cell. 8 (2005) 241–254. doi:10.1016/j.ccr.2005.08.010.

[5] K.R. Levental, H. Yu, L. Kass, J.N. Lakins, M. Egeblad, J.T. Erler, et al., Matrix Crosslinking Forces Tumor Progression by Enhancing Integrin Signaling, Cell. 139 (2009) 891–906. doi:10.1016/j.cell.2009.10.027.

[6] C.C. DuFort, M.J. Paszek, V.M. Weaver, Balancing forces: architectural control of mechanotransduction, Nat Rev Mol Cell Biol. 12 (2011) 308–319. doi:10.1038/nrm3112.

[7] F.L. Miles, R.A. Sikes, Insidious changes in stromal matrix fuel cancer progression, Mol. Cancer Res. 12 (2014) 297–312. doi:10.1158/1541-7786.MCR-13-0535.

[8] D. Duscher, Z.N. Maan, V.W. Wong, R.C. Rennert, M. Januszyk, M. Rodrigues, et al., Mechanotransduction and fibrosis, Journal of Biomechanics. 47 (2014) 1997–2005. doi:10.1016/j.jbiomech.2014.03.031.

[9] C. Margadant, A. Sonnenberg, Integrin-TGF-beta crosstalk in fibrosis, cancer and wound healing, EMBO Rep. 11 (2010) 97–105. doi:10.1038/embor.2009.276.

[10] T.R. Cox, J.T. Erler, Remodeling and homeostasis of the extracellular matrix: implications for fibrotic diseases and cancer, Dis Model Mech. 4 (2011) 165–178. doi:10.1242/dmm.004077.

[11] M. Zeisberg, R. Kalluri, Cellular Mechanisms of Tissue Fibrosis. 1. Common and organ-specific mechanisms associated with tissue fibrosis, AJP: Cell Physiology. 304 (2013) C216–C225. doi:10.1152/ajpcell.00328.2012.

[12] J.L. Astarita, V. Cremasco, J. Fu, M.C. Darnell, J.R. Peck, J.M. Nieves-Bonilla, et al., The CLEC-2–podoplanin axis controls the contractility of fibroblastic reticular cells and lymph node microarchitecture, Nat Immunol. 16 (2014) 75–84. doi:10.1038/ni.3035.

[13] S.E. Acton, A.J. Farrugia, J.L. Astarita, D. Mourão-Sá, R.P. Jenkins, E. Nye, et al., Dendritic cells control fibroblastic reticular network tension and lymph node expansion, Nature. 514 (2015) 498–502. doi:10.1038/nature13814.

[14] A.L. Fletcher, S.E. Acton, K. Knoblich, Lymph node fibroblastic reticular cells in health and disease, Nat Rev Immunol. 15 (2015) 350–361. doi:10.1038/nri3846.

[15] V. Vogel, Mechanotransduction involving multimodular proteins: converting force into biochemical signals, Annu Rev Biophys Biomol Struct. 35 (2006) 459–488. doi:10.1146/annurev.biophys.35.040405.102013.

[16] W.C. Little, R. Schwartlander, M.L. Smith, D. Gourdon, V. Vogel, Stretched Extracellular Matrix Proteins Turn Fouling and Are Functionally Rescued by the Chaperones Albumin and Casein, Nano Lett. 9 (2009) 4158–4167. doi:10.1021/nl902365z.

[17] M. Chabria, S. Hertig, M.L. Smith, V. Vogel, Stretching fibronectin fibres disrupts binding of bacterial adhesins by physically destroying an epitope, Nature Communications. 1 (2010) 135–9. doi:10.1038/ncomms1135.

[18] S. Hertig, M. Chabria, V. Vogel, Engineering mechanosensitive multivalent receptor-ligand interactions: why the nanolinker regions of bacterial adhesins matter, Nano Lett. 12 (2012) 5162–5168. doi:10.1021/nl302153h.

[19] D.J. Tschumperlin, G. Dai, I.V. Maly, T. Kikuchi, L.H. Laiho, A.K. McVittie, et al., Mechanotransduction through growth-factor shedding into the extracellular space, Nature. 429 (2004) 83–86. doi:10.1038/nature02543.

[20] C. Ricciardelli, R.J. Rodgers, Extracellular matrix of ovarian tumors, Seminars in Reproductive Medicine. 24 (2006) 270–282.

[21] D.J. O'Shannessy, E.B. Somers, L.K. Chandrasekaran, N.C. Nicolaides, J. Bordeaux, M.D. Gustavson, Influence of tumor microenvironment on prognosis in colorectal cancer: Tissue architecture-dependent signature of endosialin (TEM-1) and associated proteins, Oncotarget. 5 (2014) 3983–3995.

[22] M.V. Gulubova, T.I. Vlaykova, Significance of tenascin-C, fibronectin, laminin, collagen IV, alpha5beta1 and alpha9beta1 integrins and fibrotic capsule formation around liver metastases originating from cancers of the digestive tract, Neoplasma. 53 (2006) 372–383.

[23] Y.K. Bae, A. Kim, M.K. Kim, J.E. Choi, S.H. Kang, S.J. Lee, Fibronectin expression in carcinoma cells correlates with tumor aggressiveness and poor clinical outcome in patients with invasive breast cancer, Hum. Pathol. 44 (2013) 2028–2037. doi:10.1016/j.humpath.2013.03.006.

[24] J. Park, J.E. Schwarzbauer, Mammary epithelial cell interactions with fibronectin stimulate epithelial-mesenchymal transition, Oncogene. 33 (2014) 1649–1657. doi:10.1038/onc.2013.118.

[25] A. Leask, D.J. Abraham, TGF-β signaling and the fibrotic response, The FASEB Journal. (2004).

[26] G. Baneyx, L. Baugh, V. Vogel, Coexisting conformations of fibronectin in cell culture imaged using fluorescence resonance energy transfer, Proc. Natl. Acad. Sci. U.S.a. 98 (2001) 14464–14468. doi:10.1073/pnas.251422998.

[27] M.L. Smith, D. Gourdon, W.C. Little, K.E. Kubow, R.A. Eguiluz, S. Luna-Morris, et al., Force-Induced Unfolding of Fibronectin in the Extracellular Matrix of Living Cells, Plos Biol. 5 (2007) e268. doi:10.1371/journal.pbio.0050268.sv001.

[28] I. Schoen, B.L. Pruitt, V. Vogel, The Yin-Yang of Rigidity Sensing: How Forces and Mechanical Properties Regulate the Cellular Response to Materials, Annu. Rev. Mater. Res. 43 (2013) 589–618. doi:10.1146/annurev-matsci-062910-100407.

[29] B. Henderson, S. Nair, J. Pallas, M.A. Williams, Fibronectin: a multidomain host adhesin targeted by bacterial fibronectin-binding proteins, FEMS Microbiology Reviews. 35 (2010) 147–200. doi:10.1111/j.1574-6976.2010.00243.x.

[30] L. Cao, M.K. Zeller, V.F. Fiore, P. Strane, H. Bermudez, T.H. Barker, Phage-based molecular probes that discriminate force-induced structural states of fibronectin in vivo, Proc. Natl. Acad. Sci. U.S.a. 109 (2012) 7251–7256. doi:10.1073/pnas.1118088109.

[31] R. Kalluri, The biology and function of fibroblasts in cancer, Nat Rev Cancer. 16 (2016) 582–598. doi:doi:10.1038/nrc.2016.73.

[32] E. Scandella, B. Bolinger, E. Lattmann, S. Miller, S. Favre, D.R. Littman, et al., Restoration of lymphoid organ integrity through the interaction of lymphoid tissue-inducer cells with stroma of the T cell zone, Nat Immunol. 9 (2008) 667–675. doi:10.1038/ni.1605.

[33] R.L. Coffman, A. Sher, R.A. Seder, Vaccine Adjuvants: Putting Innate Immunity to Work, Immunity. 33 (2010) 492–503. doi:10.1016/j.immuni.2010.10.002.

[34] D.A. Rytand, The number and size of mammalian glomeruli as related to kidney and to body weight, with methods for their enumeration and measurement, American Journal of Anatomy. (1938) 507–520.

[35] R. Kalluri, M. Zeisberg, Fibroblasts in cancer, Nat Rev Cancer. 6 (2006) 392–401. doi:10.1038/nrc1877.

[36] M.S. Samuel, J.I. Lopez, E.J. McGhee, D.R. Croft, D. Strachan, P. Timpson, et al., Actomyosin-Mediated Cellular Tension Drives Increased Tissue Stiffness and b-Catenin Activation to Induce Epidermal Hyperplasia and Tumor Growth, Cancer Cell. 19 (2011) 776–791.

doi:10.1016/j.ccr.2011.05.008.

[37] J.L. Leight, A.P. Drain, V.M. Weaver, Extracellular Matrix Remodeling and Stiffening Modulate Tumor Phenotype and Treatment Response, Annu. Rev. Cancer Biol. 13 (2016) 17.1–17.22. doi:10.1146/annurev-cancerbio-050216-034431.

[38] M. Sixt, N. Kanazawa, M. Selg, T. Samson, G. Roos, D.P. Reinhardt, et al., The Conduit System Transports Soluble Antigens from the Afferent Lymph to Resident Dendritic Cells in the T Cell Area of the Lymph Node, Immunity. 22 (2005) 19–29. doi:10.1016/j.immuni.2004.11.013.

[39] V. Dugina, A. Alexandrova, C. Chaponnier, J. Vasiliev, G. Gabbiani, Rat fibroblasts cultured from various organs exhibit differences in alpha-smooth muscle actin expression, cytoskeletal pattern, and adhesive structure organization, Exp. Cell Res. 238 (1998) 481–490. doi:10.1006/excr.1997.3868.

[40] F. Kai, H. Laklai, V.M. Weaver, Force Matters: Biomechanical Regulation of Cell Invasion and Migration in Disease, Trends in Cell Biology. (2016) 1–12. doi:10.1016/j.tcb.2016.03.007.

[41] R. Malik, P.I. Lelkes, E. Cukierman, Biomechanical and biochemical remodeling of stromal extracellular matrix in cancer, Trends Biotechnol. 33 (2015) 230–236. doi:10.1016/j.tibtech.2015.01.004.

[42] B. Hinz, The extracellular matrix and transforming growth factor-β1: Tale of a strained relationship, Matrix Biol. 47 (2015) 54–65. doi:10.1016/j.matbio.2015.05.006.

[43] P. Castellani, G. Viale, A. Dorcaratto, G. Nicolo, J. Kaczmarek, G. Querze, et al., The fibronectin isoform containing the ED-B oncofetal domain: A marker of angiogenesis, Int. J. Cancer. 59 (1994) 612–618.

[44] S. Sauer, P.A. Erba, M. Petrini, A. Menrad, L. Giovannoni, C. Grana, et al., Expression of the oncofetal ED-B-containing fibronectin isoform in hematologic tumors enables ED-B-targeted 131I-L19SIP radioimmunotherapy in Hodgkin lymphoma patients, Blood. 113 (2009) 2265–2274. doi:10.1182/blood-2008-06-160416.

[45] A. Villa, E. Trachsel, M. Kaspar, C. Schliemann, R. Sommavilla, J.-N. Rybak, et al., A high-affinity human monoclonal antibody specific to the alternatively spliced EDA domain of fibronectin efficiently targets tumor neo-vasculature in vivo, Int. J. Cancer. 122 (2008) 2405–2413. doi:10.1002/ijc.23408.

[46] H.E. Barker, T.R. Cox, J.T. Erler, The rationale for targeting the LOX family in cancer, Nat Rev Cancer. 12 (2012) 540–552. doi:10.1038/nrc3319.

[47] K.E. Kubow, R. Vukmirovic, L. Zhe, E. Klotzsch, M.L. Smith, D. Gourdon, et al., Mechanical forces regulate the interactions of fibronectin and collagen I in extracellular matrix, Nature Communications. 6 (2015) 1–11. doi:10.1038/ncomms9026.

[48] J.-F. Groulx, D. Gagné, Y.D. Benoit, D. Martel, N. Basora, J.-F. Beaulieu, Collagen VI is a basement membrane component that regulates epithelial cell-fibronectin interactions, Matrix Biol. 30 (2011) 195–206. doi:10.1016/j.matbio.2011.03.002.

[49] P. Sabatelli, P. Bonaldo, G. Lattanzi, P. Braghetta, N. Bergamin, C. Capanni, et al., Collagen VI deficiency affects the organization of fibronectin in the extracellular matrix of cultured fibroblasts, Matrix Biol. 20 (2001) 475–486.

[50] C. Gialeli, A.D. Theocharis, N.K. Karamanos, Roles of matrix metalloproteinases in cancer progression and their pharmacological targeting, FEBS Journal. 278 (2010) 16–27. doi:10.1111/j.1742-4658.2010.07919.x.

[51] M. Egeblad, Z. Werb, New functions for the matrix metalloproteinases in cancer progression, Nat Rev Cancer. 2 (2002) 161–174. doi:10.1038/nrc745.

[52] S.E. Acton, C. Reis e Sousa, Dendritic cells in remodeling of lymph nodes during immune responses, Immunol. Rev. 271 (2016) 221–229. doi:10.1111/imr.12414.

[53] A. Ariel, R. Hershkoviz, L. Cahalon, D.E. Williams, S.K. Akiyama, K.M. Yamada, et al., Induction of T cell adhesion to extracellular matrix or endothelial cell ligands by soluble or matrix-bound interleukin-7,

Eur. J. Immunol. 27 (1997) 2562–2570. doi:10.1002/eji.1830271015.

[54] N.C. Henderson, T.D. Arnold, Y. Katamura, M.M. Giacomini, J.D. Rodriguez, J.H. McCarty, et al., Targeting of alpha-v integrin identifies a core molecular pathway that regulates fibrosis in several organs, Nat Med. 19 (2013) 1617–1624. doi:10.1038/nm.3282.

[55] N.C. Henderson, D. Sheppard, Integrin-mediated regulation of TGFβ in fibrosis, Biochimica Et Biophysica Acta (BBA) - Molecular Basis of Disease. 1832 (2013) 891–896. doi:10.1016/j.bbadis.2012.10.005.

[56] S. Preibisch, S. Saalfeld, P. Tomancak, Globally optimal stitching of tiled 3D microscopic image acquisitions, Bioinformatics. 25 (2009) 1463–1465. doi:10.1093/bioinformatics/btp184.

Supplementary information

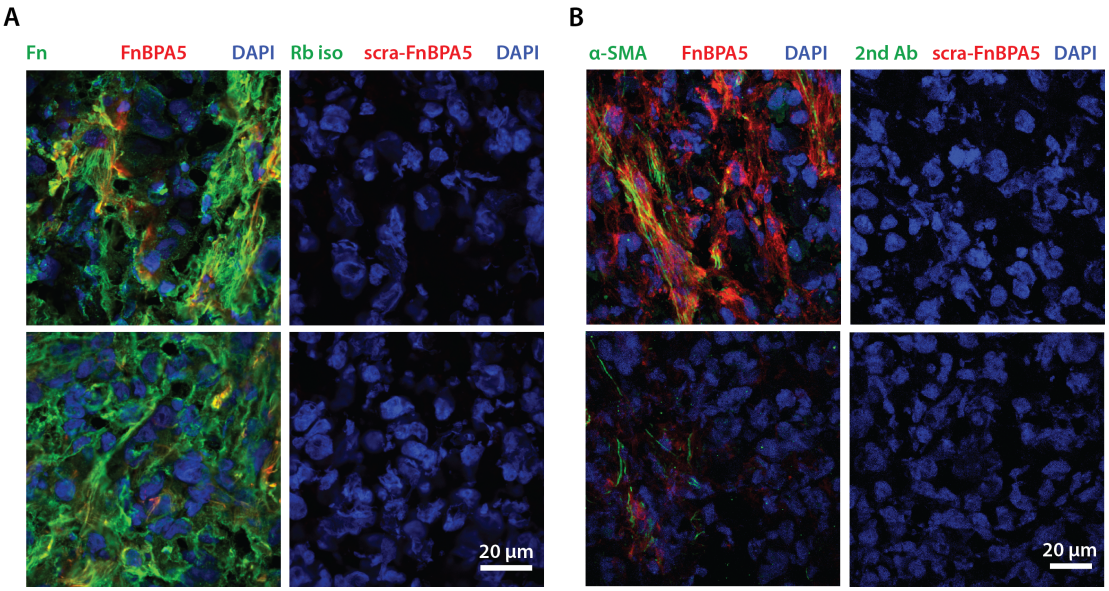

Supplementary figure 4.1: Scrambled negative control of FnBPA5 peptide experiments. **(A)** 2 representative images of PC-3 tumor tissue stained with anti Fn antibody and FnBPA5-Cy5 on the left panel and respective negative control of the same tissue stained with Cy5 labeled scrambled control of FnBPA5 and rabbit IgG isotype control with respective secondary antibody on the right panel. **(B)** 2 representative images of PC-3 tumor tissue stained with anti α-SMA antibody and FnBPA5-Cy5 on the left panel and respective negative control of the same tissue stained with Cy5 labeled scrambled control of FnBPA5 and secondary antibody only, on the right panel.

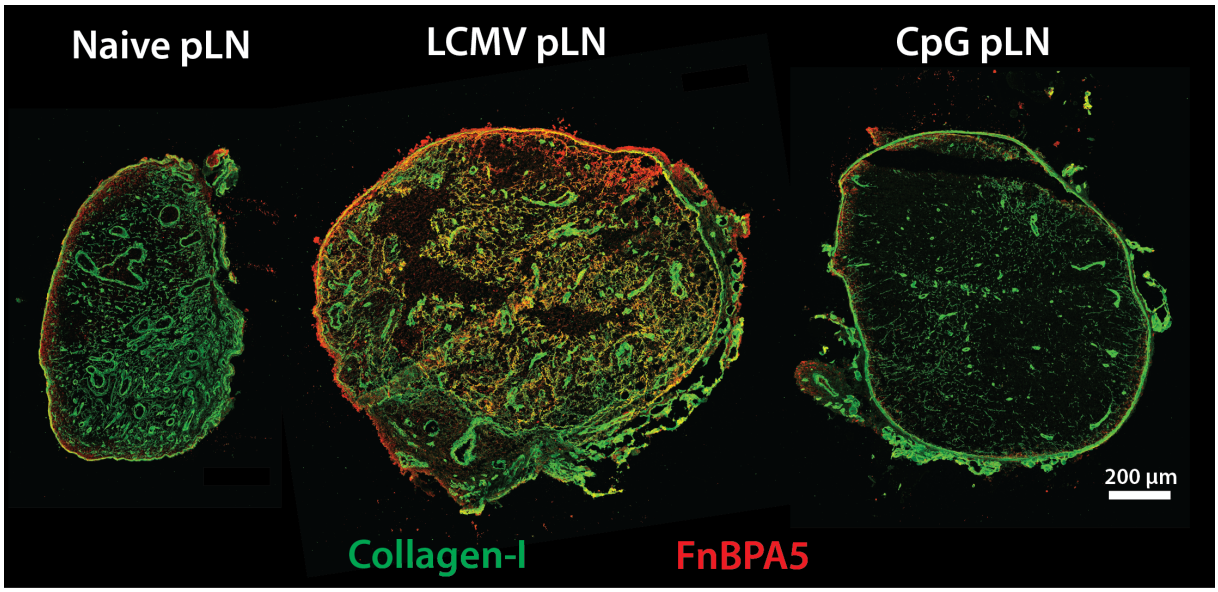

Supplementary figure 4.2: Lymph node sections stained for Collagen-I (ab34710, abcam, Cambridge, UK) and FnBPA5-Cy5 imaged at Leica-SP8 confocal microscope. Shown images are stitched together from individual tile images.

Chapter 5

Influence of glycosaminoglycan sulfation on Fn binding and binding competition with FnBPA5

The preliminary data set presented in this chapter is still in preparation. Simon Arnoldini, Sarah Vogel, Ute Hempel and Viola Vogel are the authors of this manuscript. Simon Arnoldini conducted all imaging and data analysis, as well as all experiments involving manually pulled Fn fibers in this chapter, and put together all figures presented herein. Sarah Vogel conducted all cell culture work and cell stimulation experiments in this chapter and provided synthetically sulfated hyaluronic acid, as well as low molecular weight hyaluronic acid. Simon Arnoldini wrote the manuscript

Abstract

Glycosaminoglycans (GAGs) are an integral part of the extracellular matrix (ECM) and of great importance as binding sites and co-receptors for many growth factors. Heparin (Hep) represents a major sulfated GAG binding to ECM protein fibronectin (Fn) at two different binding sites. Heparin also binds to fibroblast growth factor (FGF), and is capable to change conformation of Fn to open up cryptic binding sites for vascular endothelial growth factor (VEGF) on Fn. It is however not yet clear, how other GAGs share similar functional properties with heparin and what chemical features govern these processes. Here we show that synthetic sulfation of hyaluronic acid leads to Fn binding capacity and the ability to change Fn conformation in the ECM of human bone marrow derived stromal cells, measured via Fn-FRET if compared to unsulfated control or chondroitin sulfate (CS). Effect of synthetically sulfated hyaluronic acid (sHA) could be reversed in presence of cell contractility inhibitor Blebbistatin, whereas heparin induced effect was still observable, suggesting a different mechanism of the two GAGs. Binding studies of sHA to manually pulled Fn fibers alongside heparin reveal no strain sensitive binding of sHA to Fn. As one heparin binding site on Fn is overlapping with the bacterial peptide binding site we tested for possible blocking capacity of heparin and clinically used low molecular weight heparin derivatives, as well as hyaluronic acid (HA) and sHA using manually pulled Fn fibers. Binding competition showed no effect in case of sHA and HA, whereas heparin non-significantly decreases attachment of bacterial adhesin. Our results indicate, that although GAGs have severe impact on Fn conformation in cell culture they do not significantly compete with the N-terminal binding site of bacteria and rather use the more prominently described heparin binding site at $FnIII_{12\text{-}14}$. We anticipate that this study offers a starting point for further investigation of different GAG derivatives in terms of sulfation (negative charge) and chemical composition to link these chemical parameters with previously reported physiological functions of GAGs.

Introduction

The interaction of extracellular matrix (ECM) protein fibronectin (Fn) with several glycosaminoglycans (GAGs) has been reported already in 1980 [1], and was characterized to be highly dependent on ionic conditions of the surroundings and was under physiological conditions only observable for heparin [2]. These findings suggest, that binding of other GAGs might strongly depend on the degree of sulfation. It is however, up to now not fully understood to what extent disaccharide repeat units of GAGs or overall sulfation and thus negative charge is influencing the previously observed binding properties and additional effects of GAGs on Fn conformation [3-5].

GAGs are polymers with disaccharide repeat units that can be differently sulfated at oxygen or nitrogen species. These disaccharide repeats are linked via glycosidic bonds. The most abundant GAGs are heparan sulfate (HS), heparin (Hep), chondroitin sulfate (CS), hyaluronic acid (HA), dermatan sulfate and keratan sulfate. Depending on the amount of sulfation, their size and sugar isomers, GAGs can vary in their degree of negative charge and thus in their functional properties [6]. Due to tissue specific differences and also large variations in composition, size, charge and physicochemical properties, functional properties of GAGs are still not characterized to the same extent as for ECM proteins. Heparan sulfates (HS) are GAGs that naturally occur as part of heparan sulfate proteoglycans (HSPG) in the ECM, on cell surfaces or in secretory vesicles with a multitude of functions [7] consisting of partially sulfated repeating sequences of glucosamine-hexuronic acid disaccharide units with a molecular weight range of 10-70 kDa. The highly sulfated chemical HS isoform heparin (Hep) (on average 2.3 sulfate groups per disaccharide, compared to HS having approximately 0.8 sulfate groups per disaccharide [7]), being mainly composed of the iduronic epimer of the hexuronic acid residue [8,9] is produced by mast cells and exclusively found in mast cell granules, where it is stored together with other mast cell specific factors, such as histamine and released upon mast cell activation during an inflammatory process [10]. A unique property of heparin is its tight binding to antithrombin III, leading to a subsequent activation of this factor and a downstream inhibitory effect on a number of proteases in the coagulation cascade, thus representing a potent inhibitor of blood coagulation [11,12]. After the discovery of this principle heparin and low molecular weight derivatives of heparin are frequently used in clinics as anti-coagulation medication [13,14]. The animal-derived heparin however had certain drawbacks in terms of purity and impurities can lead to severe clinical complications [15]. Recently, a pentasaccharide structure within heparin has been identified to be the responsible unit of antithrombin binding and a new synthetic pentasaccharide drug called Fondaparinux has been approved in 2004 [16].

Hyaluronic acid (HA) does, unlike HS not form proteoglycan complexes and is completely unsulfated. Its disaccharide repeat unit consists of glucuronic acid and N-acetylglucosamine linked alternatively via 1,4 and 1,3-glycosidic bonds, and is frequently found in synovial fluids and the ECM of loose connective tissue and acts as lubricant and shock absorber in joints and bones. HA chains can be extremely large and reach a molecular weight of up to 8000 kDa [6]. Figure 5.1 summarizes the chemical structures of different GAGs as used in this study together with their known physiological functions and their interaction sites with other molecular entities.

Two different binding sites for heparin respectively heparan sulfate on the Fn molecule have been identified: one next to the integrin binding site at the Fn type III domains 12-14 (Hep II binding site) [17,18] and a second one close to the N-terminus of Fn (Hep I) [19,20], overlapping with the binding site for many Fn binding peptides of bacteria [21,22]. Heparin exhibits a moderate binding affinity to Hep II on Fn with a dissociation constant of around 5-10 μM and an even lower affinity to the Hep I domain, with a dissociation constant at around 300 μM [3,4]. It has been reported that low binding affinity of heparin and heparan sulfate can be overcome via clustering of ligands as observed in fibronectin fibers and high avidity can thus still be reached under physiological conditions [7]. Heparan sulfate and heparin binding to Fn has functional implications as these GAGs can act as coligands for cell attachment being part of transmembrane syndecans [23], for many growth factors, such as fibroblast growth factor (FGF)[24,25], or vascular endothelial growth factor (VEGF)[9,26] as well as for chemokines [27]. Heparin binding to Fn has also been hypothesized to be able to expose cryptic binding sites of Fn, thus playing a catalytic role [9]. This has recently been experimentally proven using both a dual-antibody technique to evaluate the conformation of the Hep II domain of Fn [28] as well as via the usage of a FRET probe for Fn measuring the extension respectively the strain of the molecule [29]. Interestingly, in a recent study it was shown using Fn-FRET, that synthetically sulfated HA (sHA) is, unlike native HA, capable of binding to Fn and changing Fn conformation as similarly observed for heparin. However, in contrast to Hep and HA, sHA exclusively showed additional effects on Fn matrix production and exhibited a pro-osteogenic effect in human bone marrow stromal cells (hBMSC), that yet need to be further examined [5].

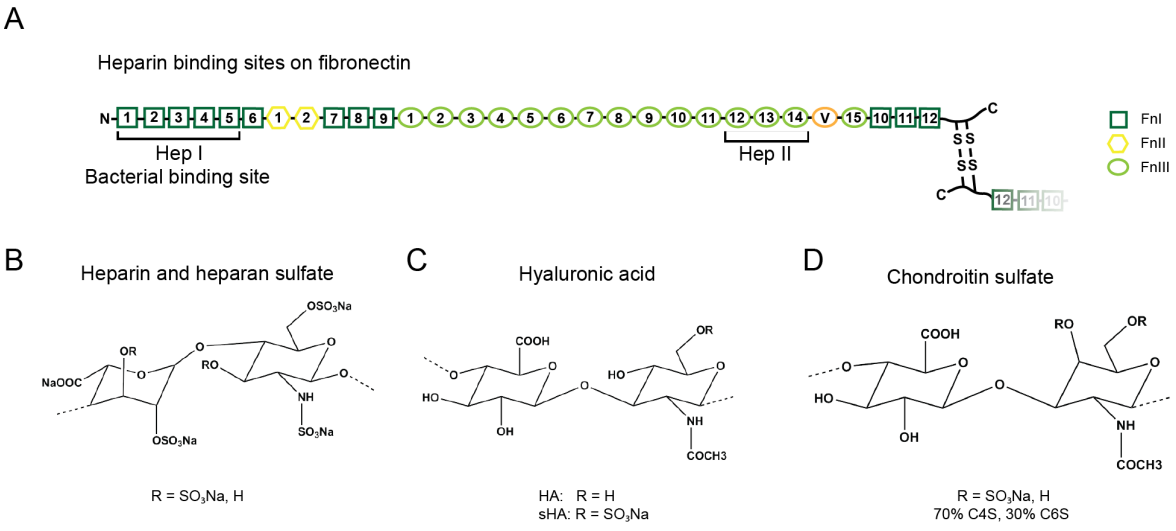

Figure 5.1: Fibronectin binding sites and molecular structure of different GAGs. **(A)** Fibronectin's multimodular structure with two heparin binding sites and bacterial binding site partially overlapping with Hep I binding site. **(B)** Molecular structure of heparin and heparan sulfate disaccharide repeat unit. The iduronic acid epimer is depicted in this illustration. Degree of sulfation of heparin is around 2.2 per disaccharide and for HS it may vary depending on the location, but is generally lower. **(C)** Molecular structure of the hyaluronic acid disaccharide repeat unit. HA is completely unsulfated, whereas low sulfated HA (sHA) has a degree of sulfation of 1 per disaccharide repeat unit, with a sulfate group at the C6 position. **(D)** Chondroitin sulfate repeat unit. Mixture of chondroitin sulfate with 70% C4S and 30% C6S was used.

In this study we first further characterized the effect of GAGs on Fn matrix conformation in human bone marrow stromal cells (hBMSCs), and therefore studied whether and how other known factors influencing and affecting Fn conformation, such as ascorbic acid, Jasplakinolid, or Blebbistatin [30,31] change or ablate the known effects of different GAGs on Fn [5,29]. In a second set of experiments we then tried to elucidate how different GAGs exhibit mechanosensitive binding to manually pulled Fn fibers. Given the fact that the Hep I domain on Fn is also a major attachment site for many bacterial Fn binding proteins, crucially important in bacterial host infection [32] and evidence that heparin and derivatized dextrans are capable of inhibiting bacterial adhesion to Fn coated surfaces [33,34], we ultimately tested, whether GAGs could be utilized to inhibit or compete with bacterial binding peptides in binding to manually pulled Fn fibers. This consequently also gives information about the dominant binding site for heparin and sHA on Fn. Binding competition was tested both for HA and synthetically sulfated HA, as well as for heparin and its clinically used low molecular weight derivatives dalteparin, enoxaparin and for the synthetic pentasaccharide fondaparin.

Results

As previous work has shown that synthetic sulfation of HA leads to an extension of Fn fibers, similar to heparin, as observed via reduction of Fn-FRET ratio in hBMSC derived ECM [5], we first asked whether addition of chondroitin sulfate (CS), a sulfated GAG, that did not significantly bind to Fn under physiological conditions in earlier reports [2], is similarly capable of changing Fn conformation. In Figure 5.2 A representative ratiometric color-coded FRET images of control (CTRL), chondroitin sulfate (CS) and synthetically sulfated hyaluronic acid (Atto655-sHA) are shown. In figure 5.2 B boxplot of means of images of three different cell donors (10 images per donor) are shown. Treatment with sHA leads to a significant reduction of FRET ratio if compared with the control (p=0.014), whereas treatment with CS does not lead to a significant change in Fn conformation. Figure 5.2 C shows representative histograms of FRET ratios from 10 field of views from one donor. Vertical lines are FRET values obtained from chemical denaturation of Fn-FRET in 0, 1, 2 or 4M guanidinium hydrochloride solution (GdnHCl).

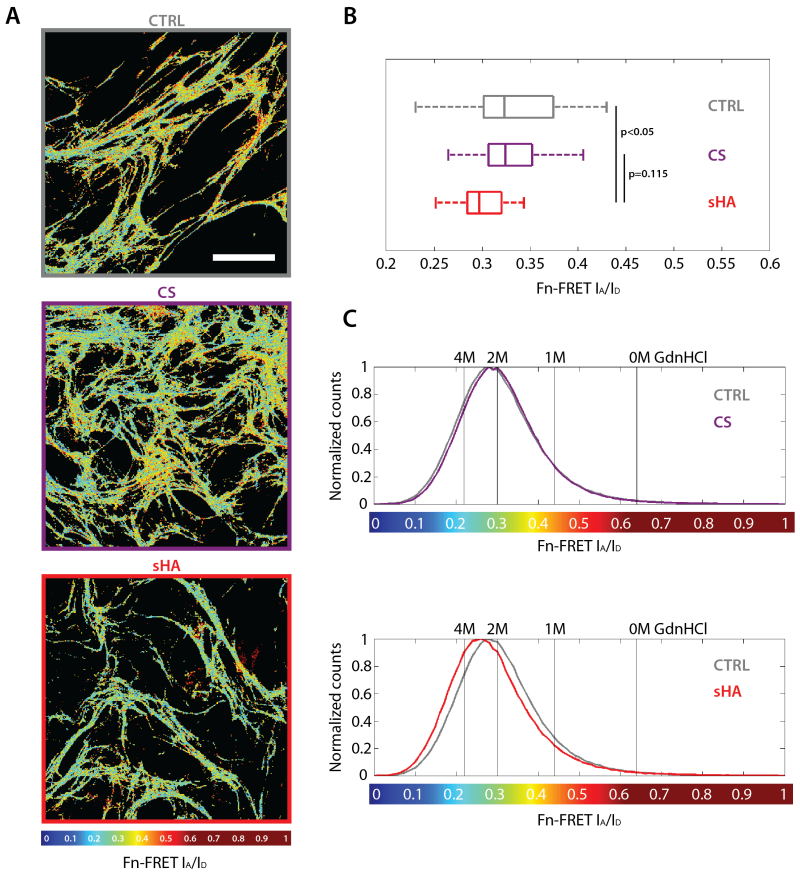

Figure 5.2: Influence of CS and sHA on Fn FRET ratio in hBMSCs. **(A)** Representative images of ratiometric FRET images for control (CTRL, gray) or treated with 200 µg/ml chondroitin sulfate (CS, purple) or sulfated hyaluronan (sHA, red). Scale bar is 50 µm. **(B)** Boxplot of 3 experiment with cells from different donors using mean FRET ratio for 10 fields of view per experiment. Treatment with sHA leads to a significant (p=0.014) decrease in FRET ratio, whereas CS treatment does not lead to any significant change, if compared to control. **(C)** Histograms of FRET ratios of 10 fields of view per treatment of a single donor shows shift of distribution of FRET ratio of different treatments. FRET ratios for chemical denaturation with GdnHCl are shown as vertical lines for 0, 1, 2 or 4 M GdnHCl.

Chemical inhibitors influence previously observed effects of GAGs on Fn conformation

As Fn matrix extension is known to be influenced by both, matrix composition and cellular forces we next asked, whether a manipulation of these variables via external stimuli may also change the previously observed effects of different GAGs on Fn matrix [5]. We therefore supplemented the cell culture medium with 300 µM ascorbic acid, 15 nM Jasplakinolid, or 10 µM Blebbistatin. Ascorbic acid is known to increase deposition of fibrillar Collagen-I network, thus leading to a changed matrix composition going along with a relaxation of Fn fibers [31]. Jasplakinolid is a potent inducer of actin polymerization and stabilizes actin fibers, whereas Blebbistatin decreases cellular forces via inhibition of myosin II [35]. Treatment with ascorbic acid (Fig. 5.3 A) and Jasplakinolid (Fig. 5.3 B) lead to a quite large variation of Fn-FRET ratios in different samples with no statistically significant changes between groups, thus both abolishing the previously observed effect of heparin and synthetically sulfated hyaluronic acid on conformation of Fn fibers within the ECM. Treatment with Blebbistatin, as shown in figure 5.3 C leads to the abolishment of the difference in Fn-FRET between control and sHA treated sample, albeit heparin treated samples still show a significantly reduced Fn-FRET ratio compared to the control ($p < 0.05$).

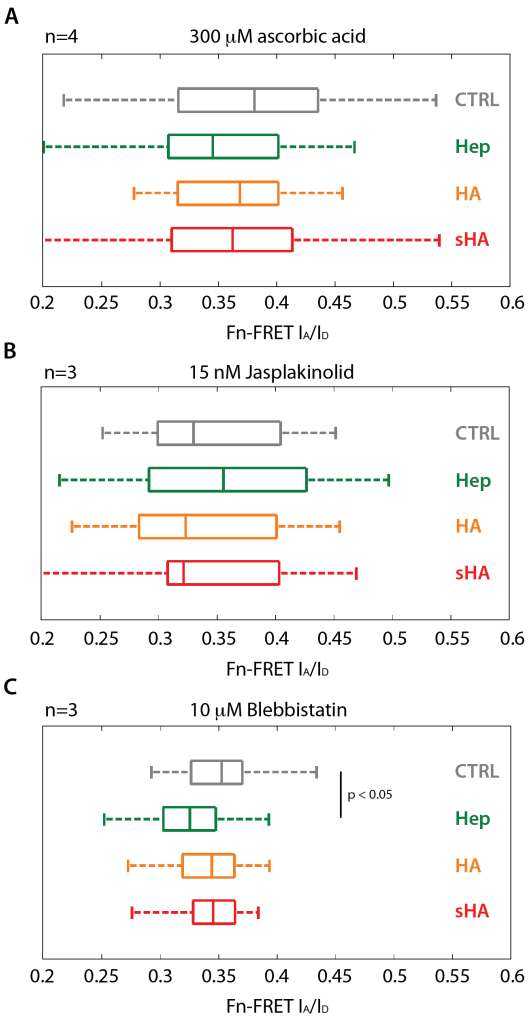

Figure 5.3: Influence of ascorbic acid, Jasplakinolid or Blebbistatin on Fn FRET ratio in hBMSCs matrices. **(A)** Treatment with 300 μM ascorbic acid leads to abrogation of effect of both, heparin and sHA on lowering Fn-FRET ratio, as no significant differences between differently treated groups could be observed. **(B)** Similar to ascorbic acid treated samples also treatment with 15 nM Jasplakinolid led to statistical insignificant FRET values between differently treated groups. **(C)** Treatment with 10 μM Blebbistatin leads to an abolishment of effect of sHA not showing a statistical difference between sHA treated samples and control, while heparin treated sample still exhibits significantly reduced Fn-FRET ratios ($p<0.05$) compared to control samples.

As FRET data from samples treated with ascorbic acid showed a quite high variability, we investigated the amount of deposited collagen-I within the matrix of these samples. For this we analyzed all four donors individually and could see a quite high variability in collagen expression between donors and a therefore resulting spread of Fn-Fret ratios of imaged samples. In supplementary figure 5.1 representative images of collagen-I staining for all donors are shown.

sHA and heparin significantly bind to Fn fibers

To investigate binding behavior of sulfated (sHA) and unsulfated hyaluronic acid (HA) and heparin we incubated manually pulled Fn fibers at different mechanical strains as described previously [36] with sHA-Atto655, HA-Atto655 or heparin-FITC, respectively. Unsulfated hyaluronic acid only showed unspecific binding to both stretched and relaxed Alexa-546 labeled Fn fibers, as expected from previous cell-culture based studies [5], whereas sHA showed significantly higher binding to Fn fibers. sHA was furthermore shown, although not significantly, to have the tendency to preferentially bind to relaxed Fn fibers compared to stretched ones, as shown in figure 5.4 A. Heparin-FITC also showed significant binding to Cy5 labeled Fn fibers, however in contrast to sHA, heparin exhibited an insignificant higher binding to stretched fibers than to relaxed ones (Fig. 5.4 B).

Co-incubation of sHA and heparin shows binding competition to Fn fibers

To estimate a possible overlap of binding sites between sHA and heparin, respectively the competition of binding of these two sulfated GAGs to manually pulled Fn fibers, we next evaluated GAG binding ratio of single and co-incubation of sHA and heparin respectively. In figure 5.4 C the intensity ratios of sHA-655 / Fn-546 and heparin-FITC / Fn-546 are shown for single incubation of GAGs or co-incubation with the respective other glycosaminoglycan. Data from figure 5.4 C shows a significant reduction in sHA binding of around 90% in presence of heparin ($p<0.001$), whereas heparin binding ratio was not significantly changed in presence of sHA. This indicates that although there is a competition between heparin and sHA, as seen in the reduction of binding of sHA in presence of heparin, heparin exhibits a higher affinity to Fn fibers than sHA as its binding was not significantly altered in presence of sHA.

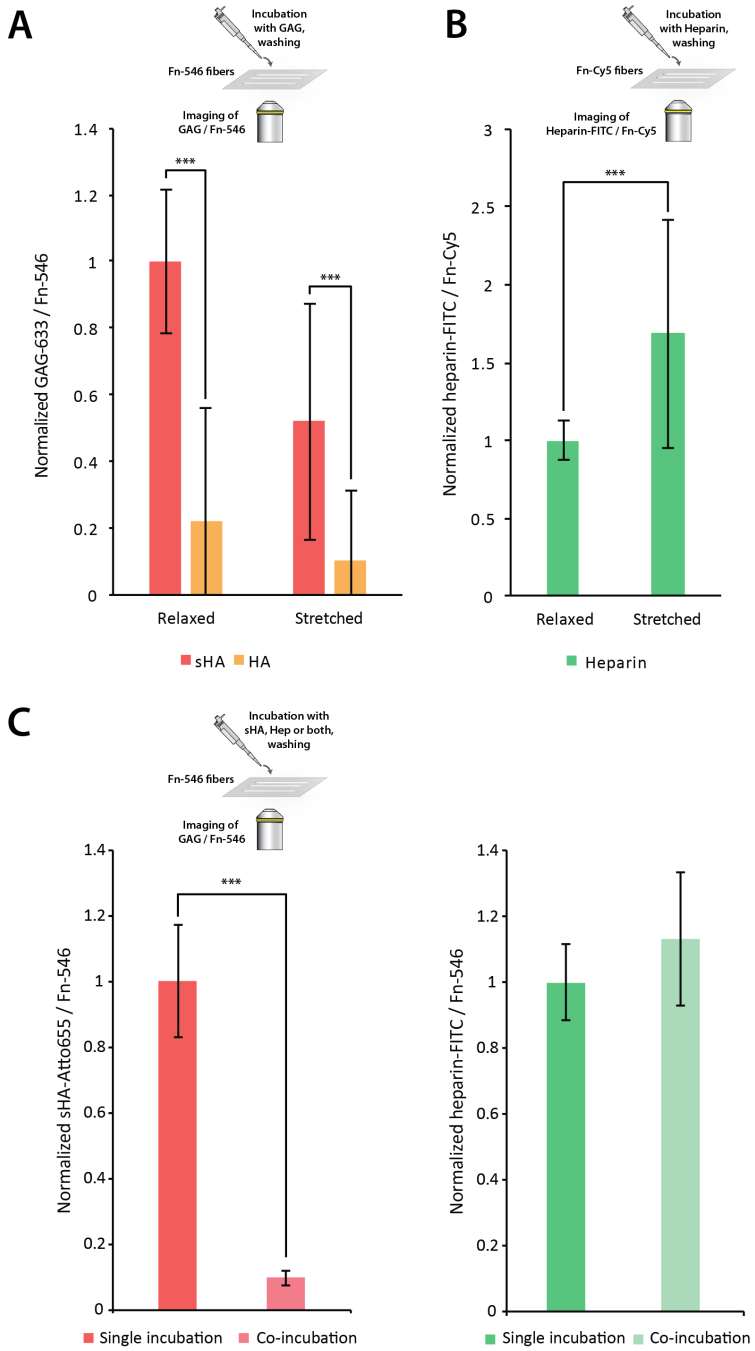

Figure 5.4: Binding of sulfated and natural hyaluronic acid and heparin to manually pulled Fn fibers and competition between different GAGs. **(A)** Relaxed and stretched manually pulled Fn fibers were incubated with 200 µg/ml Atto 655 labeled synthetically sulfated hyaluronic acid (sHA) or Atto 655 labeled hyaluronic acid. sHA showed stronger binding to relaxed fibers than to stretched ones, albeit this trend does not show statistical significance. HA showed little to no binding to manually pulled Fn fibers regardless of the mechanical strain state (>30 fibers from three independent experiments were analyzed). **(B)** Binding of FITC labeled heparin to stretched or relaxed Cy5 labeled Fn fibers showed no statistical significant preference towards a certain strain state. Heparin-FITC exhibited an insignificant, small trend towards stronger binding to stretched fibers (>30 fibers from three independent experiments were analyzed). **(C)** Assessment of binding competition of sHA and heparin to relaxed Fn fibers. Alexa-546 labeled Fn fibers were either incubated with sHA-Atto655 or heparin-FITC or with both labeled GAGs. Binding ratio of single incubation was normalized to 1 and respective results from co-incubation experiment are illustrated as percentage of value of single incubation showing a significant decrease in sHA1 binding to Fn in presence of heparin-FITC ($p<0.001$), whereas heparin-FITC / Fn-546 ratio stays unchanged in presence of sHA, if compared to single incubation control (>10 fibers from one experiment).

sHA and HA do not compete with FnBPA5 binding to relaxed or stretched Fn fibers

To test whether GAGs compete with bacterial binding peptides in binding to N-terminal FnI_{1-5} domains of fibronectin we pre-incubated relaxed and stretched manually pulled Fn fibers with GAGs at a concentration of 200 µg/ml and assessed, whether FnBPA5 binding is altered. In figure 5.5 A representative ratiometric sample images of FnBPA5-488 / Fn-546 ratio are shown, no obvious change in ratio depending on pre-incubation with HA or sHA is visible. In figure 5.5 B quantification of multiple fibers reveals that no significant difference in FnBPA5/Fn ratio can be observed depending on GAG pre-incubation. This is indeed supported by data presented in figure 5.5 C and supplementary figure 5.2 showing that GAG binding before and after FnBPA5 is not affected by FnBPA5 incubation, as passive unbinding in absence of FnBPA5 shows an even higher decrease in sHA binding after 2 hours (Supplementary figure 5.2).

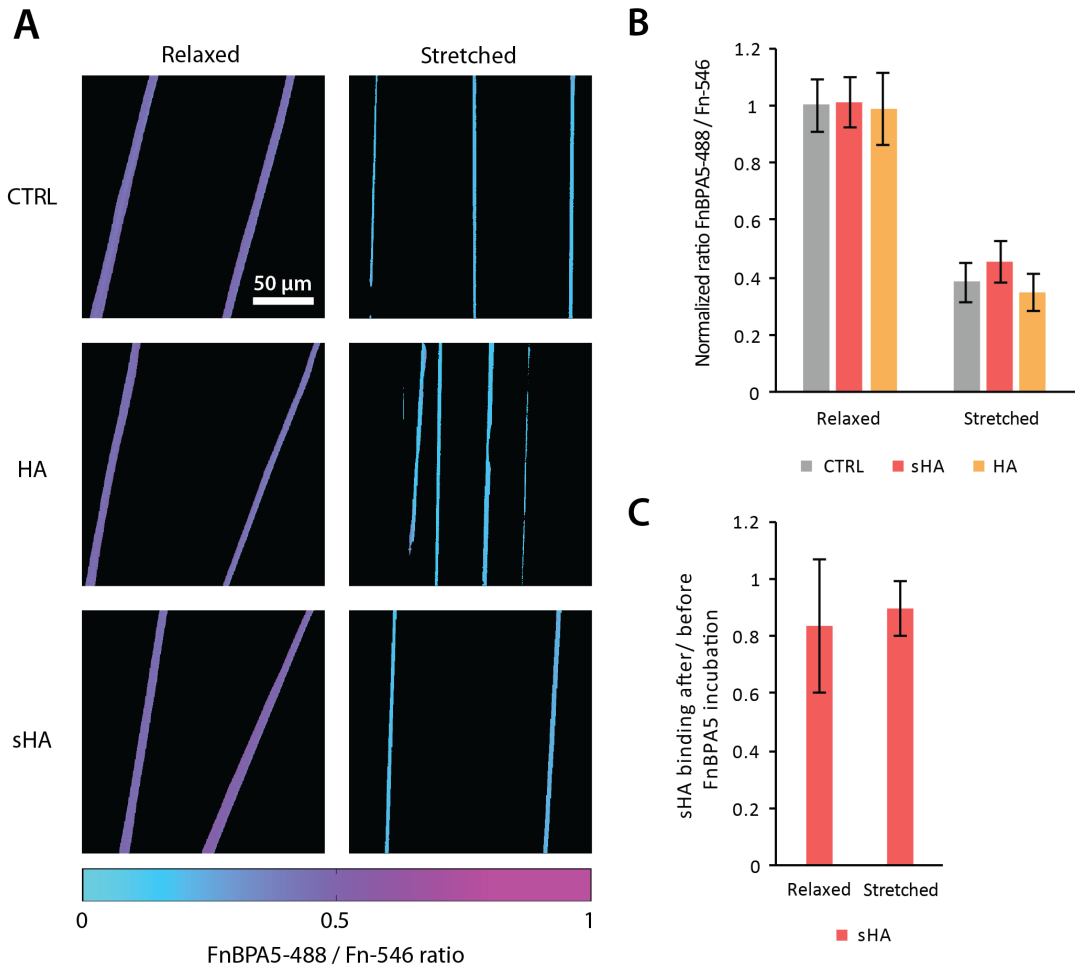

Figure 5.5: Binding competition assay of different GAGs and FnBPA5 to relaxed and stretched manually pulled Fn fibers. **(A)** Representative images of ratiometric analysis of binding of FnBPA5-488 to Fn-546 fibers for differently treated Fn fibers being either relaxed or stretched. **(B)** Bar graph analysis of FnBPA5 / Fn ratio for fibers being incubated with sHA or HA show no significant change in compared to control. Strain sensitive binding of FnBPA5 remains unchanged even in presence of GAGs ($p<0.001$), analysis data from 2 independent experiments. **(C)** Percentage of GAG binding before and after FnBPA5 incubation show no significant decrease from initial 100%, indicating that there is no measurable competition between sHA, HA and FnBPA5 binding to manually pulled Fn fibers, analysis data from 2 independent experiments.

Different heparin derivatives cannot sufficiently block FnBPA5 binding to relaxed Fn fibers

As heparin and low molecular weight derivatives are frequently used in clinical settings as blood anticoagulants we next investigated whether preincubation of these GAGs are capable of blocking binding sites of bacterial Fn binding peptides, as they share the HepI binding site close to the N-terminus of Fn as shown in figure 5.1 A. In figure 5.6 A representative ratiometric images of FnBPA5-488/Fn-Cy5 are shown for control Fn fibers and fibers treated with 100 µg/ml of heparin or a low molecular weight heparin derivative. In figure 5.6 B a schematic illustration of the experimental setup is given. The analysis of multiple experiments presented in figure 5.6 C illustrated, that there are only small reductions in FnBPA5 binding in case of preincubation of heparin or low molecular weight derivatives. Statistical analysis revealed that only Enoxaparin leads to a significant decrease in binding of FnBPA5 compared to the untreated control ($p<0.01$), whereas all other groups did not show any significant difference.

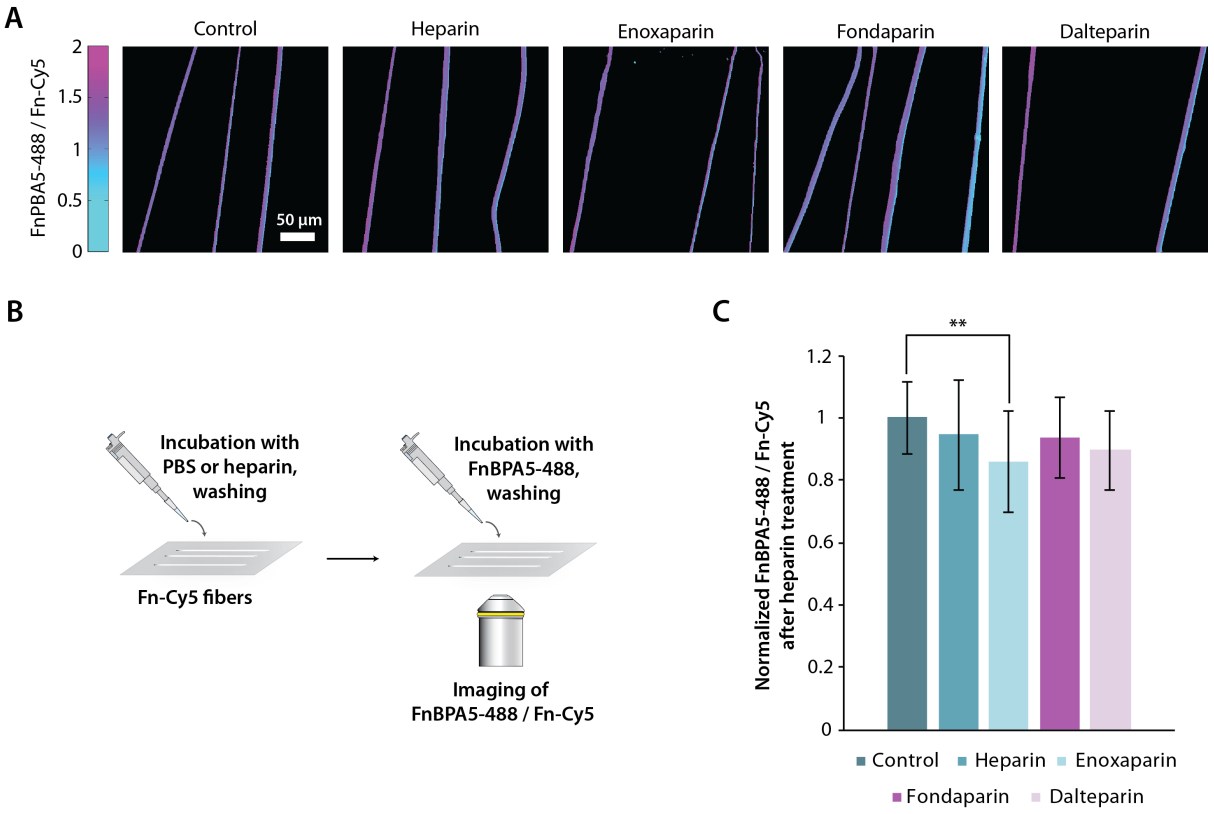

Figure 5.6: Influence of heparin and clinically used low molecular weight derivatives, Enoxaparin, Fondaparin and Dalteparin FnBPA5 binding to relaxed Fn fibers. **(A)** Representative images of FnBPA5-488 / Fn-Cy5 intensity ratio of manually pulled, relaxed Fn fibers. All samples except the control were pre-treated with 100 µg/ml of a heparin derivative. **(B)** Scheme of experimental setup with heparin pre-incubation and subsequent FnBPA5 incubation before imaging. **(C)** Evaluation of binding ratio for multiple experiments show significant decrease in FnBPA5 binding only for Enoxaparin, compared to control ($p < 0.01$) all other groups of two are not significantly different from each other, ANOVA test with a post-hoc Bonferroni test was carried out for statistical analysis, data is from 3 independent experiment except for Fondaparin, where only two experiments were carried out.

Discussion

Glycosaminoglycans play a major role in extracellular matrix organization, ligand interaction and stem cell differentiation. Despite increasing knowledge on structure and function of different GAGs only little is known to date on the impact of their charge and compositional variabilities on their interaction with ECM protein fibronectin. Furthermore, the question to what extent GAG binding to Fn competes with other binding ligands to the same binding sites is currently still not sufficiently answered in the literature.

We show here that synthetically sulfated hyaluronic acid specifically led to a decrease of Fn-FRET ratio in comparison to untreated control or cells treated with chondroitin sulfate (Fig. 5.2). As Chondroitin sulfate, a naturally sulfated GAG does not influence Fn-FRET ratio it is concluded here that degree of sulfation is not the exclusive factor in binding to and changing Fn conformation. Indeed, our data and previous findings indicate that a combination of both the composition of the disaccharide repeat unit, as well as the degree and position of sulfation of respective GAGs play an important role in the interaction with Fn as unsulfated hyaluronic acid was previously reported to have no influence on Fn conformation if compared to its synthetically sulfated derivative and heparin [5,37]. To elucidate, whether change in Fn-FRET ratio is induced via a chemical interaction between Fn and GAGs with a subsequent conformational change or via an active process involving cellular forces, treatments with ascorbic acid and chemical agents Jasplakinolid and Blebbistatin of human bone marrow stromal cell samples were done showing abrogation of effect of sHA on Fn fiber conformation in all samples, if compared to control (Fig. 5.3). Results for ascorbic acid and Jasplakinolid treated samples showed a high variation of FRET ratios with no significant differences between control and different GAG treatments (Fig. 5.3 B,C), especially for ascorbic acid treatment this variation could be attributed to donor to donor differences in collagen expression of cells (Supplementary figure 5.1), majorly influencing Fn-FRET values [31]. Astonishingly, Blebbistatin treatment led to a significant decrease ($p<0.05$) in FRET ratio only for heparin treated samples, if compared to control, similar as reported previously for samples without Blebbistatin treatment [5], albeit and in contrast to results from figure 5.2, sHA does not show a significant effect on Fn conformation in presence of Blebbistatin (Fig. 5.3 A). This could indicate a cell contractility dependent mechanism in the change of Fn conformation for sHA, whereas effect of heparin seems to be independent from cellular contractility, as it was unaffected by the myosin inhibitor Blebbistatin, also in line with published literature reporting a cell-independent conformational change of fibronectin upon heparin binding [9,26,29,37]. This is especially interesting in light of previous findings of sHA promoting osteogenic differentiation of mesenchymal stromal cells *in vitro* depending on sulfation pattern and degree of sulfation of used GAGs [38-40], as cell-induced stretching of Fn due to sHA treatment could then act as positive feedback loop for osteogenic commitment, considering reports of mesenchymal stromal cells showing enhanced osteogenic differentiation on stretched compared to relaxed single Fn fibrils [41].

As nothing is known on a potential strain sensitive binding behavior of heparin and other glycosaminoglycans to Fn fibers we assessed, whether there is such an effect observable for the binding of sHA, HA and heparin and

whether heparin and sHA compete for binding sites on Fn fibers. In figure 5.4 results of interaction of Atto655-sHA and Atto655-HA with relaxed and stretched manually pulled Fn fibers are presented, showing a significant higher binding of sulfated HA to both relaxed and stretched Fn fibers compared to natural, unsulfated HA derivative. An insignificant trend toward higher binding to relaxed fibers for sHA could be observed (Fig. 5.4 A). These results confirm previous reports stating that unsulfated hyaluronic acid is not binding to Fn [5,37], partly contradicting older findings reporting an interaction of HA with fibronectin [1]. Heparin-FITC was shown to bind significantly stronger ($p<0.001$) to stretched compared to relaxed fibers (Fig. 5.4 B), potentially exploiting exposure of cryptic binding sites after stretch induced mechanical strain of Fn fibers. Binding competition of heparin and sulfated hyaluronic acid to relaxed manually pulled Fn fibers revealed a drastic, significant decrease in binding of sHA if co-incubated with heparin, compared to single incubation, whereas heparin binding was unaffected regardless of co-incubation with sHA (Fig. 5.4 C). This results indicate a much higher affinity of heparin to Fn, compared to sHA with both higher binding and lower unbinding rates, as sHA is almost completely blocked from Fn fibers in presence of heparin. This could be due to the higher overall degree of sulfation of heparin having 2.3 sulfate groups per disaccharide, whereas sHA only has 1 sulfate group per repeat unit, comparable to typical heparan sulfates [7], or by sugar backbones with specific arrangement of charges and sugar epimers influencing binding, as reported for the interaction of heparin with antithrombin [7].

Further we sought to determine which of the two different heparin binding sites of fibronectin (Fig. 5.1) dominates binding of heparin and sHA. For this a competitive study with the bacterial Fn binding peptide FnBPA5 from S. *aureus,* exhibiting specific, high affinity binding to the HepI domain at $FnI_{2\text{-}5}$ [21,42] was carried out using relaxed or stretched manually pulled Fn fibers. Neither unsulfated hyaluronic acid nor sHA pre-incubation of Fn fibers showed a significant effect on binding of FnBPA5 to Fn fibers compared to untreated control, whereas previously reported strain sensitive binding behavior of bacterial peptides to Fn fibers [43,44] was clearly observed for FnBPA5 regardless of GAG pre-incubation (Fig. 5.5 A,B). Data from figure 5.5 thus suggests, that the HepI binding site of Fn is indeed not the dominant attachment position, being supported by our finding, that sHA binding before and after FnBPA5 incubation is not significantly influenced by the presence of FnBPA5 (Fig. 5.5 C, Supplementary figure 5.2). The higher affinity of heparin towards Fn, led to a subtle decrease of FnBPA5 binding to relaxed Fn fibers in presence of heparin or its low molecular weight derivatives used in clinics. These differences were however, except for Enoxaparin, not significant (Fig. 5.6). These findings can be interpreted as such, that heparin although binding to the same domain as FnBPA5 is due to its drastically lower affinity not able to significantly block FnBPA5 attachment. This hypothesis is in line with findings of heparin being able to significantly block a shorter version of FnBPA5 binding only two FnI domains and consequently having a lower overall affinity to Fn [43]. Regarding the different Hep binding domains it can thus be concluded, that the Hep I domain is not the dominating domain for GAG binding being in line with previously reported lower affinity values for the Hep I binding site compared to the HepII binding site of Fn [3,4]. It can further be concluded that sHA, heparin or its low molecular weight derivatives are not a suitable mean to efficiently block attachment of bacterial adhesins to fibronectin.

In conclusion, sHA has been shown to be a potential mediator of Fn matrix conformation with potential impact towards osteogenic commitment of stem cells opening up fields of application in bone tissue engineering and regenerative medicine. However further comparative studies are needed to fully elucidate the impact of size, charge and exact sugar epimer constitution of sHA on the ECM and thus on cells. A blocking of bacterial adhesion attachment to Fn could not be sufficiently achieved neither with sHA nor with heparin or small molecular weight heparin derivatives, most probably due to moderate binding affinity of GAGs to the HepI binding domain of Fn. Taken together the study of glycosaminoglycans in the context of extracellular matrix interaction and tissue engineering will continue with synthetically sulfated hyaluronic acid representing a valid model system to test for the effect of sulfation and sugar composition if compared to other compounds.

Materials and Methods

Fn purification and labeling

Blood plasma derived fibronectin was used for this study. Purification of human plasma (Zürich Blutspendedienst, SRK, Switzerland) was carried out as previously described [45,46] via usage of gelatine-sepharose chromatography. Briefly, plasma was thawed and removed from aggregates via passing it through a PD-10 column (GE Healthcare, Germany). After aggregate removal, the effluent was passed through a gelatin sepharose column, bound fibronectin was after a washing step eluted with a 6M urea solution and stored at -80°C. Fn was labeled using Alexa-Fluor C5 546 maleimide dye (Invitrogen) as acceptor and Alexa-Fluor 488 succinimidyl ester (Invitrogen) as donor fluorophore. For maleimide labeling Fn was incubated in 4M guanidinium hydrochloride for exposure of cryptic cysteine residues on $FnIII_7$ and $FnIII_{15}$ and incubated with a 30-fold molar excess of maleimide dye for 1 hour at room temperature. Free dye was excluded via passage through a PC-10 column and single labeled Fn was rebuffered into a 0.1 M $NaHCO_3$ solution in PBS. Second labeling step was carried out with a 70 fold molar excess of the succinimidyl ester dye for 1 hour at room temperature and subsequent removal of free dye using a PD-10 column with physiological saline solution (PBS) as final solvent for double-labeled fibronectin. Single labeling was similarly done using Alexa-Fluor C5 546 maleimide dye (Invitrogen) or Cy5-maleimide Dye (GE Healthcare) with removal of the second labeling step, respectively using Alexa-Fluor 488 succinimidyl ester without prior GdnHCl denaturation, with PBS being the buffer of all labeled Fn derivatives used in this study.

Binding ligands, GAGs and bacterial peptide FnBPA5

Labeled, synthetically sulfated hyaluronic acid and labeled low molecular weight natural hyaluronic acid were produced by Innovent e.V., Jena, and provided by collaborators from the TU Dresden and specific preparation and characteristics of these derivatives were described previously [5]. Heparin (Sigma, Switzerland), CS (70% C4S, 30% C6S mixture, Kraeber, Germany) and FITC labeled heparin derivative (Invitrogen) were commercially bought from suppliers. Alexa 488 labeled bacterial peptide derivative FnBPA5 was commercially synthesized, labeled and purified (Peptide Specialty Laboratories GmbH, Heidelberg, Germany).

Cell culture experiments

Experiments involving human bone marrow stromal cells (hBMSCs) were conducted with cells obtained from the Bone Marrow Transplantation Center of the University Hospital Dresden and was ethically approved by the ethics commission of the University of Technology Dresden and carried out with the consent of the donors. Samples were prepared as previously described [5], briefly approximately 14000 cells/cm^2 were seeded on to 8-well chamber slides. After 2 hours of cell attachment, the samples were treated with 50 μg/ml fibronectin (90% unlabeled, 5% double-labeled), or in experiments involving inhibitors first treated with respective inhibitor or chemical (10 μM Blebbistatin (Sigma), 15 nM Jasplakinolid (Sigma), 300 μM ascorbic acid (Sigma), and 2h after

addition of inhibitors, 50 μg/ml fibronectin (90% unlabeled, 5% double-labeled) was added. After a culture period of 24 hours 200 μg/ml GAG were added and samples were subsequently fixed 48 hours after start of GAG incubation using 4% paraformaldehyde. Samples were then embedded in Mowiol and sealed for further imaging.

Experiments involving manually pulled Fn fibers

Manually pulled fibers were produced as described previously [36,43], briefly a fibronectin solution of 0.5 μg/μl (95% unlabeled and 5% single-labeled) in PBS was prepared. A droplet of Fn solution was deposited onto a flexible silicone sheet (SMI, USA) and fibers were manually pulled out of this Fn droplet and deposited onto the sheet using a sharp pipette tip. Depending on the desired mechanical strain state of the fiber samples the sheet was either pre-stretched and after pulling of Fn fibers relaxed, or was stretched after pulling of Fn fibers. Stretched fibers have a strain of around 380% and relaxed fibers of around 7%, as defined earlier [47]. For binding assays fibers were blocked in 4% albumin solution in PBS for 30 minutes and after a washing step incubated with respective binding ligands for 1 hour. Binding ligands were low molecular weight hyaluronic acid (Atto655-HA LMW, 27 kDa, Innovent e.V., Jena, Trr67 project A2), sulfated hyaluronic acid (Atto655-sHA, D.S.=1, 27 kDa, Innovent e.V., Jena, Trr67 project A2), heparin (≈ 15 kDa, Sigma), Enoxaparin (≈ 4.5 kDa, Lovenox®, Sanofi-Aventis), Fondaparin (≈ 1.7 kDa, Arixtra®, GlaxoSmithKline) and Dalteparin (≈ 5 kDa, Fragmin®, Pfizer). Depending on the experiment GAGs were pre-incubated and subsequent incubation with FnBPA5-488 peptide was carried out after GAG pre-incubation. After ligand incubation, the samples were washed again for 3 times and subsequently analyzed by means of confocal microscopy.

Imaging of hBMSC samples and Fn fiber samples

All imaging was done using an Olympus FV-1000 confocal microscope, equipped with a 40x water immersion objective (NA 0.9). For hBMSC samples donor and acceptor channel were recorded using a single photo multiplier tube, sequentially detecting 20 nm bandwidth (510-530 nm for donor, 560-580 nm for acceptor), as described previously [30]. Pinhole diameter (200 μm), PMT voltage and pixel dwell was kept constant in all experiment to avoid artifacts. Bleed-through from donor into acceptor channel was corrected and set to 20% as done previously [30] and FRET ratios from cell culture samples were set into context to FRET values from Fn-FRET upon chemical denaturation using guanidinium hydrochloride (GdnHCl). For fiber experiments, different channels were imaged and microscope settings were chosen for optimal imaging of respective samples. Briefly, z-stacks of a minimum of 10 fibers per samples were acquired using a z-step size of 1 μm.

Image analysis of Fn-FRET samples

FRET analysis was carried out using Matlab (MathWorks, Switzerland) similar to previously described procedures [5,46]. Briefly, dark current background was subtracted from donor and acceptor images, images were smoothened using a 2x2 pixel-averaging filter. Unspecific signal below a lower threshold and saturated pixels were excluded from analysis. Acceptor channel was corrected for donor bleed through (linear subtraction of

20% of intensity) and then pixel-wise divided by donor channel. Resulting FRET ratios were represented in color-codes images.

Image analysis of manually pulled Fn fiber samples

Images from manually pulled Fn fibers were analyzed using Fiji/ImageJ and Matlab (MathWorks, Switzerland). Individual z-stacks were projected by means of maximum intensity and after subtraction of background and exclusion of pixels below threshold or at saturation, smoothened using a 2x2 pixel-averaging filter. Then pixel-by-pixel ratio of two channels was calculated similarly to FRET analysis, visualized using color-coded images and statistically evaluated as indicated.

References

[1] K.M. Yamada, D.W. Kennedy, K. Kimata, R.M. Pratt, Characterization of fibronectin interactions with glycosaminoglycans and identification of active proteolytic fragments, J. Biol. Chem. 255 (1980) 6055–6063.

[2] K. Sekiguchi, S. Hakomori, M. Funahashi, I. Matsumoto, N. Seno, Binding of fibronectin and its proteolytic fragments to glycosaminoglycans. Exposure of cryptic glycosaminoglycan-binding domains upon limited proteolysis, J. Biol. Chem. 258 (1983) 14359–14365.

[3] K.C. Ingham, S.A. Brew, D.H. Atha, Interaction of heparin with fibronectin and isolated fibronectin domains, Biochemical Journal. 272 (1990) 605–611. http://www.biochemj.org/content/ppbiochemj/272/3/605.full.pdf.

[4] W. Kang, S. Park, J.-H. Jang, Kinetic and functional analysis of the heparin-binding domain of fibronectin, Biotechnol Lett. 30 (2007) 55–59. doi:10.1007/s10529-007-9522-3.

[5] S. Vogel, S. Arnoldini, S. Möller, M. Schnabelrauch, U. Hempel, Sulfated hyaluronan alters fibronectin matrix assembly and promotes osteogenic differentiation of human bone marrow stromal cells, Sci. Rep. (2016) 1–13. doi:10.1038/srep36418.

[6] N.S. Gandhi, R.L. Mancera, The Structure of Glycosaminoglycans and their Interactions with Proteins, Chemical Biology & Drug Design. 72 (2008) 455–482. doi:10.1111/j.1747-0285.2008.00741.x.

[7] S. Sarrazin, W.C. Lamanna, J.D. Esko, Heparan sulfate proteoglycans, Cold Spring Harbor Perspectives in Biology. 3 (2011). doi:10.1101/cshperspect.a004952.

[8] R. Raman, S. Raguram, G. Venkataraman, J.C. Paulson, R. Sasisekharan, Glycomics: an integrated systems approach to structure-function relationships of glycans, Nat. Methods. 2 (2005) 817–824. doi:10.1038/nmeth807.

[9] M. Mitsi, K. Forsten-Williams, M. Gopalakrishnan, M.A. Nugent, A catalytic role of heparin within the extracellular matrix, J. Biol. Chem. 283 (2008) 34796–34807. doi:10.1074/jbc.M806692200.

[10] S. Wernersson, G. Pejler, Mast cell secretory granules: armedfor battle, Nat Rev Immunol. 14 (2014) 478–494. doi:10.1038/nri3690.

[11] Z. Shriver, R. Raman, G. Venkataraman, K. Drummond, J. Turnbull, T. Toida, et al., Sequencing of 3-O sulfate containing heparin decasaccharides with a partial antithrombin III binding site, Proc. Natl. Acad. Sci. U.S.a. 97 (2000) 10359–10364. doi:10.1073/pnas.97.19.10359.

[12] M. Sundaram, Y. Qi, Z. Shriver, D. Liu, G. Zhao, G. Venkataraman, et al., Rational design of low-molecular weight heparins with improved in vivo activity, Proc. Natl. Acad. Sci. U.S.a. 100 (2003) 651–656. doi:10.1073/pnas.252643299.

[13] A. Bisio, D. Vecchietti, L. Citterio, M. Guerrini, R. Raman, S. Bertini, et al., Structural features of low-molecular-weight heparins affecting their affinity to antithrombin, Thromb Haemost. 102 (2009) 865–873. doi:10.1160/TH09-02-0081.

[14] C.D. Sommers, H. Ye, R.E. Kolinski, M. Nasr, L.F. Buhse, A. Al-Hakim, et al., Characterization of currently marketed heparin products: analysis of molecular weight and heparinase-I digest patterns, Anal Bioanal Chem. 401 (2011) 2445–2454. doi:10.1007/s00216-011-5362-z.

[15] T.K. Kishimoto, K. Viswanathan, T. Ganguly, S. Elankumaran, S. Smith, K. Pelzer, et al., Contaminated Heparin Associated with Adverse Clinical Events and Activation of the Contact System, N Engl J Med. 358 (2008) 2457–2467. doi:10.1056/NEJMoa0803200.

[16] M. Petitou, C.A.A. van Boeckel, A Synthetic Antithrombin III Binding Pentasaccharide Is Now a Drug! What Comes Next? Angew. Chem. Int. Ed. Engl. 43 (2004) 3118–3133. doi:10.1002/anie.200300640.

[17] F.J. Barkalow, J.E. Schwarzbauer, Localization of the major heparin-binding site in fibronectin, J. Biol. Chem. 266 (1991) 7812–7818.

[18] A. Sharma, J.A. Askari, M.J. Humphries, E.Y. Jones, D.I. Stuart, Crystal structure of a heparin-and integrin-binding segment of human fibronectin, The EMBO Journal. 18 (1999) 1468–1479. doi:10.1093/emboj/18.6.1468.

[19] H. Pande, J.E. Shively, NH2-terminal sequences of DNA-, heparin-, and gelatin-binding tryptic fragments from human plasma fibronectin, Archives of Biochemistry and Biophysics. 213 (1982) 258–265. doi:10.1016/0003-9861(82)90460-X.

[20] R. Kishore, M. Samuel, M.Y. Khan, J. Hand, D.A. Frenz, S.A. Newman, Interaction of the NH2-terminal domain of fibronectin with heparin. Role of the omega-loops of the type I modules, J. Biol. Chem. 272 (1997) 17078–17085.

[21] U. Schwarz-Linek, J.M. Werner, A.R. Pickford, S. Gurusiddappa, J.H. Kim, E.S. Pilka, et al., Pathogenic bacteria attach to human fibronectin through a tandem beta-zipper, Nature. 423 (2003) 177–181. doi:10.1038/nature01589.

[22] T.J. Foster, J.A. Geoghegan, V.K. Ganesh, M. Höök, Adhesion, invasion and evasion: the many functions of the surface proteins of Staphylococcus aureus, Nature Reviews Microbiology. 12 (2014) 49–62. doi:10.1038/nrmicro3161.

[23] M.R. Morgan, M.J. Humphries, M.D. Bass, Synergistic control of cell adhesion by integrins and syndecans, Nat Rev Mol Cell Biol. 8 (2007) 957–969. doi:10.1038/nrm2289.

[24] J. Folkman, M. Klagsbrun, J. Sasse, M. Wadzinski, D. Ingber, I. Vlodavsky, A heparin-binding angiogenic protein-basic fibroblast growth factor-is stored within basement membrane, The American Journal of Pathology. 130 (1988) 393–400.

[25] M.V. Galanternik, K.L. Kramer, T. Piotrowski, Heparan Sulfate Proteoglycans Regulate Fgf Signaling and Cell Polarity during Collective Cell Migration, CellReports. 10 (2015) 414–428. doi:10.1016/j.celrep.2014.12.043.

[26] M. Mitsi, Z. Hong, C.E. Costello, M.A. Nugent, Heparin-Mediated Conformational Changes in Fibronectin Expose Vascular Endothelial Growth Factor Binding Sites, Biochemistry. 45 (2006) 10319–10328. doi:10.1021/bi060974p.

[27] Y. Monneau, F. Arenzana-Seisdedos, H. Lortat-Jacob, The sweet spot: how GAGs help chemokines guide migrating cells, Journal of Leukocyte Biology. 99 (2016) 935–953. doi:10.1189/jlb.3MR0915-440R.

[28] B. Hubbard, J.A. Buczek-Thomas, M.A. Nugent, M.L. Smith, Heparin-dependent regulation of fibronectin matrix conformation, Matrix Biol. 34 (2014) 124–131. doi:10.1016/j.matbio.2013.10.006.

[29] B. Li, Z. Lin, M. Mitsi, Y. Zhang, V. Vogel, Heparin-induced conformational changes of fibronectin within the extracellular matrix promote hMSC osteogenic differentiation, Biomater. Sci. (2014). doi:10.1039/C3BM60326A.

[30] W.R. Legant, C.S. Chen, V. Vogel, Force-induced fibronectin assembly and matrix remodeling in a 3D microtissue model of tissue morphogenesis, Integr. Biol. 4 (2012) 1164–1174. doi:10.1039/c2ib20059g.

[31] K.E. Kubow, R. Vukmirovic, L. Zhe, E. Klotzsch, M.L. Smith, D. Gourdon, et al., Mechanical forces regulate the interactions of fibronectin and collagen I in extracellular matrix, Nature Communications. 6 (2015) 1–11. doi:10.1038/ncomms9026.

[32] K. House-Pompeo, Y. Xu, D. Joh, Pietro Speziale, M. Höök, Conformational Changes in the Fibronectin Binding MSCRAMMs Are Induced by Ligand Binding, J. Biol. Chem. 271 (1996) 1379–1384.

[33] P. Vaudaux, T. Avramoglou, D. Letourneur, D.P. Lew, J. Jozefonvicz, Inhibition by heparin and derivatized dextrans of Staphylococcus aureus adhesion to fibronectin-coated biomaterials, Journal of Biomaterials Science, Polymer Edition. 4 (1993) 89–97. doi:10.1163/156856292X00321.

[34] P. Francois, D. Letourneur, D.P. Lew, J. Jozefonwicz, P. Vaudaux, Inhibition by heparin and derivatized dextrans of Staphylococcus epidermidis adhesion to in vitro fibronectin-coated or explanted polymer surfaces, Journal of Biomaterials Science, Polymer Edition. 10 (1999) 1207–1221. doi:10.1163/156856299X00027.

[35] M. Kovacs, J. Toth, C. Hetenyi, A. Malnasi-Csizmadia, J.R. Sellers, Mechanism of Blebbistatin Inhibition of Myosin II, J. Biol. Chem. 279 (2004) 35557–35563. doi:10.1074/jbc.M405319200.

[36] W.C. Little, M.L. Smith, U. Ebneter, V. Vogel, Assay to mechanically tune and optically probe fibrillar fibronectin conformations from fully relaxed to breakage, Matrix Biology. 27 (2008) 451–461. doi:10.1016/j.matbio.2008.02.003.

[37] T.P. Ugarova, C. Zamarron, Y. Veklich, R.D. Bowditch, M.H. Ginsberg, J.W. Weisel, et al., Conformational transitions in the cell binding domain of fibronectin, Biochemistry. 34 (1995) 4457–4466.

[38] U. Hempel, S. Möller, C. Noack, V. Hintze, D. Scharnweber, M. Schnabelrauch, et al., Sulfated hyaluronan/collagen I matrices enhance the osteogenic differentiation of human mesenchymal stromal cells in vitro even in the absence of dexamethasone, Acta Biomaterialia. 8 (2012) 4064–4072. doi:10.1016/j.actbio.2012.06.039.

[39] U. Hempel, C. Matthäus, C. Preissler, S. Möller, V. Hintze, P. Dieter, Artificial matrices with high-sulfated glycosaminoglycans and collagen are anti-inflammatory and pro-osteogenic for human mesenchymal stromal cells, J. Cell. Biochem. 115 (2014) 1561–1571. doi:10.1002/jcb.24814.

[40] U. Hempel, C. Preissler, S. Vogel, S. Möller, V. Hintze, J. Becher, et al., Artificial extracellular matrices with oversulfated glycosaminoglycan derivatives promote the differentiation of osteoblast-precursor cells and premature osteoblasts, Biomed Res Int. 2014 (2014) 938368. doi:10.1155/2014/938368.

[41] B. Li, C. Moshfegh, Z. Lin, J. Albuschies, V. Vogel, Mesenchymal Stem Cells Exploit Extracellular Matrix as Mechanotransducer, Sci. Rep. 3 (2013). doi:10.1038/srep02425.

[42] N.A.G. Meenan, L. Visai, V. Valtulina, U. Schwarz-Linek, N.C. Norris, S. Gurusiddappa, et al., The tandem beta-zipper model defines high affinity fibronectin-binding repeats within Staphylococcus aureus FnBPA, J. Biol. Chem. 282 (2007) 25893–25902. doi:10.1074/jbc.M703063200.

[43] M. Chabria, S. Hertig, M.L. Smith, V. Vogel, Stretching fibronectin fibres disrupts binding of bacterial adhesins by physically destroying an epitope, Nature Communications. 1 (2010) 135–9. doi:10.1038/ncomms1135.

[44] S. Hertig, M. Chabria, V. Vogel, Engineering mechanosensitive multivalent receptor-ligand interactions: why the nanolinker regions of bacterial adhesins matter, Nano Lett. 12 (2012) 5162–5168. doi:10.1021/nl302153h.

[45] P. Speziale, L. Visai, S. Rindi, A. Di Poto, Purification of human plasma fibronectin using immobilized gelatin and Arg affinity chromatography, Nat Protoc. 3 (2008) 525–533. doi:10.1038/nprot.2008.12.

[46] M.L. Smith, D. Gourdon, W.C. Little, K.E. Kubow, R.A. Eguiluz, S. Luna-Morris, et al., Force-Induced Unfolding of Fibronectin in the Extracellular Matrix of Living Cells, Plos Biol. 5 (2007) e268. doi:10.1371/journal.pbio.0050268.sv001.

[47] E. Klotzsch, M.L. Smith, K.E. Kubow, S. Muntwyler, W.C. Little, F. Beyeler, et al., Fibronectin forms the most extensible biological fibers displaying switchable force-exposed cryptic binding sites, Proc. Natl. Acad. Sci. U.S.a. 106 (2009) 18267–18272.

Supplementary figures

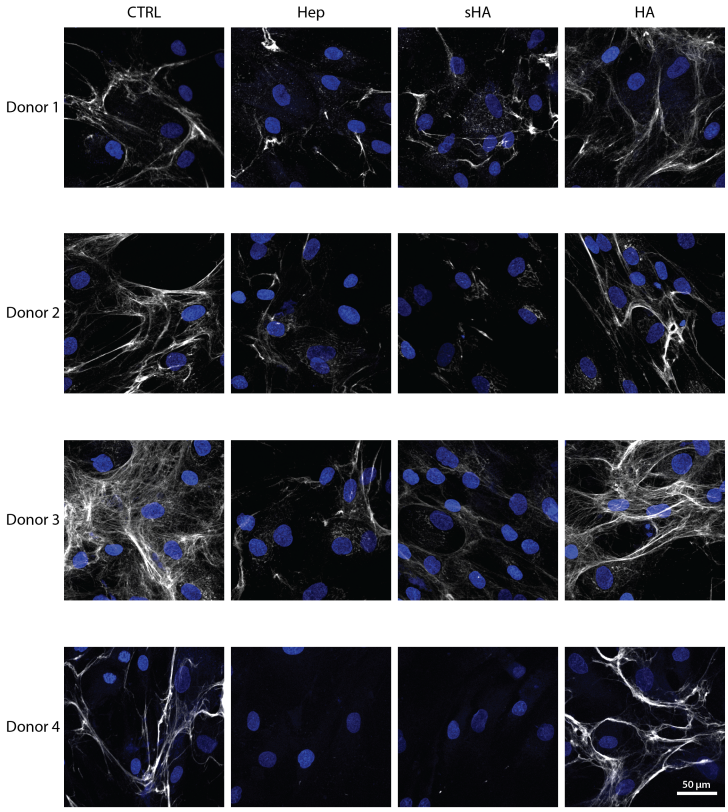

Supplementary figure 5.1: Collagen-I antibody staining (grey) and cell nuclei DAPI staining (blue) of hBMSCs treated with heparin, hyaluronic acid, synthetically sulfated hyaluronic acid or untreated control of four different donors treated with ascorbic acid (AA). Interestingly, samples treated with heparin or sHA show less collagen fibers in all different donors, albeit relative collagen expression levels vary quite drastically between cells from different donors. Used collagen-I antibody was from Sigma (mouse anti collagen-I, C2456)

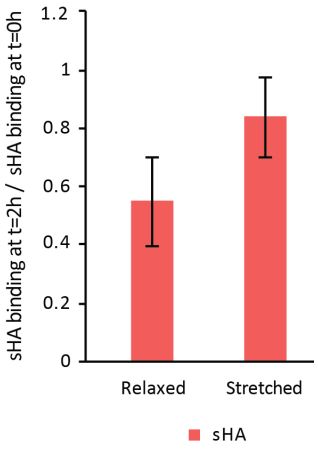

Supplementary figure 5.2: Passive unbinding of sHA from relaxed and stretched Fn fibers after 2 hours. Ratio of sHA-655 / Fn-546 after 2 hours (t=2h) divided by ratio of sHA / Fn directly after incubation (t=0) to relaxed and stretched Fn fibers reveals significant unbinding of sHA from fibers of both of both strain states (>10 fibers from one experiment).

Chapter 6

Implications and Outlook

Implications of tissue stainings and *in vivo* findings

In vivo biodistribution of radiolabeled FnBPA5 derivative in a PC-3 tumor xenograft mouse model showed a specific accumulation in many organs, predominantly in liver, spleen and tumor (Fig. 3.5, 3.6). Interestingly, in a previous study investigating *in vivo* biodistribution of labeled Fn, liver and spleen uptake of endogenously labeled plasma fibronectin was reported in rats [1], indicating a possible role of plasma Fn as carrier molecule for FnBPA5 within the blood stream. As it is shown here, that FnBPA5 is indeed able to bind to plasma Fn in solution with nanomolar affinity (Fig. 3.2 D), we suggest that *in vivo* kinetic of FnBPA5 strongly depends on its binding to plasma Fn. This notion is supported by the literature reporting that other Fn binding peptides use plasma Fn as carrier [2] and stressing the importance of this interaction in bacterial virulence [3]. Interestingly, we could observe a prolonged retention of FnBPA5 peptide in tumors, compared to the other organs with specific uptake, such as the liver or spleen. Indeed, FnBPA5 levels in liver and spleen exponentially decreased at later post-injection time points. This could be explained by both a higher binding of FnBPA5 to Fn in tumor or the incorporation of FnBPA5-pFn complex into the tumor stroma, as reported for other peptides selected to bind clotted plasma [4]. An additional promoting factor could be a lower degree of unbinding of FnBPA5 from Fn in tumor tissue due to changed strain state of Fn fibers as assessed in *ex vivo* tissue stainings (Fig. 3.4). Indeed, results from tissue stainings from PC-3 tumor xenograft mice support the notion of a plasma fibronectin dependent kinetic of FnBPA5 within the bloodstream, as no significant binding of FnBPA5 to tissue sections from liver, kidney, heart, and lung could be observed, compared to tumor sections, respectively to the scrambled negative control (Fig. 4.1). From this data, it seems evident, that specific *in vivo* uptake of FnBPA5 in liver and potentially also in the spleen are indeed dependent on plasma Fn acting as a carrier vehicle for FnBPA5 bound to it. On the other hand, specific binding of FnBPA5 to tumor tissue sections, as presented in figure 3.4 and figure 4.1 demonstrates that observed *in vivo* uptake and prolonged retention is, at least in part, due to disturbances in tissue organization as frequently reported for tumors [5-7]. These changes in tissue organization likely have an impact on the strain state of fibronectin's bacterial binding site, and thus promote binding of FnBPA5. Our herein presented data show, that the current dogma, relating increased tissue rigidity, cell contractility and an aligned matrix structure directly to a stretched extracellular matrix and to stretched individual protein fibers within the ECM, is likely to be challenged in the future with further development of this and other probes to assess mechanical strain of proteins in tissue.

Conceptual design of diagnostic probes based on Fn binding peptides

Cancer, fibrosis and lymph node swelling were previously reported [5,6,8-11] and shown herein to go along with changes in mechanical forces and ECM organization, as strain sensitive peptide FnBPA5 only showed binding to cancer tissue, respectively virus infected lymph node tissue sections (Fig. 4.1, 4.3). For an envisioned development of novel diagnostic markers based on this technology, the further characterization of underlying molecular mechanisms resulting in relaxed strain state of Fn fibers in these circumstances is necessary. This was partly done already in this work, as both collagen-I and alpha smooth muscle actin have been shown in PC-3 tumor xenograft tissue sections to correlate with enhanced binding of FnBPA5 (Fig. 3.4, 4.2). The discovery of further additional cancer markers, correlating with FnBPA5 binding would be greatly beneficial for a reliable prediction of malignancy and disease progression. Additionally, the clarification of *in vivo* fate of FnBPA5 would help greatly in deepening the mechanistic understanding of FnBPA5 dynamics upon intravenous injection. Plasma Fn null mice, as used in previous studies [3,4], could be utilized to assess the influence of circulating fibronectin in blood plasma to distinguish to what extent our herein observed biodistribution is dependent on binding abilities of FnBPA5 to plasma Fn or whether we can observe a similar distribution also in absence of this interaction.

For a successful clinical prototype a literature review and experimental assessment of different tumor types or fibrotic diseases in terms of Fn content, tissue rigidity and abundance of highly contractile myofibroblasts should be carried out to identify the most promising targets for a clinical application. As the current design of the FnBPA5 peptide as shown in figure 3.1 is highly flexible in terms of coupling of a functional molecule to the N-terminal cysteine, an adequate marker should be introduced with a readout that is frequently used in clinics. This can be either markers for *in vivo* imaging such as radionuclides for positron emission tomography (PET), or fluorophores for *ex vivo* probing of tissue sections or biopsies. Adequate PET radionuclides would be ^{44}Sc, ^{64}Cu or ^{68}Ga as previously used in clinical PET imaging [12-14] and fluorophore linked FnBPA5 can be similarly utilized as presented herein by means of attachment of organic dyes.

Although the clinical feasibility of strain-sensitive bacterial Fn binding peptides as diagnostic marker still needs to be assessed, they would offer enormous potential in classifying diseases in terms of mechanical changes, rather than in terms of expression patterns of specific markers. This novel concept could ultimately be used to plan patient treatment for an overall improved treatment stratification. It is evident that great efforts are still necessary to reach that point, however in this work we tried to establish a starting point to reach that goal.

Experimental framework

As FnBPA5 and many other bacterial Fn binding peptides bind to Fn via a specific mechanism to FnI domains 1-5 [15-17] the herein presented probe only gives information on a change in the relative distances between these FnI modules, it however remains open to what extent, in which circumstances or whether these changes correlate or relate to an overall strain state of a Fn protein fiber in tissues. This question was addressed in terms of a correlative evaluation of Fn-FRET and FnBPA5 in human dermal fibroblast cell culture *in vitro*, indeed showing a correlation of increased FnBPA5 binding to more relaxed Fn fibers as visualized via Fn-FRET. As the organizational complexity of tissues and organs is drastically higher compared to cell culture in a petri dish, with potentially multiple intertwining factors being present, interpretation of tissue and *in vivo* data needs additional diligence and consideration. Known factors, such as ECM composition and crosslinking, endocrine factors, presence of several different cell types, vascularization and influence of the immune system need to be taken into consideration [18-20], making the interpretation of data challenging. Further groundwork with different *in vitro* model systems, such as 2D cell culture or novel 3D microtissue assays may lead to a far better understanding of individual influencing factors for FnBPA5 binding to Fn in tissue sections or *in vivo*.

Two different *in vivo* model systems have been used in this work: prostate cancer (PC-3) xenograft model [21] and swollen lymph nodes upon immunological challenge with lymphocytic choriomeningitis virus [22] or CpG adjuvant [23,24]. The PC-3 xenograft model as used herein, has the shortcoming of an immunocompromised host organism lacking a thymus and thus most of the adaptive immune system with tumor cells of human origin being inoculated subcutaneously. Tumor vasculature, stromal compartments and other compartments of the tumor not being built up by tumor cells are of murine origin and have most likely been recruited by tumor cells from the surrounding tissue. This may raise concerns in terms of interspecies comparability of results, and to what extent such xenograft models reflect physiological tumorigenesis in an organism, as most parts of the natural immune system are compromised. It can however be said that, despite these limitations of the experimental setup, the herein presented model systems give clear evidence of the usability of FnBPA5 as mechanical strain probe for Fn fibers in tissue of different origin.

Open questions

Towards clinical translation of in vitro research

The herein presented work establishes a novel probe to measure mechanical strain of Fn fibers in tissue and offers new insight into matrix changes in pathologic situations, such as cancer or fibrosis. The question how alterations on the tissue level can be deciphered and how the individual underlying factors can be found still remains challenging. Previously introduced 3D *in vitro* test platforms, commonly referred to as microtissue assays [25,26] may offer an experimental approach to test and manipulate individual factors separately and may thus lead to a better understanding of single interfering variables. Knowledge gain from these novel 3D platforms may then contribute to the rational design of animal experiments and accelerate the overall process of translation into clinics.

End-point vs. continuous probing of Fn using FnBPA5

The bacterial Fn binding peptide FnBPA5 has in this study been exclusively used as an end-point staining and potential interference of FnBPA5 with the biological system has been neglected. As bacterial peptides bind to the same N-terminal region of Fn, that is majorly involved in Fn-Fn interactions in Fn fibers [27], and one bacterial fibronectin binding peptide has previously been reported to be capable of inhibiting fibronectin matrix assembly [28] the question arises to what extent binding of bacterial peptides may disturb the biological system. Another point of consideration is the reported internalization of bacteria containing fibronectin binding proteins on their surface [29,30] and the resulting question, whether FnBPA5, or the FnBPA5-Fn-integrin complex also gets internalized by cells and what implications this has for a potential *in vivo* use. To shed light on these questions, it would be interesting to assess whether FnBPA5 is capable of inhibiting Fn-Fn interactions, therefore disturbing Fn fibrillogenesis, which could open up new hypotheses towards the use of FnBPA5 as a blocking agent for Fn matrix formation. Furthermore, a flow cytometric experiment could be carried out to assess the number of cells having internalized fluorescently labeled FnBPA5 at different time points after addition, in comparison with a positive and negative control to get an estimate on the propensity of internalized FnBPA5 at different concentrations and time points.

Deciphering TGF-β effects – enhanced contractility and higher Fn expression

The cytokine transforming growth factor beta (TGF-β) is an important mediator of fibroblast activation toward the myofibroblastic lineage, with special importance during wound healing, but also in cancer and fibrosis [8,31]. Therefore TGF-β also represents the main target for many currently used or envisioned anti-fibrotic therapies [32,33]. TGF-β is known to have a multitude of effects on fibroblasts: enhanced cell contractility and α-SMA expression in fibroblasts [34], increased expression and alternative splicing of fibronectin [35,36] with an overall enhanced fibronectin fiber assembly [37], increase expression of tenascin-C [38], as well as increased expression of collagen-I [39]. The effect of TGF-β is self-propagating, as increased forces exerted by myofibroblasts have been shown to activate TGF-β via unfolding and thus releasing the active form of TGF-β from its latency complex [40]. It remains challenging to decipher the aforementioned downstream effects of TGF-β to obtain a satisfactory answer on the overall effect on the tissue level. As we found an increased binding of FnBPA5 to regions rich in α-SMA expressing cells in tumor tissue sections, as shown in figure 3.4 and an increase in both FnBPA5 binding and Fn expression in human fibroblasts *in vitro* (Supplementary figure 3.2) the question remains open which of the versatile effects of TGF-β are responsible for increased binding of FnBPA5 to these regions. Further experiments staining for tenascin-C, elastin and other known affected mediators of TGF-β [39] are necessary to further clarify this question.

Functional impact of fibronectin fiber strain on disease outcome

It is evident from the literature that fibronectin has important functions in many cancer types [41-43], and that it represents a key mediator of cancer metastasis and poor clinical outcome [44-47]. An open question that still remains to be answered is whether and how increased presence and altered strain state of Fn is linked to cell detachment or epithelial to mesenchymal transition, and whether these effects are due to changed Fn-cell interactions or due to other factors influenced by altered strain state of fibronectin, such as matrix crosslinking or matrix cleaving or different availabilities of growth factors. We, however propose that the herein presented changed Fn strain state, as assessed using a novel Fn strain probe, has physiological relevance with future experiments elucidating the currently unknown role of the aforementioned variables.

Usage of other matrix binding peptide sequences of bacterial origin

In this study only one of several Fn binding peptides of bacterial origin has been exploited [15,30]. Apart from the canonical bacterial Fn binding peptides, attaching to the N-terminal fibronectin domains FnI_{1-5}, also a smaller fraction of bacterial peptides bind to Fn on alternative binding sites. The protein F1/Sfb1 from S. *pyogenes* has, apart from known repeats targeting the same domains on Fn as FnBPA5 [15], also an additional 43 amino acid long sequence binding to fibronectin's collagen binding site FnI_6-FnI_9 [48,49]. S. *equisimilis* has another peptide sequence binding to the same region [50], frequently used for the inhibition of Fn-collagen interactions in recent studies [51,52]. Yet, other bacterial adhesins target the $FnIII_{9-10}$ domains in both fibronectin and tenascin-C with so far unknown mechanisms [53-55]. Further interaction with fibronectin's C-terminal heparin-binding region at $FnIII_{12-14}$ is reported for different mycobacterial species, with undetermined, but likely lower affinities compared to canonical Fn binding sequences [56-58]. The question whether these non-canonical peptides can be used in conjunction with Fn binding peptides binding to the N-terminal binding site still remains open. It would certainly be of great interest for future research to develop additional probes for alternative sites on the large fibronectin molecule, it is however not known whether these other probes also exhibit a strain sensitive binding behavior to Fn. In the current state the most promising approach would rather be to further exploit canonical Fn binding peptides via rational engineering to make use of the mechanistic knowledge of their strain-sensitive binding behavior [15], as to date only very little is known on the exact mechanism and binding structure of non-canonical bacterial Fn binding peptides.

Concluding remarks

Insidious changes of tissue organization are hallmarks of the development of cancer and other fibrotic disorders. A multitude of alterations comprising enhanced cellular contractility, changed matrix protein expression, deposition and crosslinking, enhanced cell-matrix interactions and changed MMP activity drive malignancy with yet insufficient means of interfering or stopping these often progressive diseases. Little is known how globally measured properties, such as increased tissue rigidity and higher amount of contractile myofibroblasts relate to local strain states of individual protein fibers within the extracellular matrix.

Trying to shed light on these unknowns a novel peptide probe specifically binding to relaxed Fn fibers is introduced in this thesis, capable of probing fibronectin in tissue sections. This novel probe has been characterized to be capable of readily visualizing relaxed Fn fibers in murine tissue sections and *in vivo* and found to have great potential for applications in cancer and fibrosis diagnosis and therapy. Further characterization on the tissue level are made possible due to the introduction of this new probe to elucidate the multifactorial process of Fn relaxation *in vivo* with the ultimate aim to find mechanistic implications of Fn relaxation during disease progression.

References

[1] D.C. Deno, T.M. Saba, E.P. Lewis, Kinetics of endogenously labeled plasma fibronectin: incorporation into tissues, Am. J. Physiol. 245 (1983) R564–75.

[2] M.E. Akerman, J. Pilch, D. Peters, E. Ruoslahti, Angiostatic peptides use plasma fibronectin to home to angiogenic vasculature, Proc. Natl. Acad. Sci. U.S.a. 102 (2005) 2040–2045. doi:10.1073/pnas.0409844102.

[3] P. Nyberg, T. Sakai, K.H. Cho, M.G. Caparon, R. Fässler, L. Björck, Interactions with fibronectin attenuate the virulence of Streptococcus pyogenes, The EMBO Journal. 23 (2004) 2166–2174. doi:10.1038/sj.emboj.7600214.

[4] J. Pilch, D.M. Brown, M. Komatsu, T.A.H. Järvinen, M. Yang, D. Peters, et al., Peptides selected for binding to clotted plasma accumulate in tumor stroma and wounds, Proc. Natl. Acad. Sci. U.S.a. 103 (2006) 2800–2804. doi:10.1073/pnas.0511219103.

[5] K.R. Levental, H. Yu, L. Kass, J.N. Lakins, M. Egeblad, J.T. Erler, et al., Matrix Crosslinking Forces Tumor Progression by Enhancing Integrin Signaling, Cell. 139 (2009) 891–906. doi:10.1016/j.cell.2009.10.027.

[6] M. Allen, J. Louise Jones, Jekyll and Hyde: the role of the microenvironment on the progression of cancer, J. Pathol. 223 (2010) 163–177. doi:10.1002/path.2803.

[7] R. Malik, P.I. Lelkes, E. Cukierman, Biomechanical and biochemical remodeling of stromal extracellular matrix in cancer, Trends Biotechnol. 33 (2015) 230–236. doi:10.1016/j.tibtech.2015.01.004.

[8] M. Zeisberg, R. Kalluri, Cellular Mechanisms of Tissue Fibrosis. 1. Common and organ-specific mechanisms associated with tissue fibrosis, AJP: Cell Physiology. 304 (2013) C216–C225. doi:10.1152/ajpcell.00328.2012.

[9] D. Duscher, Z.N. Maan, V.W. Wong, R.C. Rennert, M. Januszyk, M. Rodrigues, et al., Mechanotransduction and fibrosis, Journal of Biomechanics. 47 (2014) 1997–2005. doi:10.1016/j.jbiomech.2014.03.031.

[10] J.L. Astarita, V. Cremasco, J. Fu, M.C. Darnell, J.R. Peck, J.M. Nieves-Bonilla, et al., The CLEC-2–podoplanin axis controls the contractility of fibroblastic reticular cells and lymph node microarchitecture, Nat Immunol. 16 (2014) 75–84. doi:10.1038/ni.3035.

[11] S.E. Acton, A.J. Farrugia, J.L. Astarita, D. Mourão-Sá, R.P. Jenkins, E. Nye, et al., Dendritic cells control fibroblastic reticular network tension and lymph node expansion, Nature. 514 (2015) 498–502. doi:10.1038/nature13814.

[12] R. Hernandez, H.F. Valdovinos, Y. Yang, R. Chakravarty, H. Hong, T.E. Barnhart, et al., 44Sc: An Attractive Isotope for Peptide-Based PET Imaging, Mol. Pharmaceutics. 11 (2014) 2954–2961. doi:10.1021/mp500343j.

[13] C.J. Anderson, F. Dehdashti, P.D. Cutler, S.W. Schwarz, R. Laforest, L.A. Bass, et al., 64Cu-TETA-octreotide as a PET imaging agent for patients with neuroendocrine tumors, Journal of Nuclear Medicine. 42 (2001) 213–221.

[14] M. Gabriel, C. Decristoforo, D. Kendler, G. Dobrozemsky, D. Heute, C. Uprimny, et al., 68Ga-DOTA-Tyr3-octreotide PET in neuroendocrine tumors: comparison with somatostatin receptor scintigraphy and CT, Journal of Nuclear Medicine. 48 (2007) 508–518.

[15] S. Hertig, M. Chabria, V. Vogel, Engineering mechanosensitive multivalent receptor-ligand interactions: why the nanolinker regions of bacterial adhesins matter, Nano Lett. 12 (2012) 5162–5168. doi:10.1021/nl302153h.

[16] M. Chabria, S. Hertig, M.L. Smith, V. Vogel, Stretching fibronectin fibres disrupts binding of bacterial adhesins by physically destroying an epitope, Nature Communications. 1 (2010) 135–9. doi:10.1038/ncomms1135.

[17] U. Schwarz-Linek, J.M. Werner, A.R. Pickford, S. Gurusiddappa, J.H. Kim, E.S. Pilka, et al., Pathogenic bacteria attach to human fibronectin through a tandem beta-zipper, Nature. 423 (2003) 177–181. doi:10.1038/nature01589.

[18] S.J. Turley, V. Cremasco, J.L. Astarita, Immunological hallmarks of stromal cells in the tumour microenvironment, Nat Rev Immunol. 15 (2015) 669–682. doi:10.1038/nri3902.

[19] H.E. Barker, T.R. Cox, J.T. Erler, The rationale for targeting the LOX family in cancer, Nat Rev Cancer. 12 (2012) 540–552. doi:10.1038/nrc3319.

[20] C. Bonnans, J. Chou, Z. Werb, Remodelling the extracellular matrix in development and disease, Nat Rev Mol Cell Biol. 15 (2014) 786–801. doi:10.1038/nrm3904.

[21] O.E. Franco, S.W. Hayward, Targeting the Tumor Stroma as a Novel Therapeutic Approach for Prostate Cancer, Advances in Pharmacology, 2012. doi:10.1016/B978-0-12-397927-8.00009-9.

[22] E. Scandella, B. Bolinger, E. Lattmann, S. Miller, S. Favre, D.R. Littman, et al., Restoration of lymphoid organ integrity through the interaction of lymphoid tissue-inducer cells with stroma of the T cell zone, Nat Immunol. 9 (2008) 667–675. doi:10.1038/ni.1605.

[23] R.S. Chu, O.S. Targoni, A.M. Krieg, P.V. Lehmann, C.V. Harding, CpG oligodeoxynucleotides act as adjuvants that switch on T helper 1 (Th1) immunity, J. Exp. Med. 186 (1997) 1623–1631.

[24] R.L. Coffman, A. Sher, R.A. Seder, Vaccine Adjuvants: Putting Innate Immunity to Work, Immunity. 33 (2010) 492–503. doi:10.1016/j.immuni.2010.10.002.

[25] W.R. Legant, A. Pathak, M.T. Yang, V.S. Deshpande, R.M. McMeeking, C.S. Chen, Microfabricated tissue gauges to measure and manipulate forces from 3D microtissues, Proc. Natl. Acad. Sci. U.S.a. 106 (2009) 10097–10102. doi:10.1073/pnas.0900174106.

[26] C.M. Bidan, P. Kollmannsberger, V. Gering, S. Ehrig, P. Joly, A. Petersen, et al., Gradual conversion of cellular stress patterns into pre-stressed matrix architecture during in vitro tissue growth, Journal of the Royal Society Interface. 13 (2016). doi:10.1098/rsif.2016.0136.

[27] S.M. Früh, I. Schoen, J. Ries, V. Vogel, Molecular architecture of native fibronectin fibrils, Nature Communications. 6:7275 (2015). doi:10.1038/ncomms8275.

[28] B.R. Tomasini-Johansson, N.R. Kaufman, M.G. Ensenberger, V. Ozeri, E. Hanski, D.F. Mosher, A 49-Residue Peptide from Adhesin F1 of Streptococcus pyogenes Inhibits Fibronectin Matrix Assembly, Journal of Biological Chemistry. 276 (2001) 23430–23439. doi:10.1074/jbc.M103467200.

[29] R.J. Bingham, E. Rudino-Pinera, N.A.G. Meenan, U. Schwarz-Linek, J.P. Turkenburg, M. Hook, et al., Crystal structures of fibronectin-binding sites from Staphylococcus aureus FnBPA in complex with fibronectin domains, Proc. Natl. Acad. Sci. U.S.a. 105 (2008) 12254–12258. doi:10.1073/pnas.0803556105.

[30] B. Henderson, S. Nair, J. Pallas, M.A. Williams, Fibronectin: a multidomain host adhesin targeted by bacterial fibronectin-binding proteins, FEMS Microbiology Reviews. 35 (2010) 147–200. doi:10.1111/j.1574-6976.2010.00243.x.

[31] B. Hinz, The extracellular matrix and transforming growth factor-β1: Tale of a strained relationship, Matrix Biol. 47 (2015) 54–65. doi:10.1016/j.matbio.2015.05.006.

[32] J.H.W. Distler, A. Jüngel, L.C. Huber, U. Schulze-Horsel, J. Zwerina, R.E. Gay, et al., Imatinib mesylate reduces production of extracellular matrix and prevents development of experimental dermal fibrosis, Arthritis Rheum. 56 (2006) 311–322. doi:10.1002/art.22314.

[33] N.C. Henderson, T.D. Arnold, Y. Katamura, M.M. Giacomini, J.D. Rodriguez, J.H. McCarty, et al., Targeting of alpha-v integrin identifies a core molecular pathway that regulates fibrosis in several organs, Nat Med. 19 (2013) 1617–1624. doi:10.1038/nm.3282.

[34] B. Hinz, G. Gabbiani, C. Chaponnier, The NH 2-terminal peptide of α–smooth muscle actin inhibits force generation by the myofibroblast in vitro and in vivo, J. Cell Biol. 157 (2002) 657–663. doi:10.1091/mbc.6.5.541.

[35] W.D. Xu, E.C. LeRoy, E.A. Smith, Fibronectin release by systemic sclerosis and normal dermal

fibroblasts in response to TGF-beta, The Journal of Rheumatology. 18 (1991) 241–246.

[36] E. Balza, L. Borsi, G. Allemanni, L. Zardi, Transforming growth factor β regulates the levels of different fibronectin isoforms in normal human cultured fibroblasts, FEBS Lett. 228 (1988) 42–44.

[37] E.E. Torr, C.R. Ngam, K. Bernau, B. Tomasini-Johansson, B. Acton, N. Sandbo, Myofibroblasts exhibit enhanced fibronectin assembly that is intrinsic to their contractile phenotype, Journal of Biological Chemistry. 290 (2015) 6951–6961. doi:10.1074/jbc.M114.606186.

[38] M. Jinnin, H. Ihn, Y. Asano, K. Yamane, M. Trojanowska, K. Tamaki, Tenascin-C upregulation by transforming growth factor-β in human dermal fibroblasts involves Smad3, Sp1, and Ets1, Oncogene. 23 (2004) 1656–1667. doi:10.1038/sj.onc.1207064.

[39] M. Pickup, S. Novitskiy, H.L. Moses, The roles of TGF-beta in the tumour microenvironment, Nat Rev Cancer. 13 (2013) 788–799. doi:10.1038/nrc3603.

[40] P.-J. Wipff, D.B. Rifkin, J.-J. Meister, B. Hinz, Myofibroblast contraction activates latent TGF-beta1 from the extracellular matrix, J. Cell Biol. 179 (2007) 1311–1323. doi:10.1083/jcb.200704042.

[41] J. Park, J.E. Schwarzbauer, Mammary epithelial cell interactions with fibronectin stimulate epithelial-mesenchymal transition, Oncogene. 33 (2014) 1649–1657. doi:10.1038/onc.2013.118.

[42] C. Ricciardelli, R.J. Rodgers, Extracellular matrix of ovarian tumors, Seminars in Reproductive Medicine. 24 (2006) 270–282.

[43] E. Ruoslahti, Fibronectin and its integrin receptors in cancer, Adv. Cancer Res. 76 (1999) 1–20.

[44] M.V. Gulubova, T.I. Vlaykova, Significance of tenascin-C, fibronectin, laminin, collagen IV, alpha5beta1 and alpha9beta1 integrins and fibrotic capsule formation around liver metastases originating from cancers of the digestive tract, Neoplasma. 53 (2006) 372–383.

[45] H. Sil, T. Sen, A. Chatterjee, Fibronectin-Integrin (α5β1) Modulates Migration and Invasion of Murine Melanoma Cell Line B16F10 by Involving MMP-9, Oncol Res. 19 (2011) 335–348. doi:10.3727/096504011X13079697132925.

[46] D.J. O'Shannessy, E.B. Somers, L.K. Chandrasekaran, N.C. Nicolaides, J. Bordeaux, M.D. Gustavson, Influence of tumor microenvironment on prognosis in colorectal cancer: Tissue architecture-dependent signature of endosialin (TEM-1) and associated proteins, Oncotarget. 5 (2014) 3983–3995.

[47] F.L. Miles, R.A. Sikes, Insidious changes in stromal matrix fuel cancer progression, Mol. Cancer Res. 12 (2014) 297–312. doi:10.1158/1541-7786.MCR-13-0535.

[48] S. Sela, A. Aviv, A. Tovi, I. Burstein, M.G. Caparon, E. Hanski, Protein F: an adhesin of Streptococcus pyogenes binds fibronectin via two distinct domains, Mol. Microbiol. 10 (1993) 1049–1055. doi:10.1146/annurev.bi.52.070183.003553.

[49] J.P. Hymes, T.R. Klaenhammer, Stuck in the Middle: Fibronectin-Binding Proteins in Gram-Positive Bacteria, Front. Microbiol. 7 (2016). doi:10.1086/421946.

[50] H. Lindmark, B. Guss, SFS, a novel fibronectin-binding protein from Streptococcus equi, inhibits the binding between fibronectin and collagen, Infect. Immun. 67 (1999) 2383–2388.

[51] J. Sottile, F. Shi, I. Rublyevska, H.Y. Chiang, J. Lust, J. Chandler, Fibronectin-dependent collagen I deposition modulates the cell response to fibronectin, AJP: Cell Physiology. 293 (2007) C1934–C1946. doi:10.1152/ajpcell.00130.2007.

[52] K.E. Kubow, R. Vukmirovic, L. Zhe, E. Klotzsch, M.L. Smith, D. Gourdon, et al., Mechanical forces regulate the interactions of fibronectin and collagen I in extracellular matrix, Nature Communications. 6 (2015) 1–11. doi:10.1038/ncomms9026.

[53] I.-M. Frick, K.L. Crossin, G.M. Edelman, L. Björck, Protein H-a bacterial surface protein with affinity for both immunoglobulin and fibronectin type III domains, The EMBO Journal. 14 (1995) 1674–1679.

[54] M. Christner, G.C. Franke, N.N. Schommer, U. Wendt, K. Wegert, P. Pehle, et al., The giant extracellular matrix-binding protein of Staphylococcus epidermidis mediates biofilm accumulation

and attachment to fibronectin, Mol. Microbiol. 75 (2010) 187–207. doi:10.1111/j.1365-2958.2009.06981.x.

[55] S. Katayama, M. Tagomori, N. Morita, T. Yamasaki, H. Nariya, M. Okada, et al., Determination of the Clostridium perfringens-binding site on fibronectin, Anaerobe. 34 (2015) 174–181. doi:10.1016/j.anaerobe.2014.11.007.

[56] J.S. Schorey, M.A. Holsti, T.L. Ratliff, P.M. Allen, E.J. Brown, Characterization of the fibronectin-attachment protein of Mycobacterium avium reveals a fibronectin-binding motif conserved among mycobacteria, Mol. Microbiol. 21 (1996) 321–329.

[57] T.L. Ratliff, J.A. McGarr, C. Abou-Zeid, G.A.W. Rook, J.L. Stanford, J. Aslanzadeh, et al., Attachment of Mycobacteria to Fibronectin-coated Surfaces, Microbiology. 134 (1988) 1307–1313. doi:10.1099/00221287-134-5-1307.

[58] C. Abou-Zeid, T.L. Ratliff, H.G. Wiker, M. Harboe, Characterization of fibronectin-binding antigens released by Mycobacterium tuberculosis and Mycobacterium bovis BCG, Infect. Immun. 56 (1988) 3046–3051.

Appendix

FnBPA5 binding to Fn knockout mouse embryonic fibroblast matrix

Mouse embryonic fibroblasts (MEFs) with knocked out Fn gene (Fn -/-) and floxed control cells (Fn fl/fl) were obtained from the group of Prof. Reinhard Fässler. Cells were seeded into a Fn coated 8-well chambered Lab-Tek coverslide at a density of 50000 cells/well. Cells were allowed to attach overnight and cell culture medium was exchanged the next day. For samples with exogenous fibronectin, 10 or 50 µg/ml plasma Fn was added to the cell culture medium. After additional two days of culturing total amount of fibronectin was stained using the C-20 goat anti-fibronectin antibody from Santa Cruz (sc-6952, 1:100) and 5 µg/ml FnBPA5-Cy5 in serum free medium for 1 hour at 37°C. The samples were after a washing step fixed in 4% paraformaldehyde, blocked for one hour in PBS with 4% donkey serum and subsequently incubated with a donkey anti goat-Alexa488 secondary antibody (Invitrogen) for 45 minutes. During the last washing step cell nuclei were stained using DAPI (1:1000) for 5 minutes and afterwards imaged using a Leica SP4 confocal microscope equipped with a 40x objective. Representative images Fn -/-, rescued Fn -/- and Fn fl/fl MEFs are shown in figure A1, showing no binding of FnBPA5 to Fn -/- cells, as no fibronectin and thus no binding sites are available. Binding can be rescued via exogenous addition of Fn to the cell culture medium. This data thus gives clear evidence, that FnBPA5 indeed binds specifically to Fn in a cellular environment, with no unspecific binding to other proteins.

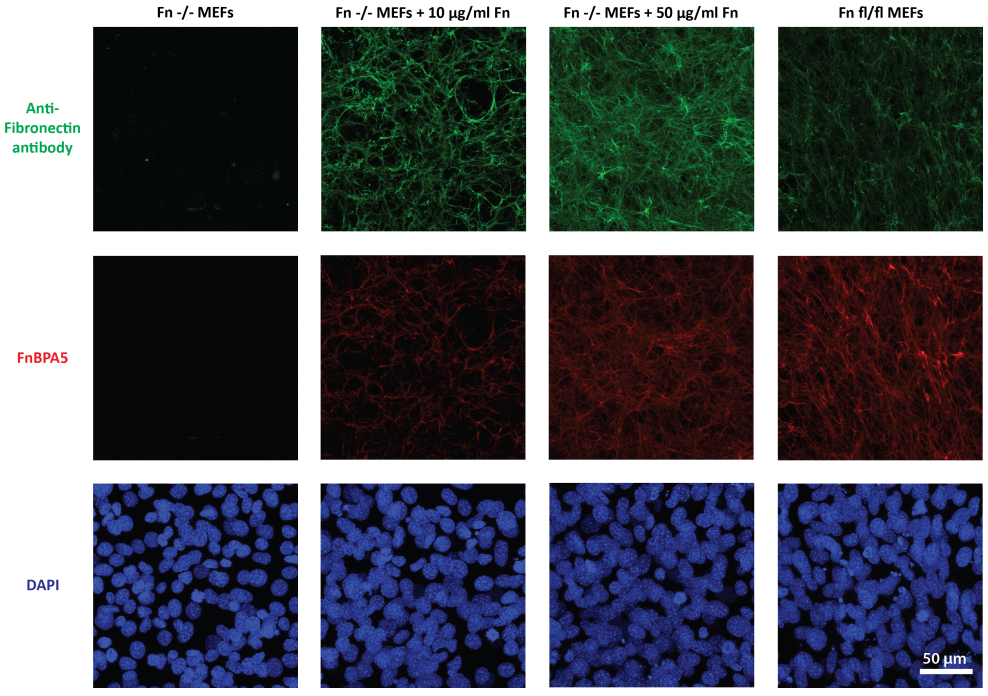

Figure A1: Staining of Fn knockout or Fn floxed mouse embryonic fibroblast (MEF) cells, with anti Fn antibody C-20 (sc-6952, Santa Cruz), FnBPA5-Cy5 and DAPI. FnBPA5 binding can be rescued via exogenous addition of plasma fibronectin (10 and 50 µg/ml respectively) to Fn knockout cells.

FnBPA5-Fn binding assessed via superresolution microscopy

This experiment was carried out together with Dr. Susanna Früh:

As Fn fibers have previously been characterized by means of sub-diffraction fluorescence microscopy [1] we asked here, whether in a similar way, we could map binding of FnBPA5 peptide at its known binding site at the N-terminus of Fn. For this human dermal fibroblasts were seeded onto sterilized Fn coated glass coverslips (18 mm diameter) at a density of 5000 cells/coverslip. After initial attachment medium was exchanged to MEM alpha with the addition of 50 µg/ml plasma fibronectin and cells were cultured overnight. The next day, samples were after a washing step incubated with 5 µg/ml Alexa-647 labeled FnBPA5 in serum free medium for 1 hour at 37°C and after washing fixed in 4% paraformaldehyde in PBS for 10 minutes. Goat anti fibronectin C-20 antibody (sc-6952, 1:50, Santa Cruz Biosciences) or goat anti fibronectin N-20 antibody (sc-6953, 1:50, Santa Cruz Biosciences) were then incubated in blocking solution with 3% bovine serum albumin (BSA) for 1 hour at room temperature. After a washing step samples were incubated with an anti-goat CF680 secondary antibody (1:10) in PBS plus BSA and incubated for 30 minutes in the dark. After a washing step samples were post-fixed with 4% paraformaldehyde in PBS for 10 minutes and again washed in PBS before being imaged with a custom-built setup used in a previous study [1].

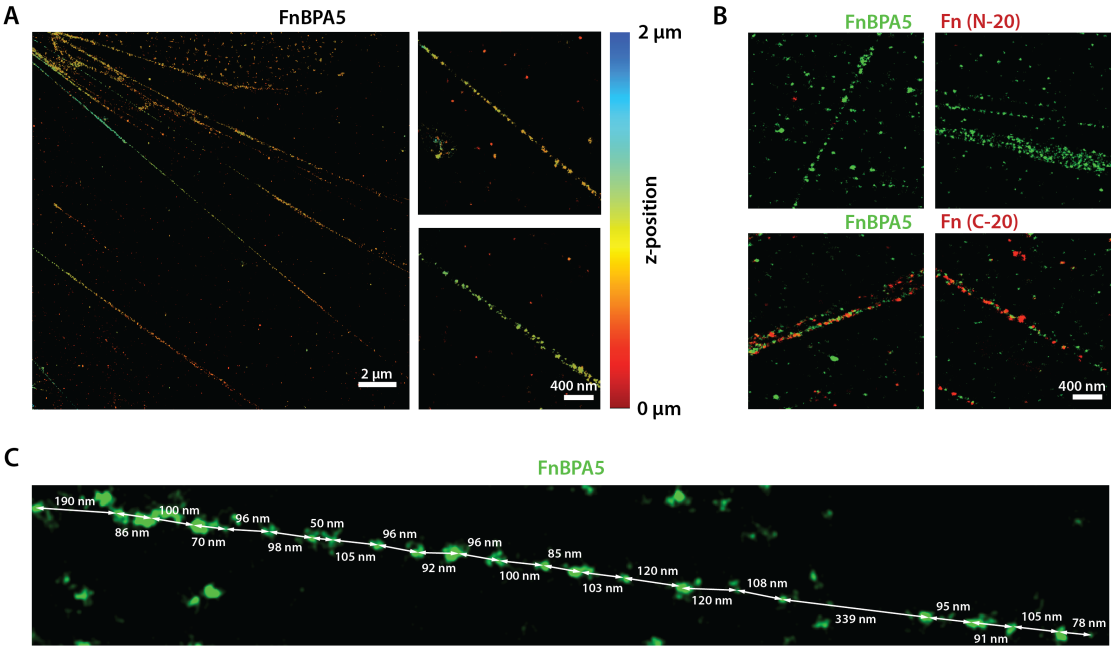

Figure A2: Superresolution images of Fn fibers from human dermal fibroblasts. **A** 3D images of FnBPA5-647 bound to Fn fibers showing a clear localization of peptide binding to fibers, with periodic signal. **B** Co-staining of FnBPA5-647 and anti-fibronectin antibodies N-20 and C-20. Whereas N-20 antibody signal was almost absent, indicating a possible blocking of antibody binding by FnBPA5, the signal of C-20 antibody was along the same Fn fibers as FnBPA5 signal. **C** Image of FnBPA5 with readout of distances between fluorophores, being in similar range as previously proposed for Fn fiber architecture [1].

References

[1] S.M. Früh, I. Schoen, J. Ries, V. Vogel, Molecular architecture of native fibronectin fibrils, Nature Communications. 6:7275 (2015). doi:10.1038/ncomms8275.

List of Abbreviations

α-SMA	alpha smooth muscle actin
AFM	atomic force microscope
CD-31	cluster of differentiation 31
CFA	complete Freud's adjuvant
cFn	cellular fibronectin
CpG	cytidine phosphate guanosine motif containing oligonucleotide sequences
CS	chondroitin sulfate
CT	computed tomography
CTRL	control
DAPI	4',6-diamidino-2-phenylindole
ECM	extracellular matrix
EDA	extra domain A
EDB	extra domain B
EMT	epithelial to mesenchymal transition
ER-TR7	antigen presented in and produced by reticular fibroblasts
FBS	fetal bovine serum
FGF	fibroblast growth factor
FITC	fluorescein isothiocyanate
Fn	fibronectin
FnBPA	fibronectin binding protein A
FnBPA5	fibronectin binding protein A 5
FRC	fibroblastic reticular cell
FRET	Förster or fluorescence resonance energy transfer
GAG	glycosaminoglycan
GdnHCl	guanidinium hydrochloride
HA	hyaluronic acid
hBMSC	human bone marrow stromal cell
Hep	heparin

HGF	hepatocyte growth factor
HS	heparan sulfate
HSPG	heparan sulfate proteoglycan
IA / g	initial activity per gram
IL-7	interleukin-7
LCMV	lymphocytic choriomeningitis virus
LOX	lysyl oxidase
MMP	matrix metalloproteinase
p.i.	post-injection
PBS	phosphate buffered saline
PC-3	human prostate cancer cell line
PDGF	platelet derived growth factor
PECAM-1	platelet endothelial cell adhesion molecule-1
PET	positron emission tomography
pFn	plasma fibronectin
PFU	plaque forming unit
pLN	popliteal lymph node
PMT	photo multiplier tube
RP-HPLC	reverse phase-high pressure liquid chromatography
sHA	sulfated hyaluronic acid
SHG	second harmonic generation
SMD	steered molecular dynamics
SPECT	single photon emission computed tomography
TGF-β	transforming growth factor-beta
VEGF	vascular endothelial growth factor
YAP	yes-associated protein

Acknowledgment

Doing a PhD was a challenging, yet interesting experience. Although many experiments and writing tasks are performed alone in this time, no one, at least in my humble opinion can achieve this degree without the significant support of others, being it the PhD advisor, committee members, colleagues in the lab, friends and family building up a supporting framework similar to the extracellular matrix in a biological context. This section here is dedicated to these important people, who significantly coined this time of my life and will have a long-lasting impact on the steps ahead.

First, I would like to express my sincere gratitude to my PhD advisor Prof. Viola Vogel. I am deeply grateful to have learned from and worked with Prof. Vogel and consider the degree of freedom given to young researchers within her group as an extraordinary environment fostering the development of people in both scientific and personal regard. Discussions and meetings were always accompanied by an understanding, kind and supporting atmosphere, for which I am especially thankful.

I want to thank the members of my PhD committee, Prof. Viola Vogel, Dr. Martin Behe and Prof. Oliver Distler for their willingness to read and give their expert opinion on the thesis and being present during the thesis examination.

I especially thank Dr. Martin Behe for the establishment of the very fruitful collaboration between our group and the PSI from which this thesis gained enormously and am especially grateful for the good discussions and his support.

Along that line I want to express my deep gratitude to Dr. Alessandra Moscaroli, representing the key collaborator during my thesis. Alessandra was able to contribute with extremely valuable scientific input, and her profoundly positive, optimistic can-do attitude often helped us to find new pathways to further develop our collaborative projects.

I want to say thank you to Sarah Vogel, who visited our lab from Dresden and introduced me to the world of glycosaminoglycans. Her pro-active approach and valuable scientific input greatly boosted the development of a collaborative project between us, parts of which are already published and parts of it are presented herein.

My sincere gratitude goes to the whole Vogel group (current and former members) for generating such a nice working environment. Special thanks go to Dr. Mamta Chabria and Dr. Samuel Hertig who started the bacterial fibronectin binding peptide project in the lab and without their groundbreaking work this project could have never been realized. A special thanks to the members of the fruit break, Dr. Susanna Früh, Dr. Florian Herzog and Lukas Braun for reminding each other that continuous vitamin input is essential for surviving the PhD and to Dr. Mario Benn, Jenna Graham, Sebastian Lickert, Dr. Ingmar Schön and Dr. Tadahiro Yamashita for having

the occasional running exercise and beverage (mostly in that order). Furthermore, I want to say a special thank you to Dr. Isabel Gerber and Chantel Spencer for their support in technical questions and for generating a safe working environment. A special thank you should go to Norma de Giuseppe for making things happen and keeping track that everything runs smoothly.

As we never walk alone, I want to express my deep gratefulness to my good friends from middle school Georg Müller and Joachim Stonig for, despite living in different cities, always being there with an open ear, honest advice and encouragement. Special thank you also to Tobias Bachmann and Andreas Wyss for struggling through undergrad together, for the mutual support and motivation during that time and onwards.

Ohne die Unterstützung meiner Familie, meiner Eltern und meines Bruders Markus wäre diese Arbeit nicht möglich gewesen. Ich möchte euch danken, dass ihr immer an mich geglaubt habt, auch in Phasen in denen der Weg uneben war und nicht sicher wohin er führt, für die Unterstützung auf diesem Weg, für die unzähligen Ermutigungen, kleinen und grossen Tipps mit neuen Herausforderungen klarzukommen und diese zu meistern und dafür, dass ihr immer vorbehaltlos hinter mir gestanden seid.

Zuletzt möchte ich Daniela danken, für deine Liebe und Unterstützung in dieser Zeit, für die Gespräche, gemeinsam gesponnenen Strategien und Visionen und, dass wir in guten und schwierigen Zeiten, füreinander da sind.